

9. SITE 750¹

Shipboard Scientific Party²

HOLE 750A

Date occupied: 14 April 1988
Date departed: 18 April 1988
Time on hole: 4 days, 7 hr, 45 min
Position: 57°35.54'S, 81°14.42'E
Bottom felt (rig floor; m, drill pipe measurement): 2041.0
Distance between rig floor and sea level (m): 10.50
Water depth (drill pipe measurement from sea level; m): 2030.5
Total depth (rig floor; m): 2501.5
Penetration (m): 460.50
Number of cores (including cores with no recovery): 26
Total length of cored section (m): 189.30
Total length of washed section (m): 271.20
Total core recovered (coring; m): 68.63
Total core recovered (washing; m): 1.88
Total core recovered (combined; m): 70.51
Core recovery (%): 15

Oldest sediment cored:
Depth (mbsf): 457.30
Nature: nannofossil chalk and limestone
Age: late Campanian
Velocity (km/s): 1.985

HOLE 750B

Date occupied: 20 April 1988
Date departed: 23 April 1988
Time on hole: 3 days
Position: 57°35.52'S, 81°14.37'E
Bottom felt (rig floor; m, drill pipe measurement): 2041.0
Distance between rig floor and sea level (m): 10.50
Water depth (drill pipe measurement from sea level; m): 2030.5
Total depth (rig floor; m): 2750.7
Penetration (m): 709.70
Number of cores (including cores with no recovery): 17
Total length of cored section (m): 57.40
Total length of washed section (m): 652.30
Total core recovered (coring; m): 24.60
Total core recovered (washing; m): 25.83
Total core recovered (combined; m): 50.43
Core recovery (%): 7

Oldest sediment cored:

Depth (mbsf): 671.70
Nature: ferruginous claystone
Age: Albian
Velocity (km/s): 1.431

Basement:

Depth (mbsf): 671.70
Nature: basalt
Measured velocity (km/s): 4.386

Principal results: Site 750 (proposed site SKP-3D; 57°35.54'S, 81°14.42'E; water depth 2030.5 m) is located on the Southern Kerguelen Plateau in the eastern part of the Raggatt Basin, west of the deep Labuan Basin, and approximately 900 km south of the present-day Polar Front. Our primary objective was to recover an expanded Cretaceous section reflecting the early tectonic and depositional history of the Southern Kerguelen Plateau. A second objective was to obtain, if feasible, basement samples from the Raggatt Basin in a zone of dipping reflectors.

Beginning with this site on 14 April 1988, *JOIDES Resolution* resumed operations on the Southern Kerguelen Plateau following an unscheduled port call to Fremantle, Australia, that required a transit of 17 days and 4400 nmi. The site was approved during the transit as a substitute for Site SKP-3B and is located 18 km to the east on the same seismic line. The basement reflector at Site 750 lies at about 0.69 s two-way traveltime (TWT) below the seafloor, and three major seismic reflectors can be traced at 0.59, 0.46, and 0.31 s TWT.

Hole 750A was wash and interval cored using a rotary core barrel (RCB) through middle and lower Eocene oozes, cherts, and cherts to 297.5 m below seafloor (mbsf); below 143 mbsf, the combination of cherts and heavy seas had their usual deleterious effect on core recovery, which was only 3% for the three rotary cores taken. After a 24-hr weather delay, continuous coring through Paleocene-Maestrichtian cherts to 423.3 mbsf yielded a nearly complete but drilling-disturbed Cretaceous/Tertiary boundary sequence at 348 mbsf; recovery was 47%.

The hole was ended at 460.5 mbsf by total bit failure (disintegration) after only 5½ hr of rotation, at which time a successful logging run was made with a combination of seismic stratigraphy tools. A second run in rough seas using lithodensity tools was foiled by damage to the cable head. Operations were suspended on 18 April 1988 with hopes of reoccupying the site after drilling at Site 751 (proposed site SKP-2C) located 46 nmi to the west.

As it developed, the site was reoccupied on 20 April 1988, and Hole 750B was washed with the RCB to 450 m, taking only one wash core on the way. After pulling a second wash barrel, the hole was continued with rotary or wash cores taken every 10–30 m through cherty Cretaceous cherts and limestones with the intention of maintaining a rate of progress of at least 10 m/hr. This rate was deemed necessary to reach basement before drilling time for the leg expired if the single bit were to survive to the projected total depth.

Drilling with a hard formation bit slowed considerably when the formation changed from marine limestone to terrestrial clay below 624 mbsf; however, a velocity inversion at that point considerably decreased the predicted depth to basement, which was encountered at 675.5 mbsf. Thereafter, a series of thick basalt flows were drilled with 67% recovery to a total depth (TD) of 709.7 mbsf.

The following lithologic units were recognized at Site 750:

Unit I (0–0.37 mbsf): lower Pleistocene to mid-Pliocene diatom ooze and lag deposit.

Repeated within the first core by a double punch of the drill string, this unit contains diatoms and foraminifers of early Pleisto-

¹ Schlich, R., Wise, S. W., Jr., et al., 1989. *Proc. ODP, Init. Repts.*, 120: College Station, TX (Ocean Drilling Program).

² Shipboard Scientific Party is as given in the list of participants preceding the contents.

cene and mid-Pliocene age with a disconformity in between. The lag contains sands and ice-rafted pebbles with heavy manganese coatings; a disconformity occurs at the base.

Unit II (0.37–357.0 mbsf): middle Eocene to lower Paleocene nanofossil ooze, chalk, and chert, divisible into two subunits.

Subunit IIA (0.37–317.2 mbsf): middle Eocene to upper Paleocene white nanofossil ooze, chalk, and chert.

Subunit IIB (317.2–357.0 mbsf): lower Paleocene white nanofossil chalk.

Crosscutting gray dissolution seams are evident below 317 mbsf. Just above the Cretaceous/Tertiary contact, the white chalk darkens downward to an olive gray color; dark specks are present, and there is a concomitant increase in magnetic susceptibility. The lowermost Danian nanofossil Zone NP1 is present, but it contains reworked Cretaceous material. The Cretaceous/Tertiary contact, which was disturbed by drilling, marks an abrupt change in lithology from well-consolidated Danian chalk to soft Maestrichtian ooze of the nanofossil *Nephrolithus frequens* Zone. The more clay-rich lower Danian section appears to show up as a positive excursion on the resistivity logs, which may allow a more precise placement of the base of this subunit.

Unit III (357.0–623.5 mbsf): upper Maestrichtian to upper Turonian nanofossil chalk, chert, and intermittently silicified limestone, divided into three subunits.

Subunit IIIA (357.0–623.5 mbsf): upper Maestrichtian to lower Maestrichtian nanofossil chalk and minor chert.

Dissolution seams characterize this subunit along with burrows, laminae, and rare stylolites. Some pale purple laminae may represent redox changes; three gray laminae contained 50% zeolite. Microfossils are exceptionally well preserved in the upper Maestrichtian; echinoid spines are a persistent component and a brachiopod shell was found at 385 mbsf.

Subunit IIIB (450.0–594.6 mbsf): lower Maestrichtian to lower Santonian with intermittently silicified limestone and calcareous chalk, poorly recovered; bioclast fragments include small molluscs, crinoid columnals, and inoceramids.

Subunit IIIC (594.6–623.5 mbsf): lower Santonian to upper Turonian chalk with dark clayey interlayers.

Cenomanian microfossils may be reworked; the darker clays may be redeposited. Pyritized wood fragments, a bivalve, and traces of glauconite are also present.

Unit IV (623.5–675.5 mbsf): Albian red to dark grey brown silty claystone with charcoal and minor conglomerate.

This unit consists of a broad range of water-laid terrigenous claystones and siltstones, with some sandy or conglomeratic intervals. Carbonized wood fragments from land plants are abundant as are coarse, authigenic siderite and pyrite grains and concretions. Where first sampled, this unit consists of a massive, plastic, reddish brown, silty claystone composed primarily of kaolinite, but with up to 25% siderite (as coarse authigenic grains), 20% opaques, 6% pyrite, and 20% altered grains that may be derived from basalt.

The next core yielded a much darker, grayish brown clayey siltstone that is more fissile and richer in organic matter (up to 7%). A highly colorful, 25-cm-thick soft pebble conglomerate displays grading, cross-stratification, and small-scale current bedding. Incorporated among the rounded to subrounded, 0.5–3 mm, silt- and claystone ferruginous grains are numerous large (centimeter scale) pieces of carbonized wood. Wood fragments are also enclosed within siderite-cemented claystones and a siderite concretion at the base of the unit.

Unit V (675.5–709.7 mbsf): Basalt flows composed of moderately to highly altered plagioclase-clinopyroxene phyric basalt.

At least four flows were recovered, of which the third flow represents the majority of the recovery, since it is a 11.5-m-thick massive basalt flow. The lower two flows are separated by a chilled margin and are overlain by highly altered volcanics. The flows are restricted in composition to olivine-hypersthene normative tholeiites. The secondary mineral assemblage consists of interlayered smectite, heulandite-clinoptilolite, calcite, and minor quartz veining.

The three major seismic reflectors observed at Site 750 above basement at 0.31, 0.46, and 0.59 s TWT are related to major changes in the lithology, physical properties, and logging data. The reflector at 0.31 s can be correlated with the boundary between Subunits IIA and IIB (317.2 mbsf). The seismic reflectors at 0.46 and 0.59 s TWT must be correlated with the top of Subunit IIIB (450 mbsf) and the

top of Subunit IIIC (594.6 mbsf), respectively. On the basis of these correlations, the calculated mean velocities for each lithologic unit or subunit are in good agreement with the measured compressional wave velocities. A clear but unusual velocity inversion is observed between 600 mbsf and the top of the basalt unit at 675.5 mbsf. A similar inversion was already recorded at Site 748 in the western Raggatt Basin.

Both the basement and the sedimentary rocks drilled at this site provide interesting contrasts with those sampled elsewhere on the Kerguelen Plateau during this leg. In terms of incompatible trace element abundances, basalts from Site 750 are the most depleted, thereby extending the array defined by samples from Sites 747 and 749. They also show slight differences in incompatible element ratios, possibly indicating differences in source characteristics.

Nevertheless, Site 750 basement is transitional in composition between normal Indian Ocean mid-ocean ridge basalts (MORB) and Kerguelen and Heard island oceanic-island basalt (OIB) lavas. The secondary mineral assemblage at this site indicates intermediate- to high-temperature alteration comparable with the temperature regimes defined at Sites 747 and 749. The alteration occurred under oxidizing conditions, and the basalts were erupted in a subaerial or shallow subaqueous environment.

Following the emplacement of the uppermost basalts at this site in Albian times, a considerable portion of the southern Kerguelen volcanic edifice was emergent and subject to intense weathering in a warm temperate or subtropical climate (in marked contrast to that in this region today). Rainfall was sufficient to weather volcanics to kaolinitic clays. The actual source rock may not have been entirely the tholeiitic basalts drilled at this site, but alkaline basalts instead that were located elsewhere in the rather extensive watershed (perhaps similar in composition to those drilled at Site 748).

The kaolinites accumulated in well-vegetated or forested, subaqueous or subaerial environments, perhaps on marshy flood plains. The soft pebble conglomerates probably denote fluvial conditions, and the authigenic siderite crystals are characteristic of coal swamps. The numerous large pieces of charcoal (up to 5 cm) and the high organic carbon contents of up to 7% further suggest a terrestrial setting. These sediments are visually similar but mineralogically different from those penetrated but poorly sampled in Unit IV at Site 748.

Foundering of this portion of the Kerguelen platform occurred by Cenomanian times. The oldest recovered chalks contain evidence of redeposition of inner shelf faunas into a deeper water environment. By the late Campanian, the subsidence had carried the site to upper slope depths; sedimentation rates increased considerably and surface temperatures cooled, so that planktonic foraminifer assemblages changed from transitional to austral in character. Only in the late Maestrichtian do the foraminifer and nanofossil assemblages lose their strong austral affinities, apparently indicating a progressive warming leading up to the close of the Cretaceous period. By then the site had deepened to perhaps bathyal depths.

Conditions at this site during the deposition of these Upper Cretaceous chalks were consistently open marine, in strong contrast to the restricted Turonian-Coniacian glauconitic siltstones and shallow-water glauconitic bioclastics that characterized the western Raggatt Basin (Site 748). Nor is there evidence of the Maestrichtian-lower Danian debris flows encountered at Site 747 to the north. The western Raggatt Basin stood structurally higher than the eastern portion of the basin throughout the Late Cretaceous, subsiding rapidly only at the end of the Maestrichtian, and Site 748 remains 740 m shallower than Site 750 today. These different histories are well reflected in our sedimentologic and seismic stratigraphic records.

Surprisingly high sedimentation rates of 11 m/m.y. characterize the Danian, which spans 40 m of section at Site 750. Danian benthic foraminifer faunas are similar to those of the upper Maestrichtian; by then, the paleodepths of the site were approaching those of the present day. Sedimentation rates increased to about 30 m/m.y. during the late early and late middle Eocene. Except for the thin Pliocene-Pleistocene veneer and lag deposit, the remainder of the Cenozoic is missing at this site.

BACKGROUND AND OBJECTIVES

The Kerguelen Plateau extends between 46°S and 64°S and can be divided into two distinct domains: the Kerguelen-Heard Plateau to the north and the Southern Kerguelen Plateau to

the south (Schlich, 1975, 1982; Houtz et al., 1977). Site 750 ($57^{\circ}35.54'S$, $81^{\circ}14.42'E$) is located on the Southern Kerguelen Plateau in the eastern part of the Raggatt Basin, west of the deep Labuan Basin, approximately 900 km south of the present-day Antarctic Convergence at a water depth of 2030.5 m (see "Introduction" chapter, this volume).

Three northeast-trending multichannel seismic reflection lines (RS02-22, RS02-24, and RS02-27), separated by approximately

50 km, one north-trending line (MD47-16), and two northwest-trending lines (MD47-05 and MD47-15) in the central part of the Raggatt Basin provide good regional control for the area close to Site 750 (Fig. 1). To the east the sedimentary coverage in the Raggatt Basin thins progressively toward the edge of the plateau. The eastern flank of the Kerguelen Plateau corresponds at this latitude to a steep slope merging into the deep Labuan Basin. To the north and to the south the sediments thin gradually,

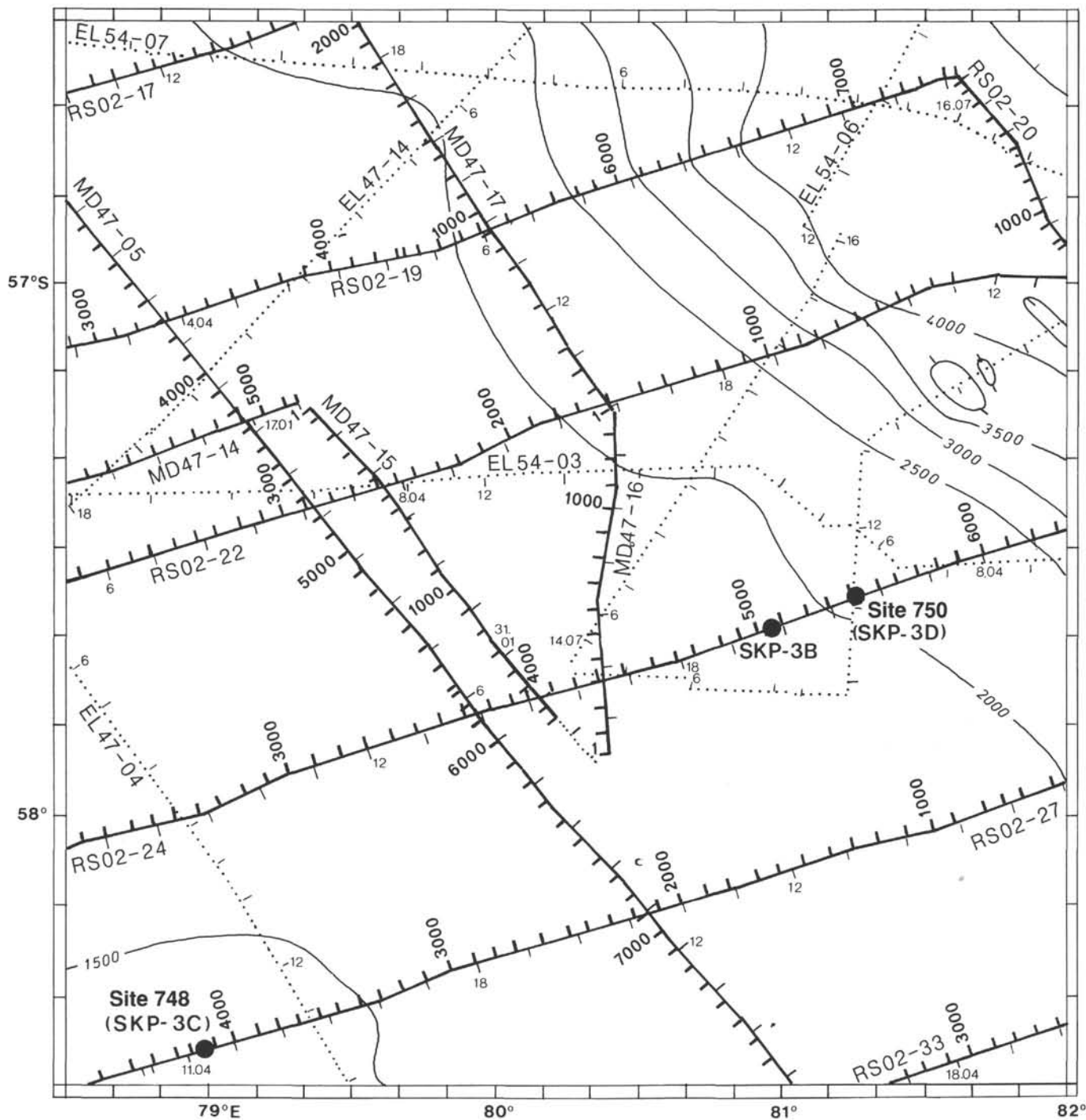


Figure 1. Track lines in the vicinity of Site 750. Bold lines denote *Rig Seismic* (RS02) and *Marion Dufresne* (MD47) multichannel seismic reflection profiles. The bathymetry is from Schlich et al. (1987).

but a lack of seismic reflection data prevents precise delineation of the basin. To the west the Raggatt Basin ends abruptly against the 77°E Graben.

The sediment cover in the central part of the Raggatt Basin reaches 2500–3000 m and rests upon a weakly defined basement reflector. Schlich et al. (1988) and Colwell et al. (1988) independently identified six seismic sequences in the basin. Joint interpretation of Australian and French multichannel seismic reflection data (Coffin et al., in press) distinguished seven seismic sequences, which can be grouped into two megasequences. The upper sequence is divided into three sequences (NQ1, PN1, and P2) and the lower megasequence into four sequences (P1, K3, K2, and K1).

Leclaire et al. (1987a, 1987b) recovered the first significant assemblage of basement rocks along the 77°E Graben. The samples are basaltic and were dated at 114 Ma, and the lowermost exposed sediments are of Late Cretaceous age. Sediments from seven cores collected north of the site along *Rig Seismic* line RS02-22 vary in age from Holocene to Maestrichtian and are composed of Neogene calcareous oozes and Eocene to Maestrichtian argillaceous calcareous oozes. The oldest sediments known from the eastern margin of the Southern Kerguelen Plateau are late Cenomanian chalks cored at 55°53'S and 81°07'E during *Eltanin* cruise 54 in 1972 (Quilty, 1973).

Site 750 (target Site SKP-3D) is on Australian multichannel seismic reflection line RS02-24 (97.2127, shot point 5410) trending northeast across the Raggatt Basin, where the basement lies at about 900 m and where a complete sedimentary section, ranging from Cretaceous to Eocene, is present. Target site SKP-3D (Site 750) lies about 18 km to the east of the original proposed Site

SKP-3B (97.1950, shot point 5055, on seismic line RS02-24). The locations of these sites on *Rig Seismic* profile RS02-24 are given in Figure 2.

Objectives

The prime objective of drilling Site 750 was to recover an expanded section of Cretaceous sediments reflecting the early tectonic history of the Southern Kerguelen Plateau (age of the sediments and unconformities, rifting episodes, vertical movements) as well as the evolution of the Cretaceous paleoenvironment. The results of this drilling were to be compared with those obtained at Site 748 (target site SKP-3C) in the western Raggatt Basin and Site 737 (target site KHP-3) drilled during Leg 119 on the Northern Kerguelen Plateau.

A second objective of drilling this site was to recover basement samples from the Raggatt Basin and to compare these rocks with those obtained at other Kerguelen Plateau basement sites (Leg 119, Site 738 in the southernmost part of the Kerguelen Plateau; Leg 120, Site 747 in the transition zone between the northern and southern Kerguelen Plateau, and Site 749 on the Banzare Bank).

As previously explained (see "Background and Objectives" section, Site 748 chapter), the original Paleogene-Mesozoic stratigraphic and tectonic site SKP-3 on seismic line RS02-24 (97.0415) was approved only to 800 m to avoid penetrating a sequence of reflections forming a pinch-out at depth, and two alternate sites (SKP-3B and SKP-3C) were proposed and approved to be drilled down to basement. For logistic and scientific reasons, priority was given on board *JOIDES Resolution* to site SKP-3C (see "Background and Objectives" section, Site 748 chapter).

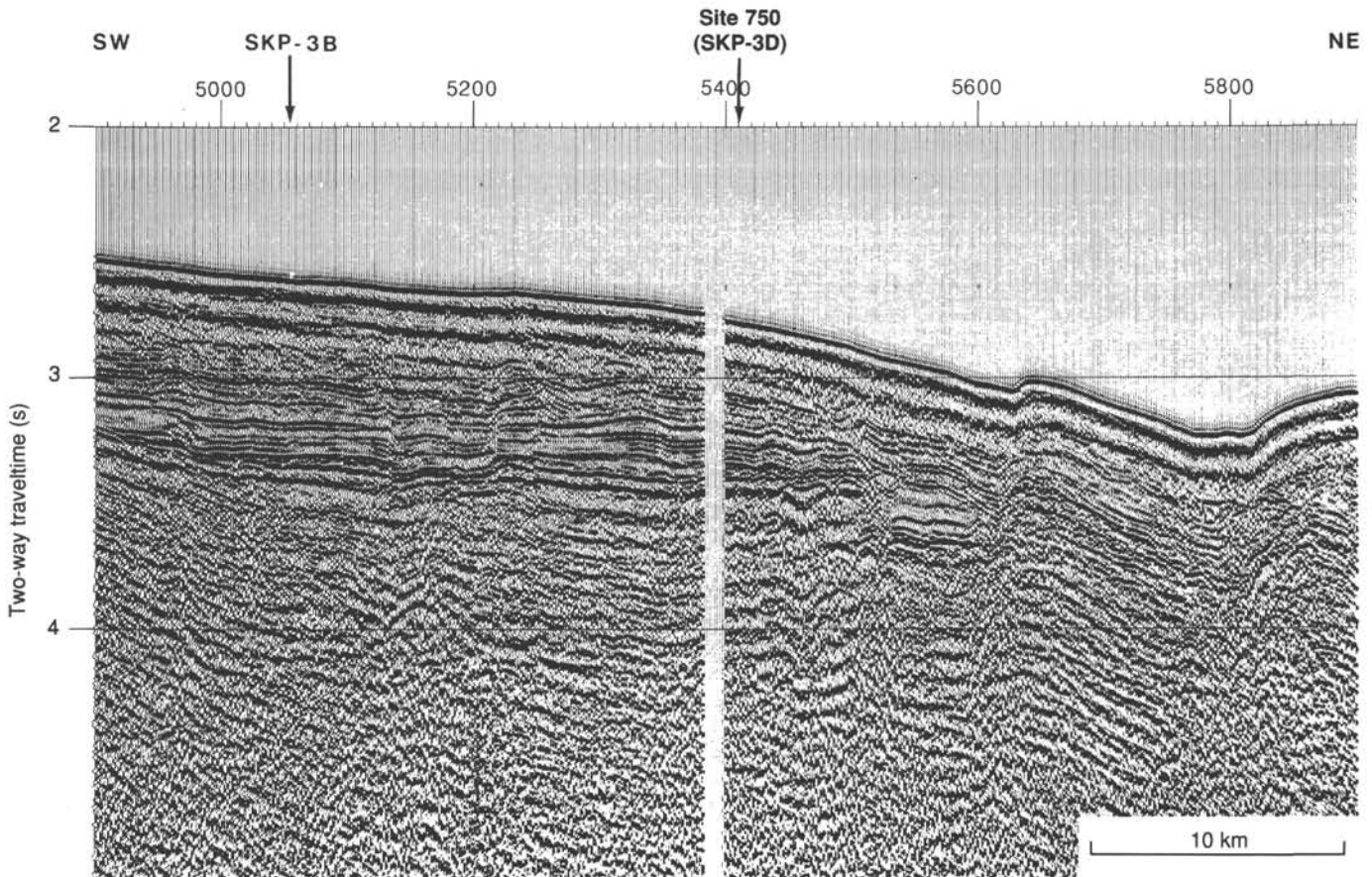


Figure 2. Seismic section RS02-24 (shot point 4900 to 5900) and location of sites SKP-3B and SKP-3D (Site 750).

After we had abandoned Site 749 due to a medical emergency and had spent 17.5 days in transit to return to the Kerguelen Plateau, we decided to use the remaining time to drill a second Paleogene-Mesozoic stratigraphic hole in the eastern Raggatt Basin rather than to reoccupy the deep basement site on the Banzare Bank (Site 749). This decision was based mainly on the results obtained at Site 748 and was taken to complete the stratigraphic and tectonic objectives related to the early history of the Kerguelen Plateau and the evolution of the Cretaceous climate. The Neogene paleoceanographic site (SKP-2C) in the central Raggatt Basin was considered a backup site.

Drilling Strategy

Due to severe time constraints, approval was requested to replace site SKP-3B, located on *Rig Seismic* line RS02-24 (97.1950, shot point 5055), with a new site SKP-3D (97.2127, shot point 5410) located on the same seismic line about 18 km to the east. All the sedimentary sequences observed at site SKP-3B can be traced at site SKP-3D, but the Paleogene sequence P1 thins by about 140 m between the two sites. The total sedimentary cover at this new site is about 910 m (i.e., about 120 m less than at the original proposed site SKP-3B), thus reducing the drilling time by almost 1 day (Fig. 2).

The drilling strategy planned for Site 750 included RCB operations (with reentry if necessary) to core the deeper part of the sedimentary section and to sample the basement. To achieve the objectives (basement and/or logging), the Paleogene and Cretaceous sections were not cored continuously; instead, only spot cores were to be taken at appropriate depths.

SITE GEOPHYSICS

JOIDES Resolution reached Fremantle, Australia, on 5 April 1988 in the early morning. The ship anchored at 0700 hr (Lt) 1.5 nmi from Rottneest Island and departed a few hours later at 1345 hr (Lt) after having completed the scheduled rendezvous (see "Operations" section, this chapter). The ship headed southwestward along a course of about 215°, changing progressively to 222°, and finally to 226°. Continuous magnetic recording started at 1650 hr (UTC) on 5 April 1988; bottom depth was not recorded due to a malfunction of the echo sounder and bad sea conditions. On 13 April 1988 at 2002 hr (UTC), the ship changed course to about 252° and headed toward Site 750 (proposed site SKP-3D).

Site 750, the second site to be drilled in the Raggatt Basin on the Southern Kerguelen Plateau, lies about 88 nmi northeast of Site 748 on *Rig Seismic* line RS02-24, time mark 97.2127, shot point 5410 (Fig. 1). *JOIDES Resolution* intersected the Australian survey profile (RS02-24) at about 2000 hr (UTC) on 13 April 1988. Just before reaching this point, the speed was reduced to 6–5 kt and the seismic profiling gear was deployed. The final site approach was made with global positioning satellite (GPS) navigation along a course of 252°, following *Rig Seismic* survey line (RS02-24) over a distance of about 12 nmi. A beacon was dropped on the initial crossing of the proposed site (SKP-3D).

The correlation of the *Rig Seismic* multichannel seismic reflection profile shot in 1985, with the *JOIDES Resolution* seismic data obtained over the site is excellent, and identification of the site location was unambiguous. The gear was retrieved at 2220 hr (UTC) on 13 April 1988, 5 min after passing the site, and the ship proceeded back to the beacon to commence drilling (Fig. 3). The final coordinates of Site 750 are 57°35.54'S and 81°14.42'E; the water depth as measured from the drill pipe (DPM) and corrected for height of the rig floor above sea level is 2030.5 m.

The sediment cover in the Raggatt Basin reaches 2500–3000 m and rests upon a weakly defined basement reflector. Interpre-

tation of the Australian and French multichannel seismic reflection profiles acquired in 1985 and 1986 over the Raggatt Basin identified seven distinct seismic sequences; these sequences can be grouped into two megasequences.

The upper megasequence is divided into three sequences (NQ1, PN1, and P2). Sequences NQ1 and PN1 are only observed in the central part of the Raggatt Basin and are truncated in all directions by toplap. Sequence P2 filled the relief of the lower megasequence by onlap.

The lower megasequence is divided into four sequences (P1, K3, K2, and K1). Sequences P1 and K3 are characterized by mounds that appear either as isolated features or in association with normal faults. The thickness of Sequence P1 remains fairly uniform in the basin whereas Sequence K3 shows significant variations in thickness. Sequences K2 and K1 filled up the center of the basin and disappeared in all directions by onlap. A major tectonic episode corresponding to normal faulting occurred at the boundary between Sequences K3 and P1; this event is related to the shift of the depocenter, which moves from west (K1, K2, and K3) to east (P1, P2, PN1, and NQ1).

Using all the available seismic data, an isochron map of the top of the acoustic basement (Fig. 4) and two isopach maps, one for the total sedimentary cover (Fig. 5) and one for the upper Sequences NQ1 and PN1 (Fig. 6), were drawn for the area close to the drill site. Site 750 is located on the eastern flank of the Raggatt Basin on a relatively shallow and flat basement high (Fig. 4) where the total sedimentary cover is less than 900 m (Fig. 5) and where the uppermost seismic sequences (NQ1 and PN1) are completely missing (Fig. 6). East of the site, a series of normal faults affect the basement structure, which slopes downward into the deep Labuan Basin. These faults are probably related to an uplift episode; their directions are not well constrained but seem to be parallel to the general northwest trend of the Southern Kerguelen Plateau's eastern margin.

The *JOIDES Resolution* survey line, shot with two 80-in.³ water guns and recorded with a 100-m hydrophone streamer, is shown on Figure 7. The similarity of this single channel seismic record with the Australian multichannel seismic reflection profile, which was used to locate Site 750, is obvious (Fig. 2). However, all the reflectors that are observed on the multichannel seismic line are not identifiable on the *JOIDES Resolution* survey line.

At Site 750 the basement reflector lies at about 0.69 s TWT below seafloor, and three major reflectors can be traced at 0.59, 0.46, and 0.31 s TWT below seafloor on the *Rig Seismic* multichannel seismic reflection profile. These reflectors correspond to the boundary between the different seismic sequences (K2/K3, K3/P1, and P1/P2) identified in the Raggatt Basin from seismic stratigraphic studies. The basement reflector at 0.69 s and the reflector at 0.46 s between K3 and P1 are visible on the *JOIDES Resolution* survey line, although it is almost impossible to scale the other reflectors observed on the multichannel seismic line. These reflectors are masked by the noise level and the bubble pulse of the source.

The correlation of the *Rig Seismic* and *JOIDES Resolution* seismic sections at Site 750 is shown on Figure 8. The vertical velocity distribution was estimated from sonobuoy experiments carried out in the Raggatt Basin during *Marion Dufresne* cruise 47 (1986) and from seismic reflection stack velocities. Considering these results, the basement was expected at 910 mbsf (0.69 s TWT), the K2/K3 boundary at about 745 mbsf (0.59 s TWT), the K3/P1 boundary at about 530 mbsf (0.46 s TWT), and the P2/P1 boundary at about 355 mbsf (0.31 s TWT).

Site 750 was drilled and partially cored down to a depth of 460.5 mbsf when the core bit failed after only 5–6 hr of rotating hours. The seismic stratigraphic logging combination was performed, and the ship left the site on 18 April 1988 at 0600 hr

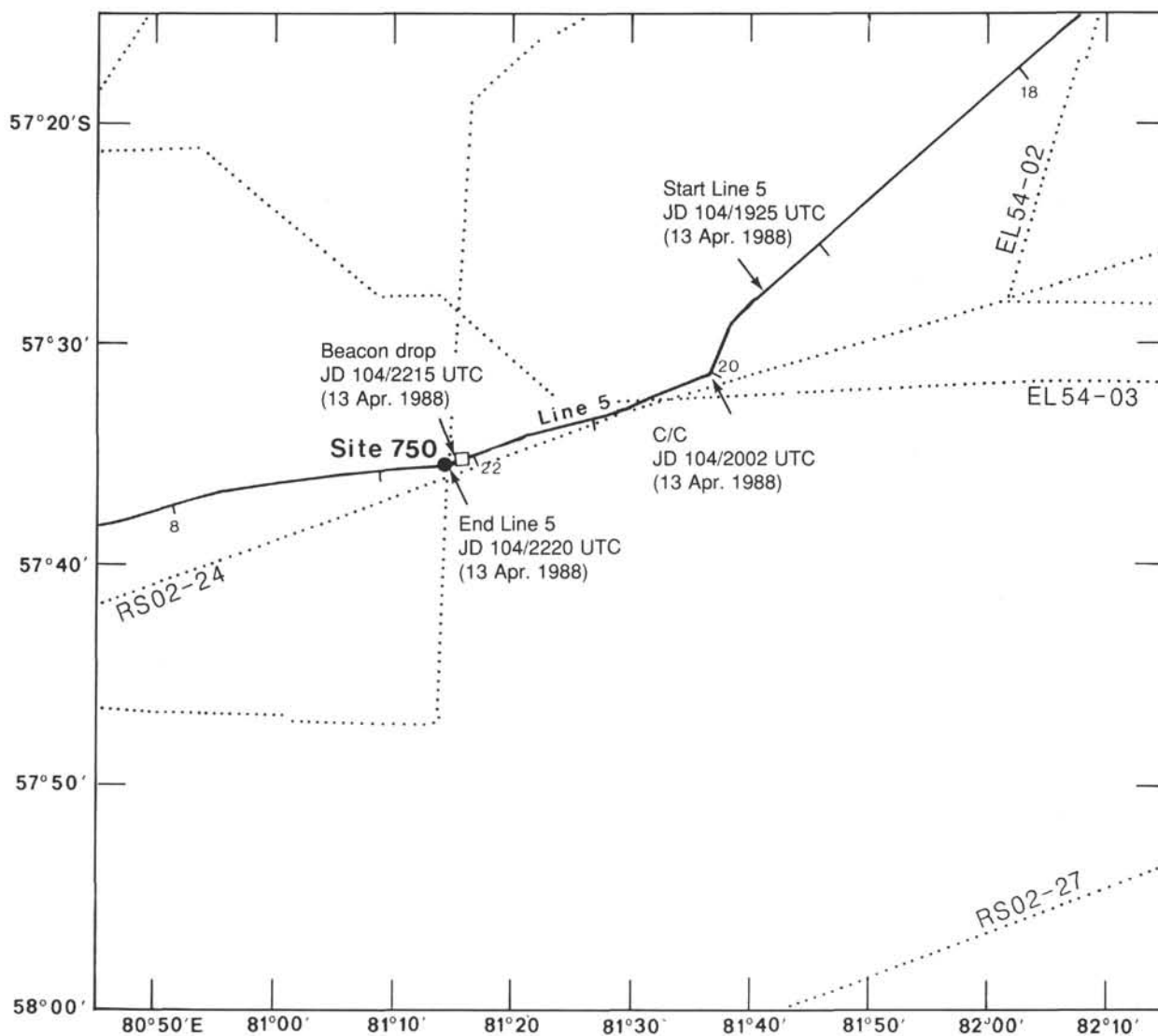


Figure 3. *JOIDES Resolution* site approach and Site 750 location.

(UTC) heading west toward Site 751 (see “Operations” section, this chapter).

Site 750 was reoccupied on 19 April 1988 at 2000 hr (UTC) without any complementary geophysical survey. Hole 750B was drilled to a depth of 450 m and then intermittently cored down to basement. Departure from Site 750 was on 22 April 1988 at 2000 hr (UTC); the magnetometer was deployed at 2030 hr (UTC), and the ship headed toward Fremantle along a course of 043°. Later, this course was slightly modified to provide a track complementary to those previously acquired during the leg.

OPERATIONS

Site 749 to Fremantle

Good speed was made the first 2 days with decreasing quartering winds and seas. On the third day, winds increased with gusts to 54 kt and combined waves to 20 ft. Minor wave damage was sustained in the port aft main deck area. After more winds to 50 kt and reduced visibility on 2 April 1988, favorable weather prevailed for the remainder of the transit to Fremantle. We maintained an average speed of 11.6 kt for the 2290-nmi voyage. At 0700 hr (local [L]), 5 April 1988, the vessel anchored in

the northern lee of Rottneest Island, about 12 nmi west of Fremantle.

Fremantle to Site 750

Arrangements had been made through the ship’s Fremantle agent for helicopter transportation. The helicopter arrived at 1130 hr with the agent and the ODP Relief Superintendent. The launch, delayed by the late arrival of supplies, arrived at 1300 hr (L). All transfers were made, and the anchor was weighed at 1345 hr (L) for the return to the Southern Kerguelen Plateau operating area.

After 3 days of good weather and transit speeds averaging over 12 kt, *JOIDES Resolution* entered the “roaring forties” on 8 April 1988. Rain squalls with wind gusts to 65 kt occurred with regularity for 3 days, and waves again caused minor damage—this time on the port wing of the bridge. The ship’s radio aircraft beacon and a small radio antenna were carried away. Shaft RPM had to be reduced to prevent overspeeding as the screws were lifted out of the water by the pitching of the vessel. Our average speed on 10 April 1988 was only 5.8 kt. Fortunately, the seas and swells (up to 35 and 25 ft, respectively) were fairly well aligned with the ship’s track, and vessel roll was limited to about 10°.

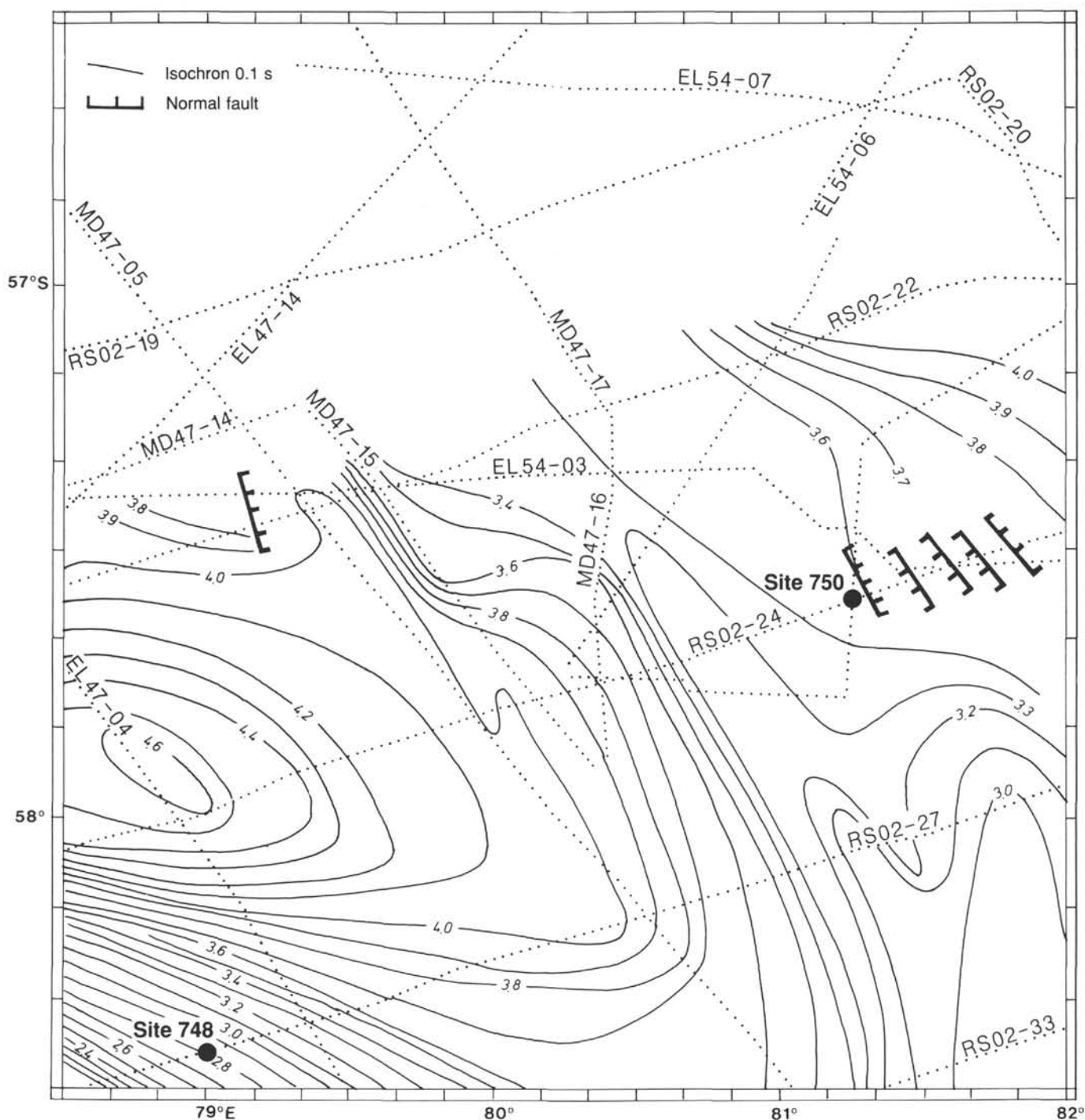


Figure 4. Isochron map of the top of the acoustic basement contoured in seconds (TWT).

The weather improved dramatically on 11 April 1988, and good speed was made for the remainder of the transit with increasing following winds. On 13 April the barometer began to fall from 1018 mbar. It reached 962 mbar 24 hr later, bottoming out just as the beacon was launched at Site 750 at 2215 hr (UTC), 13 April 1988 (0615 hr L, 14 April 1988).

Site 750 (SKP-3D)

Hole 750A

We dropped the beacon on our first pass after a direct approach from the northeast along the reference seismic line. Winds were gusting to 47 kt as the rig was positioned. They increased

to 60 kt during the pipe trip, and the barometer resumed its descent by spud time.

A seafloor "punch core" was taken, and seafloor depth was determined to be 2041.0 m. The hole was drilled ahead with "spot" cores taken at 56, 143, and 259 mbsf. Meanwhile, the barometer had reached 949 mbar, and combined sea and swell had built to 13–14 m. The roll limitation of the SEDCO Marine Operations Manual had been reached, and it was necessary to suspend coring operations at 298 mbsf to "Wait on Weather" (WOW).

During the 24-hr weather delay, the wind gusted to 65 kt in snow squalls, generating vessel roll to 15°. Continuous coring resumed on the morning of 16 April 1988. Vessel roll was within

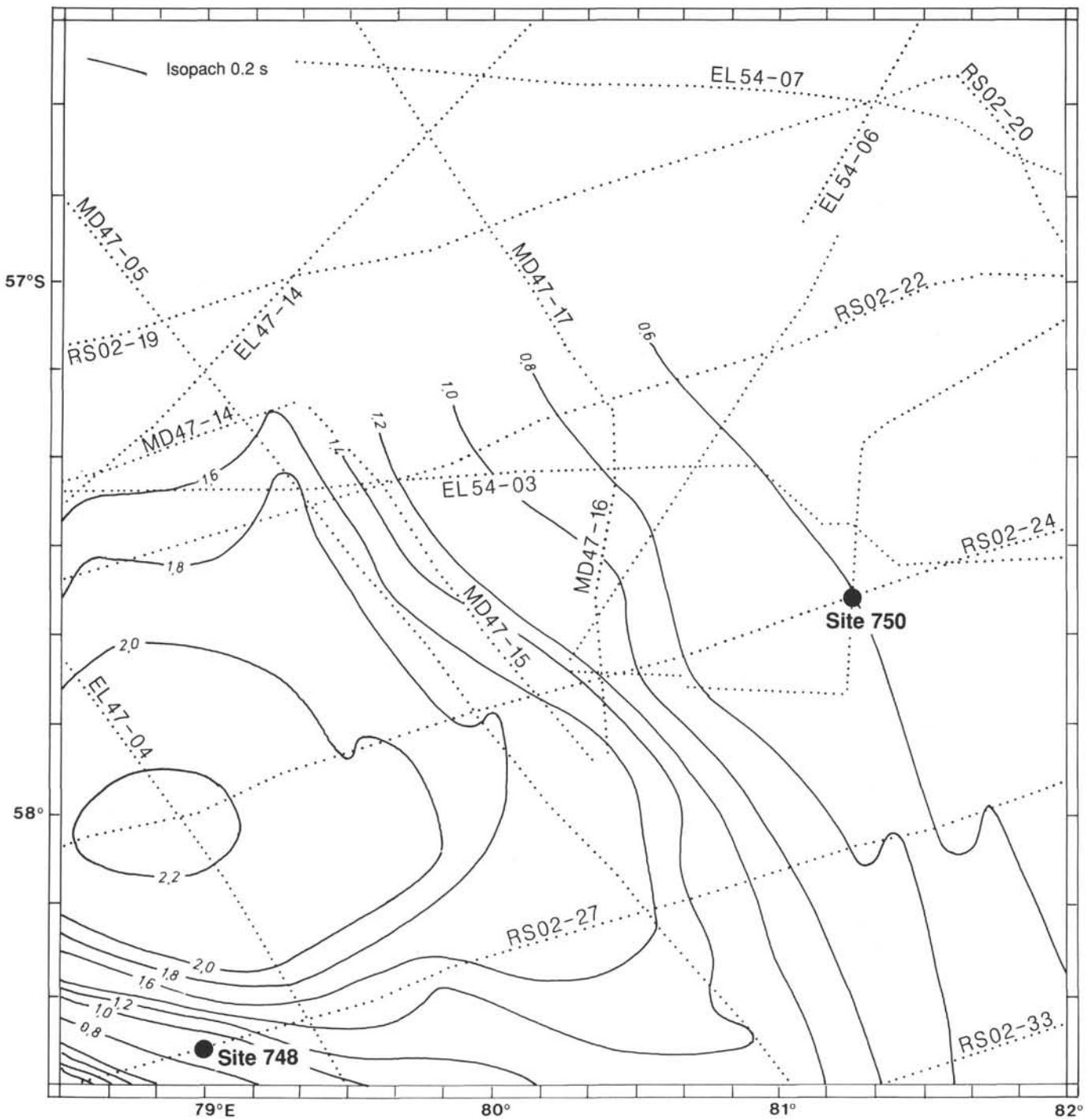


Figure 5. Total sediment isopach map contoured in seconds of reflection time (TWT).

limits, but heave (compensator stroke) occasionally bumped the 12-ft operating limit as coring continued. The drill-string motion compensator was increasingly unable to cope with the rapid heave motion associated with the confused sea state. The resulting violent motion of the drill string caused weight indicator fluctuations of 60,000 lb or more during the drilling operation, most of which is assumed to have been transmitted to the bit.

Sediments graded from a near-liquid ooze to soft chalk with depth. Scattered thin beds and nodules of chert became a factor below about 200 mbsf. They did not slow the drilling appreciably or cause hole problems, but the chert had its usual adverse

effect on core recovery. (The Cretaceous/Tertiary boundary was recovered intact, although incomplete, in Core 120-750A-15R from about 348 mbsf.) The first firm limestone beds were encountered around 447 mbsf.

Drilling became extremely rough as soon as hard material was hit. The high torque was attributed to the excessive heave, change of formation, and/or large chert fragments in the hole. Drilling torque eventually decreased, but the rate of penetration (ROP) went nearly to zero while the heave compensator motion became increasingly erratic. The inner core barrel was recovered at 460.5 mbsf after 3.2 m of penetration beyond the previous

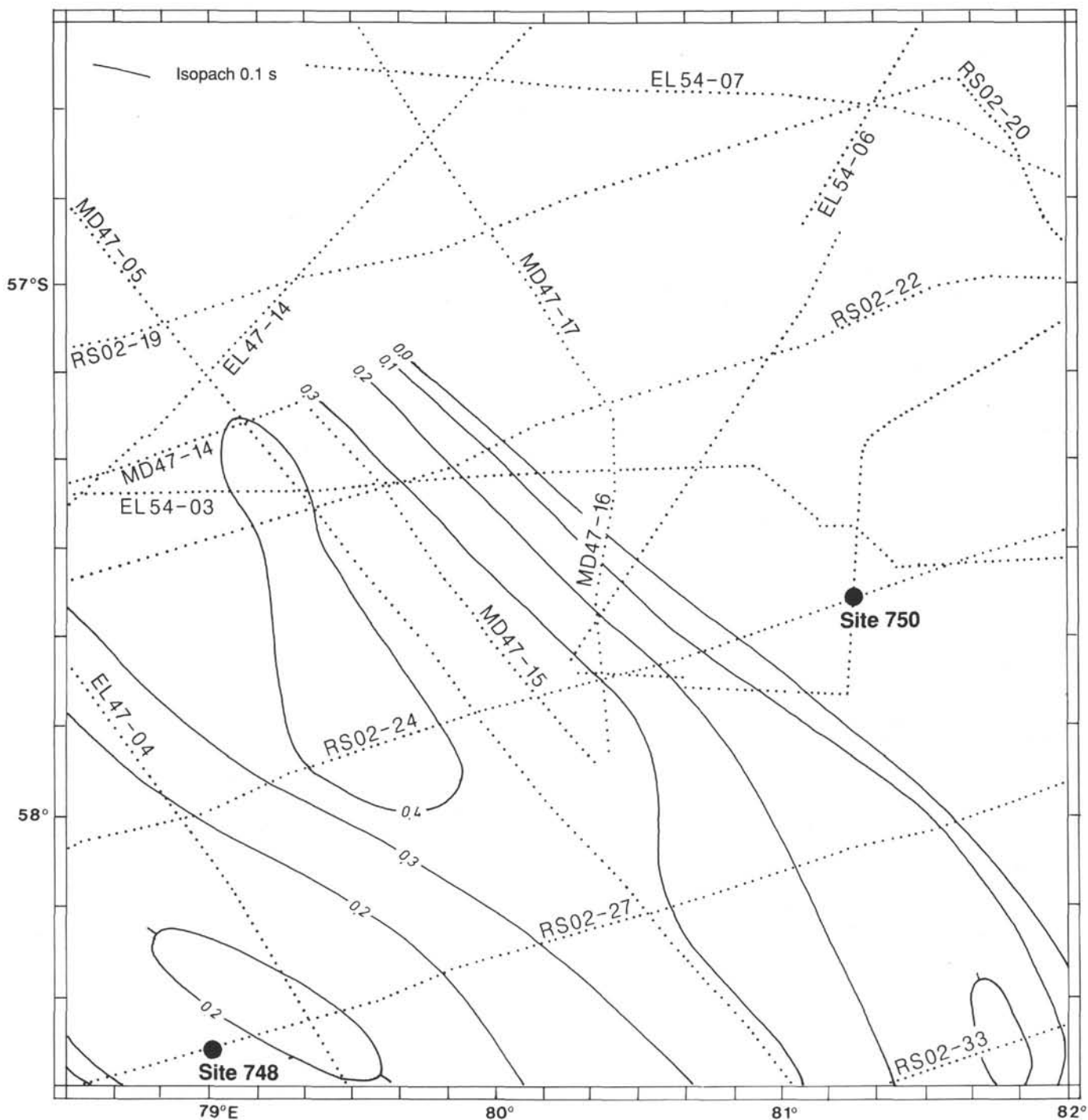


Figure 6. NQ1 and PN1 isopach map contoured in seconds of reflection time (TWT).

core. There was no core recovery, and the core-catcher sub was severely damaged, obviously from junk in the hole. The core bit had failed after only about 5½ rotating hr.

With the hole junked, free-fall funnel (FFF) deployment and reentry were out of the question. The hole was deep enough to require logging, so it was filled with weighted mud and the bit was released for logging. With the pipe at logging depth, the seismic stratigraphy tools were rigged and started down the pipe. The induction cartridge failed early, and the combination tool was recovered for a replacement cartridge. Open-hole conditions were surprisingly good, with two minor bridges at shallow

depth. The tool then went to fill about 8 m off TD, and a good log was recorded up to about 51 mbsf.

The wireline heave compensator was used for the early stages of logging. It functioned well until high heaves exceeded its maximum stroke. Operations became erratic for a period of time after the stroke limit had been reached. A lithodensity log was attempted as the second log run. The excentralizer springs dragging in the drill pipe caused considerable difficulty and time delay in getting the tool to move down the pipe and required 3 hr to run 2100 m, which was exacerbated by the strong surge from the vessel heave. The tool functioned well until it ex-

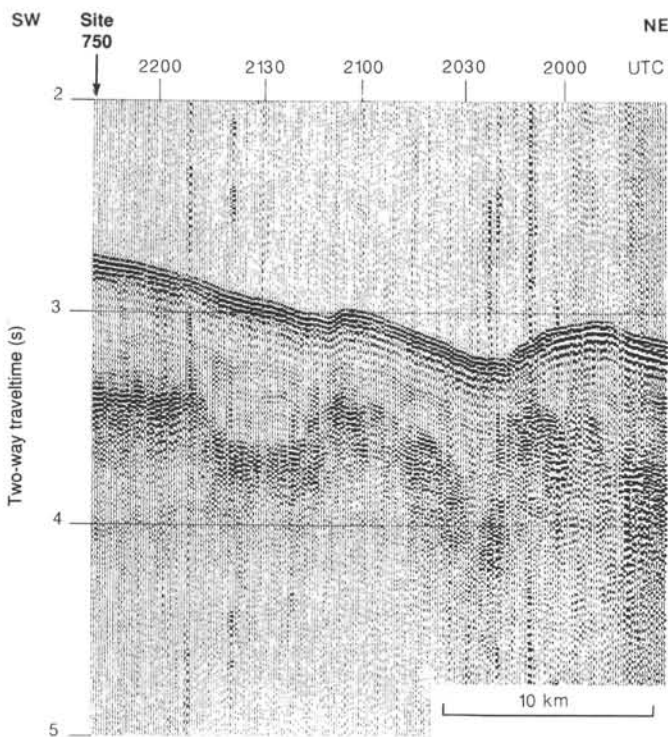


Figure 7. *JOIDES Resolution* single-channel reflection profile on approach to Site 750.

ited the pipe into the open hole. At that point, it failed electrically due to a damaged "pigtail" cable at the cable head, which was the result of forcing the tool down the pipe with the cable. In retrospect, it appears that pumping the tool down faster, adding weight via sinker bars, and taping the bow and excenterizer springs partially down would have expedited running the tool, although there would have been greater risk to the sonde.

Budgeted time had run out; the logging tools were rigged down, the pipe was recovered, and the vessel departed for prospective Site SKP-2C with the goal of achieving the remaining scientific objectives of highest priority.

Hole 750B

The return to the Site 750 beacon from Site 751 required just 4½ hr. With GPS navigation and fairly good weather conditions, the acoustic signal was detected without difficulty. The pipe trip began as soon as thrusters and hydrophones had been lowered, and Hole 750B was spudded at 1100 hr (L), 20 April 1988.

The upper 450 m of the section was drilled in only 10 hr with a core barrel in place. The barrel was pulled once, at 300 mbsf, to check the condition and function of the coring system. The opportunity was used to take a multishot measurement of hole deviation (1°). The procedure was repeated at 450 mbsf.

Because of the limitations on operating time, permission had been obtained to drill through the Cretaceous section by cutting as much as three times the normal interval each time before the inner barrel was recovered. The operation thus continued with "wash cores" of 19 and 28 m interspersed with "real" core intervals of about 9.5 m. Since Hole 750A had bottomed at the top of the indurated limestone section, the coring ROP was slower as penetration continued in firm chalk and limestone with intercalated chert. The average ROP exceeded 20 m/hr, however, which is an excellent rate for the lithology.

Core recovery, as expected, was poor due to the presence of chert nodules and irregular fragments of siliceous limestone. The normally high pump pressures were reduced over the last 5 m of each washed interval in order to enhance core recovery. At about 590 mbsf, the drilling rate dropped to about 6 m/hr, and hopes of reaching basement in the allotted time began to dim.

The reason for the drastic slowdown was clear when the core barrel was recovered. The limestone and chalk had given way to dark brown claystone. A hard formation bit (C-7) had been selected for the anticipated chert, limestone, and basalt. The bit was poorly suited for drilling the claystone with its low compressive strength. The first hole problems developed soon after the claystone was encountered, with several meters of fill accumulating in the hole during retrieval of the core barrels or when connections were made. On two occasions it was difficult to "wash" back to TD through the fill. Nevertheless, we were cautiously optimistic when the lower measured sound velocity of the claystone resulted in a revision of the estimated basement depth to a shallower figure.

Fortunately, the difficult, but scientifically interesting claystone unit was only a little over 80 m thick; and the drilling target (basaltic basement) was encountered according to drilling records at 675.5 mbsf. With the bit back in its element, the massive basalt flows were cored at an average rate of 4.2 m/hr, almost as fast as in the much softer clays above. Four basalt cores were cut before operating time ran out, with the average core recovery exceeding 60%.

No time remained for logging and, because the hole had reached igneous basement, there was no requirement to fill or plug the hole. The drill string was recovered immediately after the arrival of the final core on deck, and the bottom hole assembly (BHA) was disassembled for transit. *JOIDES Resolution* departed for Fremantle, Australia, at 0400 hr (L), 23 April 1988.

The coring summary for Site 750 appears in Table 1.

LITHOSTRATIGRAPHY AND SEDIMENTOLOGY

Introduction

Site 750 was located in 2030.5 m of water on the eastern margin of the Raggatt Basin (57°35.54' S, 81°14.42' E) with a sediment thickness estimated at over 800 m. This site was chosen to optimize severe time constraints by employing a wash-core program. It was designed to calibrate seismic stratigraphy and test whether the Cretaceous facies would be open pelagic similar to Site 747, or another restricted margin type as encountered at Site 748. Hole 750A was first drilled with a single rotary bit, spot cored to 297.8 m, and then continuously cored through a Paleocene to Campanian sequence.

Basement objectives were initially defeated by an apparent failure of the bit around 410 mbsf, followed by poor recovery and termination of the hole at 460 mbsf. After drilling nearby Site 751, we returned to Site 750 so that we could use the remaining leg time to rotary core Hole 750B with a single bit and to penetrate as much Cretaceous sediment as possible. We proceeded with a one-for-three wash-core program that provided reasonable recovery by slowing circulation while cutting the last few meters. Hole 750B was washed directly to 450 mbsf; then one-for-three wash cored. Washing imparts considerable uncertainty to the placement of lithologic boundaries, although logging of Hole 750A helped.

The sediment lithology at Site 750 comprises 675.5 m of mainly pelagic nannofossil ooze and chalk with some chert in both Eocene and Upper Cretaceous cherts. The Upper Cretaceous cherts show similarities with those at Site 747, but without evidence of volcanoclastic debris flows. The Cenozoic section differs from previous sites by having an expanded Paleo-

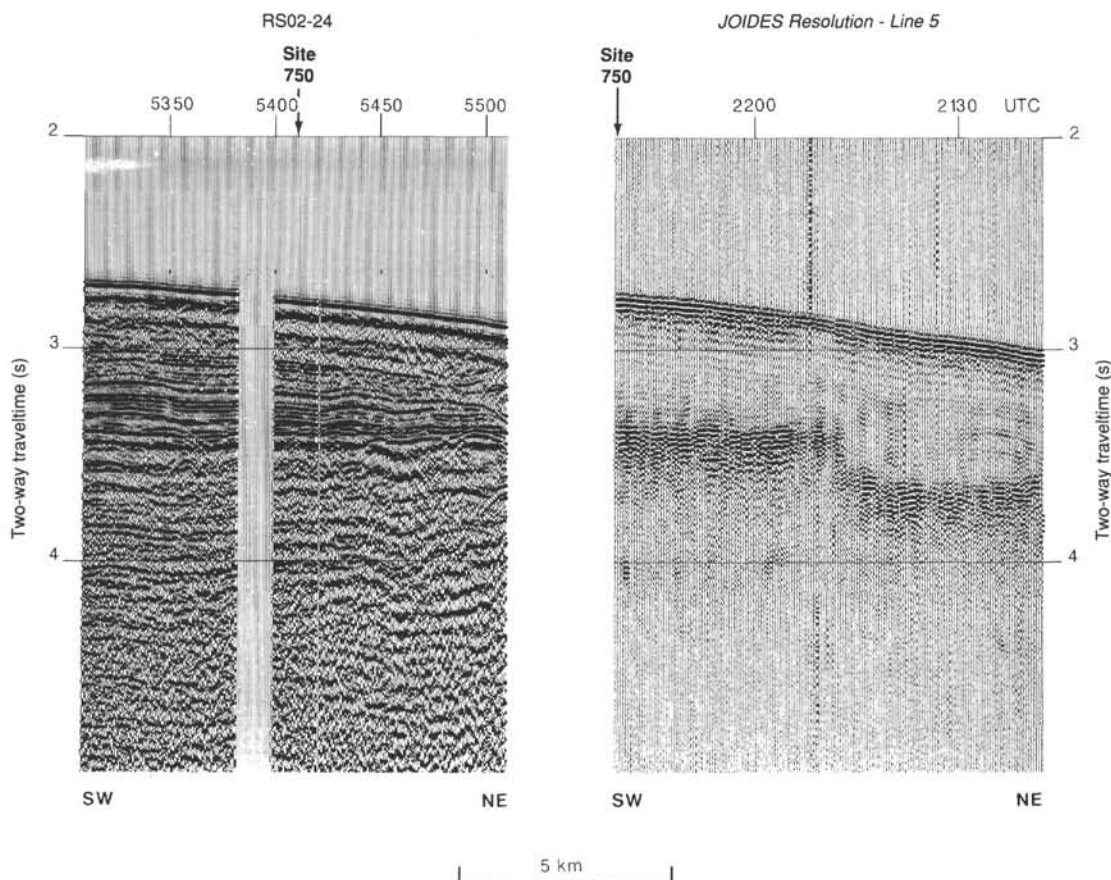


Figure 8. Comparison of the *Rig Seismic* multichannel seismic reflection profile and the *JOIDES Resolution* single-channel survey line in the vicinity of Site 750.

cene chalk section and less middle Eocene chert than at Sites 749 and 748.

Hole 750B provided unexpected discoveries. Beneath a thick upper Campanian sequence of intermittently silicified, light greenish gray pelagic chalks to limestone, we encountered softer Santonian to Turonian chalk with dark marl bands. The lithology then changed abruptly to Albian earthy red-brown ferruginous, kaolinitic claystones, rich in coaly fragments and yielding very low seismic velocities. Basement rose to the occasion, and basalt was surprisingly reached at only 675.5 mbsf. Coring in Hole 750B stopped at 709.7 mbsf after coring 34.2 m of moderately altered basalt with excellent recovery.

We separated the lithology into four main sedimentary units in order to provide a consistent basis of correlation with the other Kerguelen Plateau sites (Fig. 2). The first unit is very thin and merely comprises a lag deposit along with elements of brownish lower Pleistocene to mid-Pliocene sandy diatom ooze with foraminifers. The second unit, with long wash intervals, encompasses white, middle Eocene chalky nannofossil ooze, poorly recovered chalk, and brownish cherts as Subunit IIA, and well-recovered white Paleocene chalk as Subunit IIB. The base of Unit II is below a greenish claystone marking the Cretaceous/Tertiary contact in Section 120-750A-15R-3.

The third unit also comprises mainly pale pelagic nannofossil chalks, but these have an overall different character from those of Unit II, including more seams, darker interbeds, silicification, and cherts. Three subunits are distinguished: Subunit IIIA composed of white Maestrichtian nannofossil chalk with minor dark gray chert stringers and seams; Subunit IIIB composed of pale greenish gray burrowed Campanian chalks with pervasively silici-

fied intervals; and Subunit IIIC composed of Santonian-Turonian calcareous chalks without major silicification and with distinctive dark gray interbeds displaying abundant trace fossils.

Unit IV comprises the red-brown silty claystones with abundant land-derived organic matter.

The lithostratigraphy is given in Figure 9 and Table 2. Figure 10 and Table 3 summarize downhole grain-size trends showing the overall dominance of silty nannofossil components. Figure 10 also summarizes smear slide description trends, leaving out the long washed interval. This graph clearly shows the dominance of nannofossil components and suggests micritic lithification below 390 m. Chert abundance is not reflected.

Unit I: Diatom Ooze and Lag Deposits

Interval: Cores 120-750A-1R-1, 0–37 cm, and 120-750A-1R-6.

Depth: 0–0.37 mbsf.

Thickness: 37 cm (see text).

Age: early Pleistocene to mid-Pliocene.

Unit I has distinctive features similar to Unit I of Site 749. It is only 37 cm thick, but it is an important section with diatoms and foraminifers of early Pleistocene and mid-Pliocene age (see “Biostratigraphy” section, this chapter). It comprises a pale olive (5Y 6/4) diatom ooze with foraminifers sandwiched between gravel- to sand-size material. Bioturbation is minor, with some large, centimeter-scale vertical burrows filled with diatom-enriched nannofossil ooze. Smear slides indicate minor amounts of nannofossils, radiolarians, and some sponge spicules and silicoflagellates.

Diatom oozes were sandwiched between two polygenic lag deposits (early Pleistocene and mid-Pliocene) that include

Table 1. Coring summary, Site 750.

Core no.	Date (April 1988)	Time (local)	Depth (mbsf)	Cored (m)	Recovered (m)	Recovery (%)
120-750A-						
1R	14	1830	0-7.9	7.9	7.77	98.3
2W	14	2100	7.9-56.4	48.5	0.25	(wash core)
3R	14	2150	56.4-65.4	9.0	8.61	95.6
4W	15	0150	65.4-143.3	77.9	0.15	(wash core)
5R	15	0215	143.3-153.0	9.7	0	0
6R	15	0320	153.0-162.6	9.6	0.15	1.6
7W	15	0710	162.6-259.2	96.6	0.85	(wash core)
8R	15	0755	259.2-268.9	9.7	0.64	6.6
9W	15	1140	268.9-297.8	28.9	0.34	(wash core)
10R	16	1105	297.8-307.5	9.7	4.00	41.2
11R	16	1200	307.5-317.2	9.7	2.52	26.0
12R	16	1245	317.2-326.8	9.6	5.52	57.5
13R	16	1335	326.8-336.5	9.7	5.20	53.6
14R	16	1415	336.5-346.1	9.6	5.70	59.4
15R	16	1450	346.1-355.8	9.7	4.26	43.9
16R	16	1525	355.8-365.3	9.5	5.02	52.8
17R	16	1605	365.3-375.0	9.7	3.58	36.9
18R	16	1710	375.0-384.7	9.7	2.29	23.6
19R	16	1820	384.7-394.4	9.7	3.56	36.7
20R	16	1900	394.4-404.0	9.6	6.96	72.5
21R	16	1940	404.0-413.6	9.6	1.30	13.5
22R	16	2020	413.6-423.3	9.7	0.88	9.1
23W	16	2120	423.3-442.6	19.3	0.29	(wash core)
24R	16	2215	442.6-452.3	9.7	0.22	2.3
25R	16	2320	452.3-457.3	5.0	0.45	9.0
26R	17	0415	457.3-460.5	3.2	0	0
Coring totals				189.3	68.63	36.3
Washing totals				271.2	1.88	
Combined totals				460.5	70.51	
120-750B-						
1W	20	1650	0-299.0	299.0	0.57	(wash core)
2W	20	2100	299.0-450.0	151.0	0.32	(wash core)
3R	20	2235	450.0-459.6	9.6	0.94	9.8
4W	21	0110	459.6-478.9	19.3	3.56	(wash core)
5R	21	0200	478.9-488.5	9.6	0.56	5.8
6W	21	0320	488.5-507.9	19.4	2.09	(wash core)
7W	21	0515	507.9-527.3	19.4	2.63	(wash core)
8W	21	0710	527.3-546.7	19.4	1.96	(wash core)
9W	21	0955	546.7-566.0	19.3	2.45	(wash core)
10W	21	1330	566.0-594.6	28.6	1.19	(wash core)
11W	21	1635	594.6-623.5	28.9	2.88	(wash core)
12W	21	2145	623.5-642.8	20.3	4.23	(wash core)
13W	22	0615	642.8-671.5	27.7	3.95	(wash core)
14R	22	0950	671.5-681.2	9.7	2.04	21.0
15R	22	1250	681.2-690.5	9.3	8.40	90.3
16R	22	1605	690.5-700.2	9.7	9.69	99.9
17R	22	2010	700.2-709.7	9.5	2.97	31.2
Coring totals				57.4	24.60	42.9
Washing totals				652.3	25.83	
Combined totals				709.7	50.43	

rounded to subrounded clasts up to several centimeters in diameter of diverse igneous, metamorphic, and sedimentary affinities, most with manganese coatings (see Fig. 11). Fine to coarse sand fractions include clear subrounded quartz, feldspar, volcanic glass, amphiboles, and various other manganese-coated grains. Soft manganese nodules and other fragments were recovered from downhole cavings at the tops of several cores. These cavings augment the information on types of larger components. Ice rafting probably originally carried most of these pebbles to the site of deposition, where they were concentrated by winnowing and/or dissolution of biogenic particles. Ice-rafted and lag pebble lithologies are summarized in Table 4.

The sedimentary sequence is complicated in Core 120-750A-1R because of an apparent double punch at the mud line, which repeated Unit I in Sections 120-750A-1R-1 and 120-750A-1R-6

(Fig. 11). We chose to ignore this duplication and instead apply a realistic boundary in the assignment of unit designations.

Lag deposits unconformably overlie pure white middle Eocene chalky ooze, and together they signal a rather extensive Neogene period of erosion and slowed sedimentation.

Unit II: Nannofossil Ooze, Chalk, and Chert

Interval: Cores 120-750A-1R-1, 37 cm, to 120-750A-15R-3, 91.5 cm.

Depth: 0.37-357.0 mbsf.

Thickness: 356.6 m.

Age: middle Eocene to early Paleocene.

Subunit IIA: White Nannofossil Ooze to Chalk and Chert

Interval: Cores 120-750A-1R, 37 cm, to 120-750A-12R-1, 1 cm.

Depth: 0.37-317.2 mbsf.

Thickness: 316.8 m.

Age: middle Eocene to late Paleocene.

Nannofossil ooze in Subunit IIA (Core 120-750A-3R), although drilling disturbed, appears generally quite uniform and whiter than 2.5Y 8/1 or N8. There is no visible bioturbation, mottling, or other sedimentary structures except a sporadic pale yellow splotch (Core 120-750A-3R-1, 112 cm). The ooze has characteristically more than 85%-90% nannofossils, with ubiquitous foraminifers. Tan or yellow mottles show more foraminifers (e.g., Core 120-750A-3R-2, 65 cm) and traces of sponge spicules and radiolarians.

Lower Eocene chert was encountered at about 220 mbsf in drilling the wash interval (Core 120-750A-7W). Recovery was poor, but drilling speed suggests that the layers were not as thick or abundant as at Site 749. Logging results suggest localized zones with cherty layers around 250 and 285 mbsf. The chert varieties include: (1) massive olive to dark yellowish brown, saw-proof, translucent, conchoidal fragments; (2) brown chert; (3) smaller olive fragments with mantles of white porcellanite; (4) dark gray chert with a white patina; and (5) light gray porcellanite and chert. Cherts occur in the top of Cores 120-750A-12R to -15R, but they are thought to represent cavings because drilling and logging suggest that no further Cenozoic chert beds were encountered below about 312 mbsf.

Nannofossil chalk (>90% coccoliths) encountered to 317 mbsf is mostly pure white, N8, without visible structures but rarely displays faint, pelagic-realm burrows of *Planolites* and *Zoophycos*. Brown chert in Core 120-750A-11R-2, 64-68 cm, apparently occurs *in situ*, so the base of Subunit IIA is drawn at the top of Core 120-750A-12R.

Subunit IIB: White Nannofossil Chalk

Interval: Cores 120-750A-12R, 1 cm, to 120-750A-15R-3, 91.5 cm.

Depth: 317.2-357.0 mbsf.

Thickness: 39.8 m.

Age: early Paleocene.

Upon recovering material that could be split using the saw, we recognized the first thin zones with crosscutting gray seams in Paleocene chalk in Core 120-750A-12R-1, 147-151 cm (see Fig. 12). These appear to be dissolution seams that cut the chalk into wispy lenses. Foraminifer tests are more fragmented, and nannofossils more disaggregated. Concomitantly, we noted a few pyrite-lined burrows and splotches. Core 120-750A-13R-3, 25-100 cm, contains a bed of darker hue, with evidence of dissolution or compaction seams.

Thin submillimeter seams rarely occur in Core 120-750A-14R-2, 51 cm. Smear slides show higher foraminifer abundance (4%-7%), partly as a result of more fragmentation and debris. Chalk is very fine grained, reflecting the small sizes of Danian nannofossils. Thoracospheres and tiny one-chamber forami-

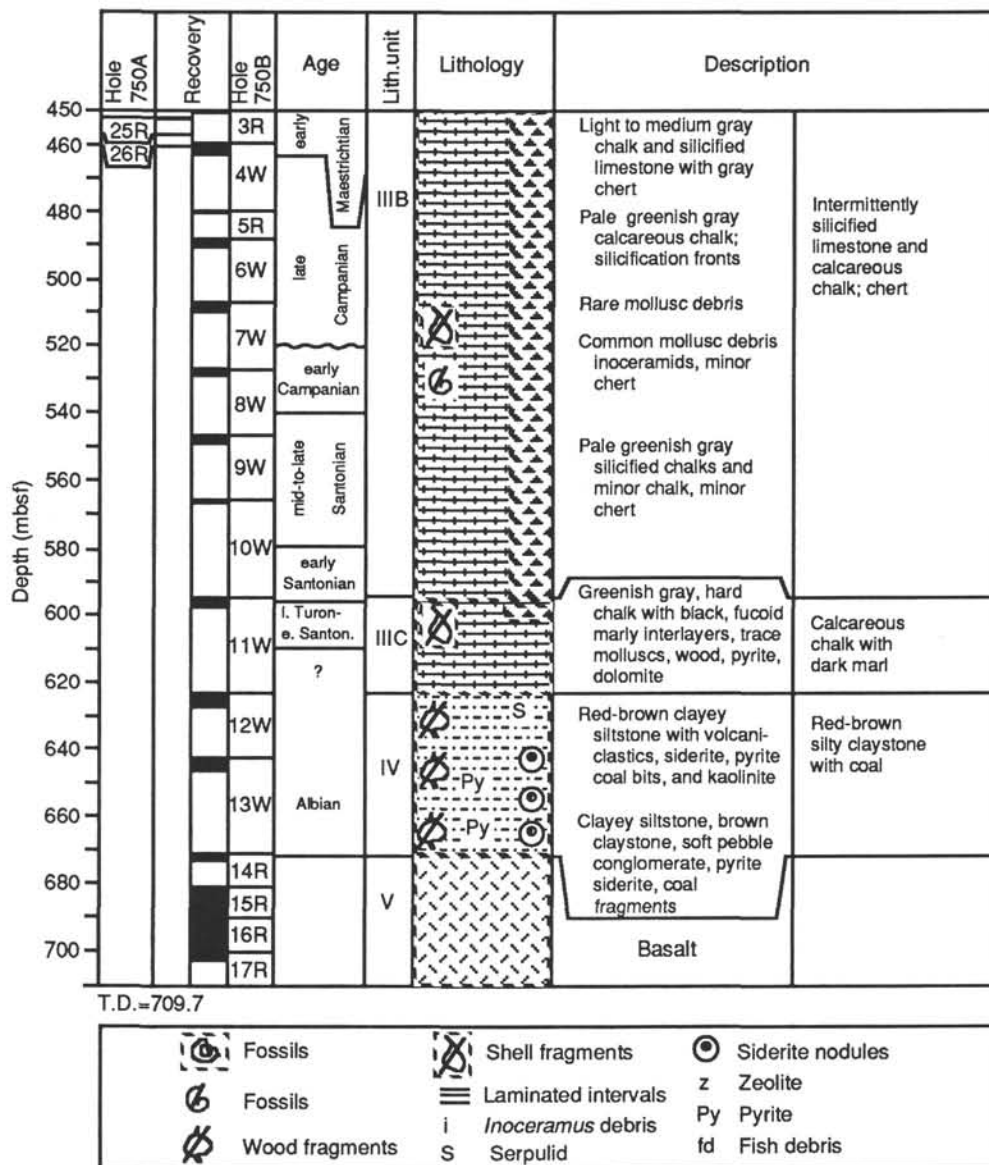


Figure 9 (continued).

fers appear as minor constituents. Both benthic and planktonic foraminifers occur with about equal abundance.

Cretaceous/Tertiary Boundary Lithology

The Cretaceous/Tertiary contact is lithologically distinct at Site 750, and forms the base of Unit II in Section 120-750A-15R-3, 91.5 cm. Core 120-750A-15R begins as uniform white nannofossil chalk. From Core 120-750A-15R-3, 20-91.5 cm, there is a conspicuously gradational bed of relatively undisturbed nannofossil chalk that darkens downward from light (N8) to darker olive gray (5Y 5/2) as clay increases, and shows a plethora of flattened burrows and seams. Dark specks that occur near the top of the bed are richer in foraminifers.

The actual Cretaceous/Tertiary boundary occurs below this bed, but the contact is disturbed by drilling that brought a pure white Maestrichtian nannofossil chalk into abrupt juxtaposition (Fig. 13). A few bits of chert drill-breccia have been drawn into the contact zone, probably by bit-twisting of the core (Fig. 13). The more clay-rich lower Danian section shows up as a positive

excursion on the resistivity logs (see "Logging" section, this chapter), so we can locate the base of Subunit IIB at 357 mbsf.

Unit III: Nannofossil Chalk to Silicified Limestone

Interval: Core 120-750A-15R-3, 91.5 cm, to the top of Core 120-750B-12W.

Depth: 357.0-623.5 mbsf.

Thickness: 266.5 m.

Age: late Maestrichtian to late Turonian.

Subunit IIIA: Nannofossil Chalk and Chert

Interval: Cores 120-750A-15R-3, 91.5 cm, to 120-750A-25R-1, 45 cm, and top of Core 120-750B-3R.

Depth: 357.0-450.0 mbsf. (The thickness is based on the logging pick for the Cretaceous/Tertiary boundary and the Core 120-785B-3R overlap, which recovered silicified chalk. Recovery in Cores 120-750A-21R to -26R was inadequate for the definition of a precise core depth.)

Thickness: 93.0 m.

Age: late Maestrichtian to early Maestrichtian.

Table 2. Summary of dominant lithologic units at Site 750.

Unit and subunit	Lithology	Features	Depth (mbsf)	Core interval	Thickness (m)	Age
I	Diatom ooze and lag deposits	Two lag beds	0–0.37	120-750A-1R-1, 0–37 cm, and 120-750A-1R-6	0.37	Early Pleistocene to mid-Pliocene
IIA	White nannofossil ooze to chalk and chert	Poorly recovered	0.37–317.2	120-750A-1R, 37 cm, to 120-750A-12R-1, 1 cm	316.8	Middle Eocene to late Paleocene
IIB	White nannofossil chalk		317.2–357.0	120-750A-12R, 1 cm, to 120-750A-15R-3, 91.5 cm	39.8	Early Paleocene
IIIA	Nannofossil chalk and chert	White to pale green with chert	357.0–450.0	120-750A-15R-3, 91.5 cm, to 120-750A-25R-1, 45 cm	93.0	Late Maestrichtian to early Maestrichtian
IIIB	Intermittently silicified limestone and calcareous chalk	Light green gray with chert	450.0–594.6	120-750B-3R-1, 0 cm, to 120-750B-11W, 0 cm	144.6	Early Maestrichtian to early Santonian
IIIC	Calcareous chalk with dark marl	Dark fucoid bands, traces of molluscs, wood, inoceramids	594.6–623.5	120-750B-11W-1, 0 cm, to 120-750B-12W-1, 0 cm	30.1	Early Santonian to late Turonian
IV	Red-brown silty claystone with coal	Siderite, pyrite, volcanic detritus, kaolinite	623.5–675.5	120-750B-12W-1, 0 cm, to 120-750B-14R-1, 23 cm	52.0	Albian
V	Basalt		Below 675.5 TD 709.7	120-750B-14R-1, 23 cm, to 120-750B-17R-6	34.2	?

Note: See text for discussion of Subunit IIIA thickness and boundary placement.

Subunit IIIA is mainly a white nannofossil chalk with minor nodular fragments or thin stringers of black chert. Although solution seams were encountered in Subunit IIB, they become a characteristic feature along with burrows, laminae, rare stylolites, and increased lithification. Just below the contact, prominent crosscutting seams occur at Intervals 120-750A-15R-3, 98, 110, 114, and 119 cm. Zones with seams alternate with sections of uniform white. The chalk is quite soft and porous. Cut surfaces are grainier, which reflects the dominance (>90%) of larger and more irregular nannofossils of the Cretaceous as well as common foraminifers. Both planktonic and benthic foraminifers occur. Smear slides show the occurrence of some foraminifer-sized calcareous capsules (calcispheres) and a trace, but persistent, component of echinoid spines as well as a few other rare calcareous fragments.

The first *in-situ* cherts in Subunit IIIA occur below 375 m as broken, dark to light gray fragments in Core 120-750A-17R-1, 58–70 cm, and 120-750A-18R-1, 30–50 cm, and as minor fragments in cores below. Some pieces have a porcellanite patina or show lighter burrow relicts.

In Core 120-750A-19R, we encountered the first rare but well-developed, light greenish gray laminae, as well as greasy purple-black pyritic swirls, outlines, and laminae. The latter contain pyritic fragments of what may have been molds of radiolarians or sponge spicules. Coarser intervals occur that have a slightly greater abundance of calcareous fragments. A brachiopod shell, possibly silicified, occurred in Core 120-750A-19R-1, 67 cm.

Solution seams are particularly common from Core 120-750A-17R downward with other types of laminae occurring as well. Three parallel greenish gray, millimeter laminae in Core 120-750A-17R-3, 19 cm, were dissolved in HCl and examined. These proved to contain more than 50% clinoptilolite(?) type, 10- μ m, ragged zeolite prisms in the residue along with a low birefringent clay and minor ferruginous debris. It is unclear whether these derived from volcanic ash. When dissolved, the thinner solution-like seams and bits of greenish gray chalk revealed only clay with minor zeolite (<10%). A few genuine incipient stylolite seams occur at the top of Section 120-750A-19R-2 and in Section 120-750A-20R-1 (Fig. 14). Some pale purple laminae appear to represent redox changes.

The preservation of nannofossils and foraminifers improves just below the top of Subunit IIIA, but it diminishes noticeably

below Section 120-750A-19R-3. Smear slides show increased nannofossil overgrowths and dissolution, foraminifer debris, and micrite. Thin subparallel olive gray wispy zones are commonly richer in clay with <5% zeolite. Rare pyritic streaks with more foraminifers and echinoid traces continue. A few peloids are noted. Thus, Core 120-750A-20R marks a transition to calcareous chalk, although nannofossil preservation is adequate to demonstrate that the basic lithologic components did not change. Gradational off-white (10YR8/1) to rather greenish gray (5GY6/1) zones occur, some with well-developed subhorizontal to horizontal *Zoophycos* tracks, others with stylolites. Recovery is extremely poor below Core 120-750A-21R. Pieces from Cores 120-750A-22R to -26R as well as the overlapping first core from Hole 750B suggest that Subunit IIIA extends to about 450 mbsf.

Subunit IIIB: Intermittently Silicified Limestone and Calcareous Chalk

Interval: top of Core 120-750B-3R-1, 0 cm, to the top of Core 120-750B-11W.

Depth: 450.0–594.6 mbsf.

Thickness: 144.6 m.

Age: early Maestrichtian to early Santonian.

Subunit IIIB recovery was poor and contained a highly disturbed sequence of drill chunks and plugs. From Cores 120-750B-3R to -10W, the general lithologic type appears uniform.

Core 120-750B-3R encountered layers of hard, white (5GY8/1) to light greenish gray (5GY7/1) calcareous cherts, lithified to limestone by pervasive silica cement. Recovery favored silicified intervals, but intermittent softer fragments with the same appearance suggest that about equal proportions of the section are unsilicified micritic calcareous cherts. The subunit is pervasively burrowed, as shown by some of the longer chalk pieces recovered (Fig. 15). Foraminifers are common and reasonably well preserved. Recognizable nannofossils are common but most of the micrite appears to consist of poorly preserved nannofossil debris. Small (fine silt to coarse sand size) calcareous fragments apparently were derived from molluscs, crinoid columnals, and other bioclast fragments (e.g., Sections 120-750B-7W-1 and 120-750B-8W-1), with a few inoceramid pieces.

Faintly darker intervals are minor but make up bundles of wispy greenish gray streaks that have higher concentrations of foraminifers, clay, and pyrite. Benthic foraminifers are com-

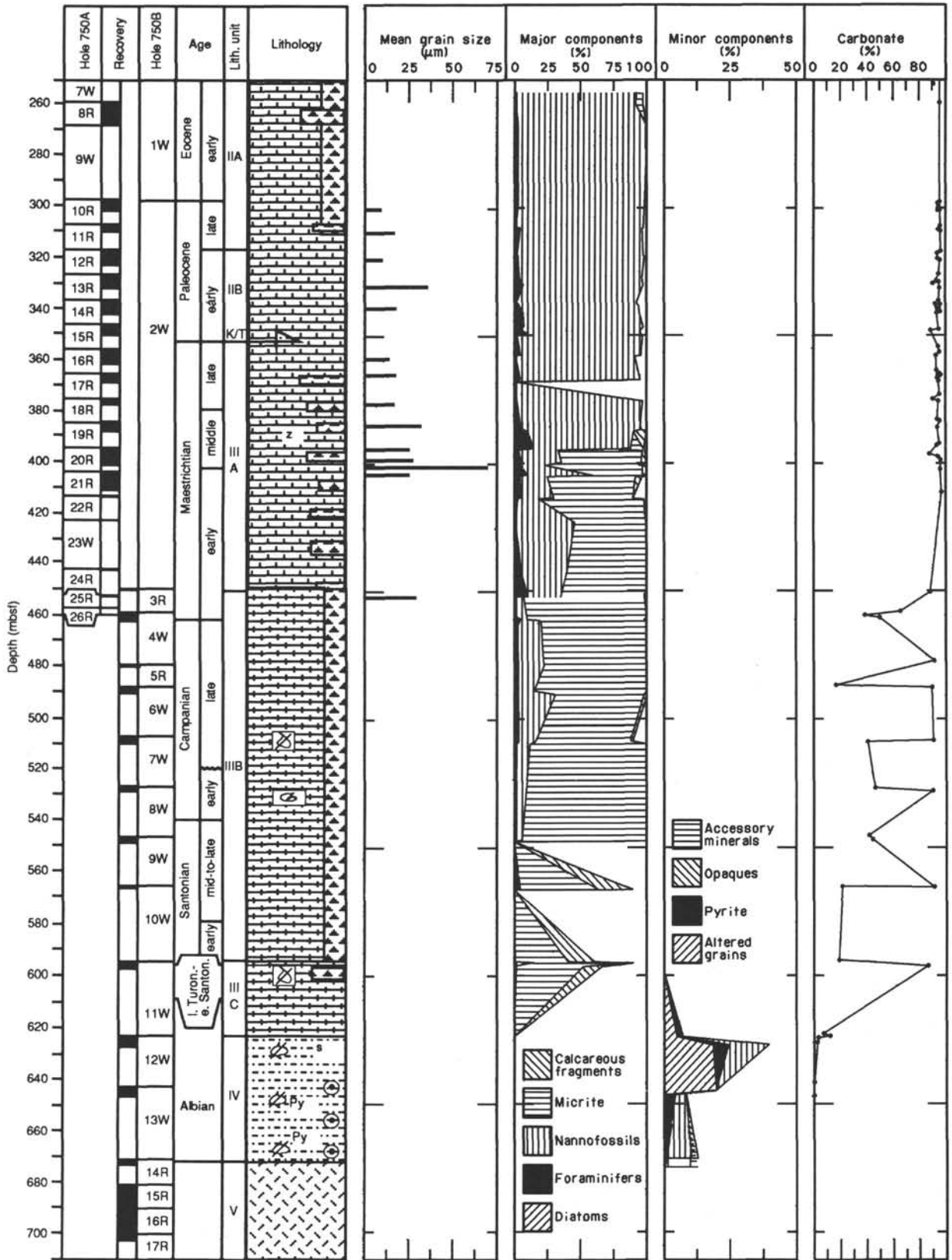


Figure 10. Lithologic summary, Site 750. Downhole grain-size trends, major and minor components from downhole smear slide and lithologic summary, and downhole plot of carbonate percentage. See Figure 9 for an explanation of symbols used.

Table 3. Mean grain size and sand/silt/clay percent, Site 750.

Core, section, interval (cm)	Depth (mbsf)	Mean grain size (μm)	Sand (%)	Silt (%)	Clay (%)
120-750A-1R-1, 22-24	0.22	28.5	15	80	5
120-750A-1R-1, 80-82	0.80	18.7	5	93	2
120-750A-3R-1, 127-129	57.67	13.3	3	85	12
120-750A-7W-1, 127-129	163.38	27.1	11	86	3
120-750A-10R-3, 21-23	301.01	9.9	3	78	19
120-750A-11R-2, 43-45	309.43	16.3	6	82	12
120-750A-12R-2, 144-145	320.14	10.0	2	82	16
120-750A-13R-3, 141-143	330.98	36.7	22	77	1
120-750A-14R-2, 79-81	338.79	18.7	7	83	10
120-750A-16R-2, 102-104	358.32	15.3	5	88	7
120-750A-17R-1, 47-49	365.77	19.6	7	89	4
120-750A-18R-2, 34-36	376.84	17.8	6	88	6
120-750A-19R-1, 79-81	385.49	32.8	22	73	5
120-750A-20R-1, 18-20	394.58	26.9	14	79	7
120-750A-20R-4, 13-14	399.03	27.0	13	85	2
120-750A-21R-1, 63-65	400.56	70.8	60	38	2
120-750A-25R-1, 6-8	404.63	27.8	13	20	7
120-750A-12W-2, 21-23	625.21	13.6	0	79	21
120-750A-12W-2, 103-105	626.03	11.1	0	71	29
120-750A-12W-3, 22-24	626.72	10.7	1	87	12

mon. Darker intervals also display trace fossils including compacted *Planolites* and *Zoophycos*. Insoluble residues generally contained some silicified foraminifer molds, quartz grains, and clay with a few zeolites. Some radiolarian fragments are preserved. Laminae appear in Core 120-750B-7W.

The intensity of silicification varies in hand specimens. Cherts are common as centimeter-size, ovoid nodular fragments with dark gray centers and medium gray exteriors. Some grade with zonally concentric bands into silicified limestone, or even white chalk; others are very irregular in outline and display tear-drop silicification fronts (Fig. 16) or enclose patchy chalk blebs. Diagenetic silicification fronts are particularly well illustrated in Cores 120-750B-7W-2 and 120-750B-9W and may conform to bedding planes. Silicification conceals primary burrow structures.

Smear slides of Subunit IIIB reveal mainly micrite (70%–90%), which apparently masks an extremely fine-grained silica component. Some of the cored pieces show compactional fractures and microfaults. One of these displays an unknown mineral on the fracture surface (Core 120-750B-9W-1, 98–105 cm) that is translucent brownish yellow, with radial flat monoclinic crystals showing low birefringence and low relief.

Subunit IIIC: Calcareous Chalk with Dark Marl Beds

Interval: top of Core 120-50A-11W-1, 0 cm, to the top of Core 120-750B-12W.

Depth: 594.6–623.5 mbsf.

Thickness: 30.1 m.

Age: early Santonian to late Turonian.

The Subunit IIIC boundary is drawn at the top of Core 120-750B-11W above the first downhole occurrence of black clayey intervals. Core recovery improves, preserving decimeter-long pieces. Minor silicification occurs but becomes very subordinate. Overall, this subunit is darker than above and is composed of mainly greenish gray (5GY6/1) hard calcareous chalk with centimeter-thick beds of burrowed, black clayey limestone (marl). Some changes from light to dark in this unit are gradational, but they do not appear to represent component grading. Smear slides show micrite to be dominant and probably derived from nanofossils, which persist as 2%–10% of the sediment. Calcareous fragments, many from foraminifers, are common. Some cut surfaces are imparted with grainy textures from foraminifers.

Diverse burrows are prominently displayed in longer pieces of dominantly light greenish gray (5GY7/1–6/1) hard marly chalk. These are flattened to flaser, burrow-mottled furoid structures. Varieties include *Planolites*, *Zoophycos*, and minor vertical burrows (*Teichinus*, *Thalassinoides*?) as well as numerous composite burrows and the first occurrences of *Chondrites* (See Fig. 17).

Significant accessories in Section 120-750B-11W-1 include: (1) centimeter-size pyritized wood fragments at 120 cm, piece 13; (2) a well-preserved bivalve cross-section with crenulated shell sculpture at 36 cm, piece 7; (3) silt-size bioclast fragments at 62 cm, piece 10; and (4) minor chert at 85–87 cm. Smear slides also contain a few single, limpid dolomite rhombs up to 20 μm in size. Acid residues contain a few radiolarian fragments and traces of possible glauconite.

A lower transition or clear boundary was not recovered.

Unit IV: Red-Brown Silty Claystone with Coal

Interval: top of Core 120-750B-12W to Core 120-750B-14R-1, 23 cm.

Depth: 623.5–675.5 mbsf.

Thickness: 52 m.

Age: Albian.

Only 7.7 m of Unit IV sediment were recovered relatively undisturbed from the basal 52 m of Hole 750B. However, consistent lithologic features noted in the recovered material suggest that it is representative of the entire interval.

Core 120-750B-12W showed no trace of pelagic chalks, but rather a major lithologic change to a tough, plastic, dominantly reddish brown, ferruginous, kaolinitic, silty claystone that clogged the drill bit. Unit IV is characterized by the overall reddish brown to dark brown color, which includes a broad range of probably terrigenous deposits from fine claystone to siltstone, with intervals richer in sandy components and a soft pebble conglomerate. It contains abundant coarse debris of coal and other land-derived organic matter, and high concentrations of coarse sand-size authigenic siderite grains, pyrite grains, and concretions.

The upper part (mainly Cores 120-750B-12W-1 to 120-750B-12W-2, 100 cm) is massive, but mottled with shades of dark brown, very dark grayish brown, rusty brown, dark reddish brown, and minor gray, black, and pea green as well as irregular yellowish seams. There is little evidence of bedding structures, laminae, or burrows, and pieces break into irregular, pedlike clods. Below this, claystones are finer grained, darker, and more fissile. Section 120-750B-12W-CC (Fig. 18) and Core 120-750B-13W contain layered siltstone and claystone (Fig. 19).

Smear slides are variable with clay (95%–35%), common opaques (15%–20%), altered grains (15%–30%), siderite (2%–25%), and pyrite (0%–6%).

The X-ray diffractograms show the clay fraction in Core 120-750B-12W to consist of kaolinite with minor goethite (Fig. 20). The coarse fractions have a conspicuous authigenic siderite component with two main habits: (1) coarse sand-size, oblong crystals with stubby terminations and occluded clay, some of which show cross- or low-angle twins; and (2) fine-sand size, more slender prismatic clear crystals, commonly with low-angle twin spray habits.

The term “altered grains” refers to abundant sand-size sub-angular grains, commonly with ferruginous coatings, but which contain transparent to cloudy particles that appear nearly isotropic to diffusely birefringent in crossed nicols. These are interpreted to be devitrified basaltic glass because of associated clasts with numerous occluded crystal relicts of iron mineral and plagioclase laths. Bulk X-ray diffractograms for Core 120-750B-

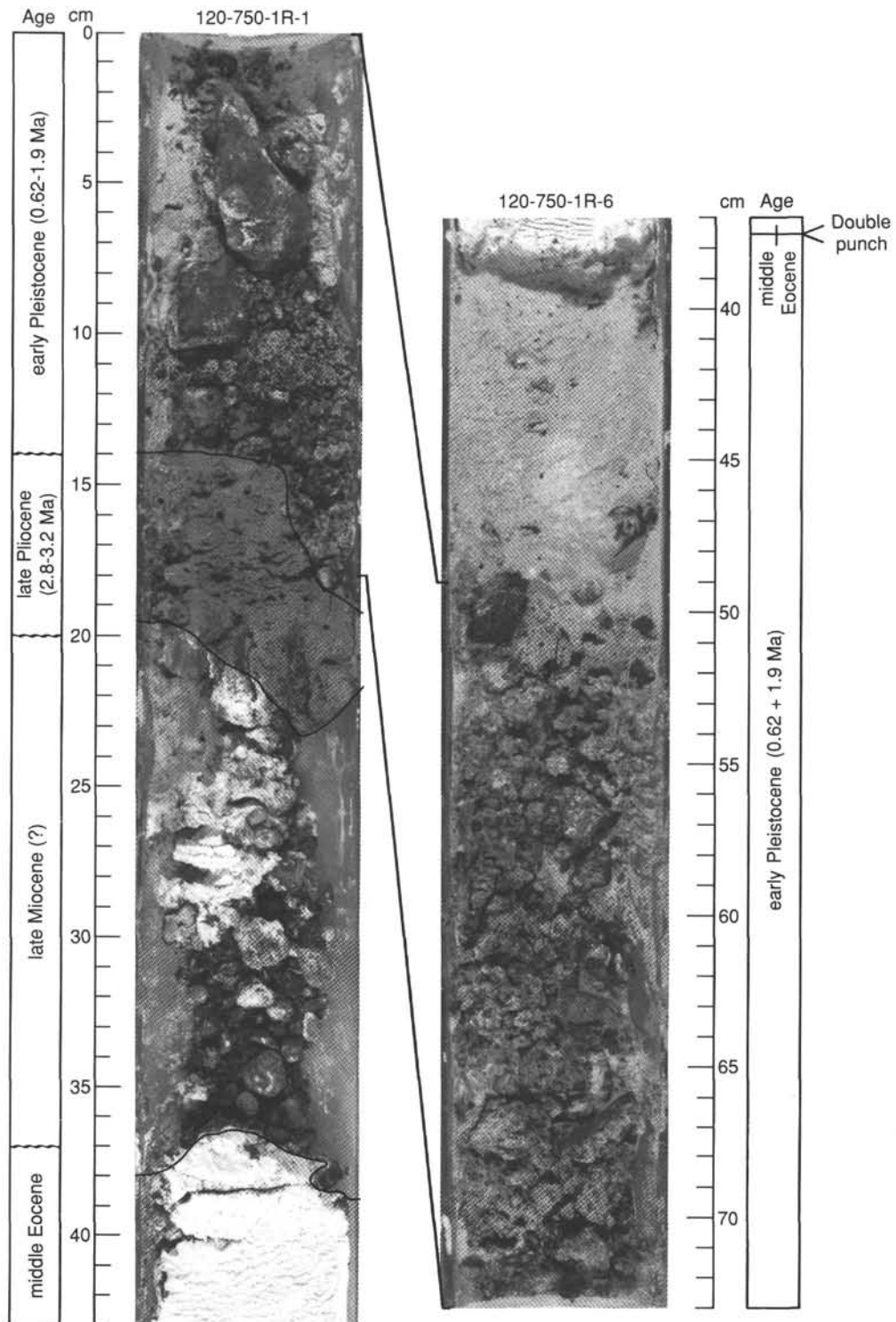


Figure 11. Unit I diatom ooze and lag deposits: Core 120-750A-1R. Photograph of Core 120-750A-1R-1, 0-43 cm, and Core 120-750A-1R-6, 38-73 cm, illustrating the correlation between the top and bottom of the core as evidence for double punching of the mud line. Differences in diatom species (see "Biostratigraphy" section, this chapter) distinguish lag deposits from two periods.

12W show hematite with silica, kaolinite, and possible apatite, but without evidence of smectite, quartz, or plagioclase (Fig. 20B).

Coal fragments range from fine to coarse sizes and appear reworked. Many have pyritic coatings. Pieces are highly angular to flaky, and cellular structures are preserved. Debris is concen-

trated along thin beds that suggest current transport. Some pieces show angular wedges that might have been derived from the compaction of soft material.

Core 120-750-13W contains clayey siltstone that is generally darker grayish brown, more fissile, and with more coaly organic material than above. The core also has parallel and current bed-

Table 4. Summary of ice-rafted and surface lag deposit clasts, Site 750.

Core, section, interval (cm)	Ice-rafted debris lithology
120-750A-1R-6	Large weathered feldspar
120-750A-1R-6	Pumice
120-750A-1R-6	Basalt
120-750A-2W-CC, 1-3	Quartzite (Q: 94%)
120-750A-2W-CC, 7-9	Epidote amphibolite
120-750A-2W-CC, 12-14	Foliated granite
120-750A-4W-CC	Granodiorite
120-750A-4W-CC	Hornblende leucogranite
120-750A-4W-CC	Altered basalt
120-750A-4W-CC, 1-3	Biotite gneiss
120-750A-6R-CC	Diorite
120-750A-6R-CC, 12-14	Metagabbro
120-750A-6R-CC, 6-9	Red quartzite sandstone
120-750A-6R-CC	Biotite schiste
120-750A-6R-CC, 1-3	Granite with orange K-feldspar
Wash 9W	Metamorphosed arkose
Wash 9W	Foliated granite
Wash 9W	Amphibolite
Wash 9W	Very coarse-grained hornblende biotite leucogranite
Wash 9W	Granite
120-750A-10R-1	Black plagioclase-pyroxene-quartz diorite

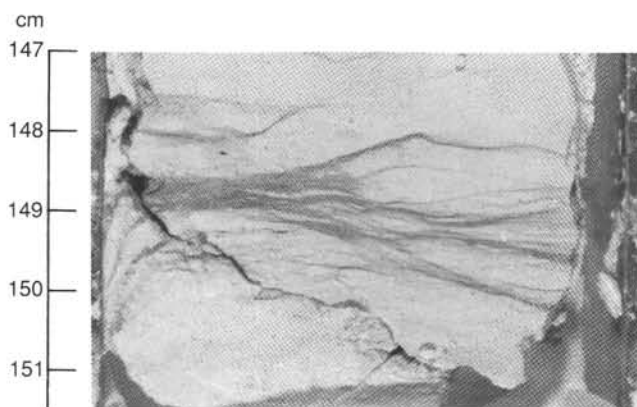


Figure 12. Dissolution seams in Paleocene chalk (Core 120-750A-12R-1, 147-151.5 cm).

ding and includes a multicolored, soft pebble conglomerate and brown sand (Core 120-750B-13W-1, 37-65 cm). Within this bed, there is evidence of grading and an abrupt change to cross-stratified sand showing small-scale current bedding (Fig. 19). Soft clasts include rust, red-brown, grayish green, and light gray clay. Hard clasts include pale yellow siderite and light gray and black claystone. Grains are rounded to subrounded in grain-to-grain contact. Sizes range from 0.5 to 3 mm.

Thin siderite laminae and small concretions appear in Section 120-750B-13W-2, along with centimeter-size pyrite nuggets. The lithology directly overlying the basalt in Section 120-750B-14R-1, 25 cm, consists of pieces of hard, brown claystone with siderite cement and a single large siderite concretion containing abundant millimeter-size, woody charcoal fragments.

Critical transitions at the base of this unit and a contact zone to the basement were not recovered in the attempt to wash through the tough claystone.

Unit V: Basalt

Interval: below Core 120-750B-14R-1, 23 cm.
 Depth: 675.5-709.7 mbsf.
 Thickness: 34.2 m.
 Age: ?

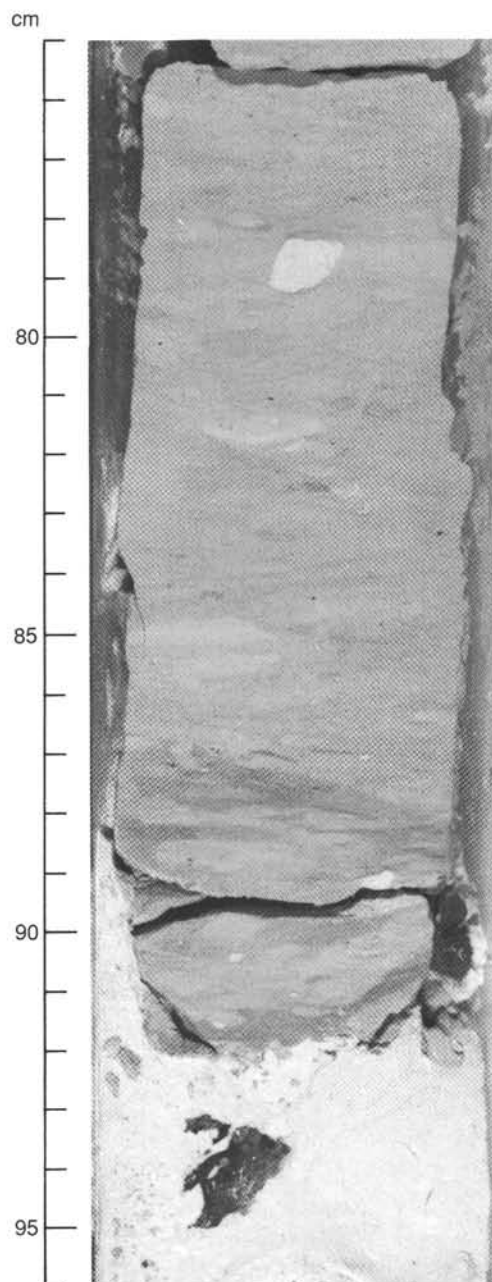


Figure 13. Close up of the Cretaceous/Tertiary contact (Core 120-750A-15R-3, 75-96 cm).

The basalt is highly altered plagioclase-clinopyroxene phyric basalt (see "Igneous Petrology" section, this chapter). The overlying sediments did not show evidence of baking. Surprisingly, ferruginous alteration colors cease at the basalt contact. The uppermost basaltic alteration product appears to be mainly a distinctive bluish green to black smectitic claystone.

BIOSTRATIGRAPHY

Introduction

The primary goal of drilling at Site 750 was to penetrate and recover a representative Cretaceous section from the eastern side of the Raggatt Basin, Southern Kerguelen Plateau. The Cretaceous at Site 750 was encountered in Holes 750A and 750B, drilled respectively before and after Site 751. Because of time constraints and operational difficulties, a modified program of

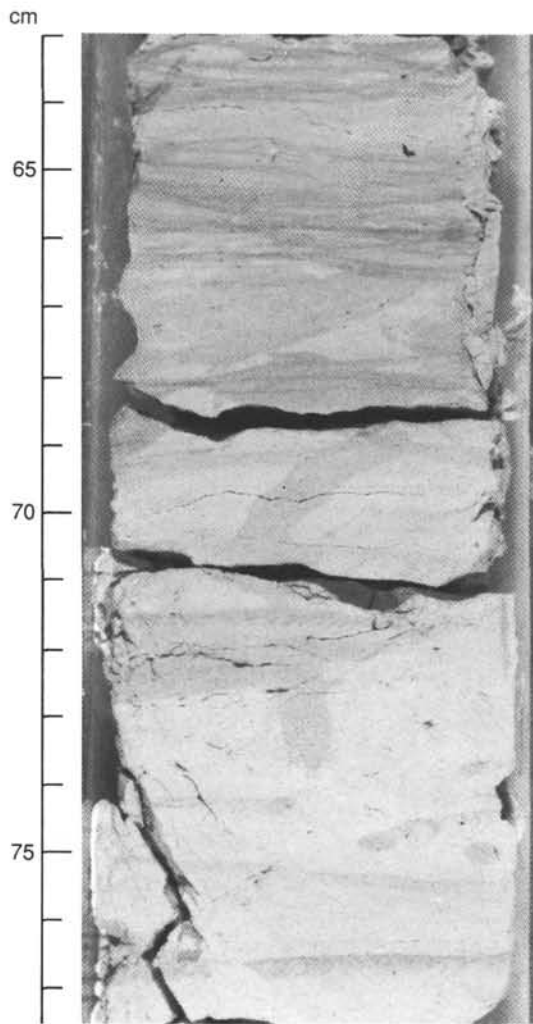


Figure 14. Stylolite seams in Maestrichtian (Subunit IIIA) chalk (Core 120-750A-20R-1, 63-77.5 cm).

coring was adopted to fulfill the primary objective. This included washing through the majority of the overlying Cenozoic section, with only a few spot cores taken. Hole 750A was washed through the Cenozoic until the lower upper Paleocene was reached. Continuous coring began at this point, proceeding across the Cretaceous/Tertiary boundary and into the Cretaceous.

Hole 750A was aborted at 460.5 mbsf (Core 120-750A-26R) due to bit failure and time constraints. Hole 750B was drilled initially with spot coring (rotary and wash cores) to Core 120-750B-5R (478.9-488.5 mbsf), where Cretaceous material was sampled from deeper levels than in Hole 750A. Hole 750B was drilled using a wash-core technique that yielded a small recovery of material from one core length out of two or three drilled. As a result, it is not clear exactly where a sample comes from within the designated interval. For example, Core 120-750B-11W recovered 2.88 m from somewhere in the interval from 594.6 to 623.5 mbsf, a drilled thickness of 28.9 m. As a fast exploration system, this technique was valuable, but it would have been better if supplementation with a sidewall coring program had been possible.

The continuously cored Paleocene section includes an expanded Danian section with excellent potential for paleontological research. The Cretaceous/Tertiary boundary is apparently not complete, as some of the lowest Danian is absent. The total

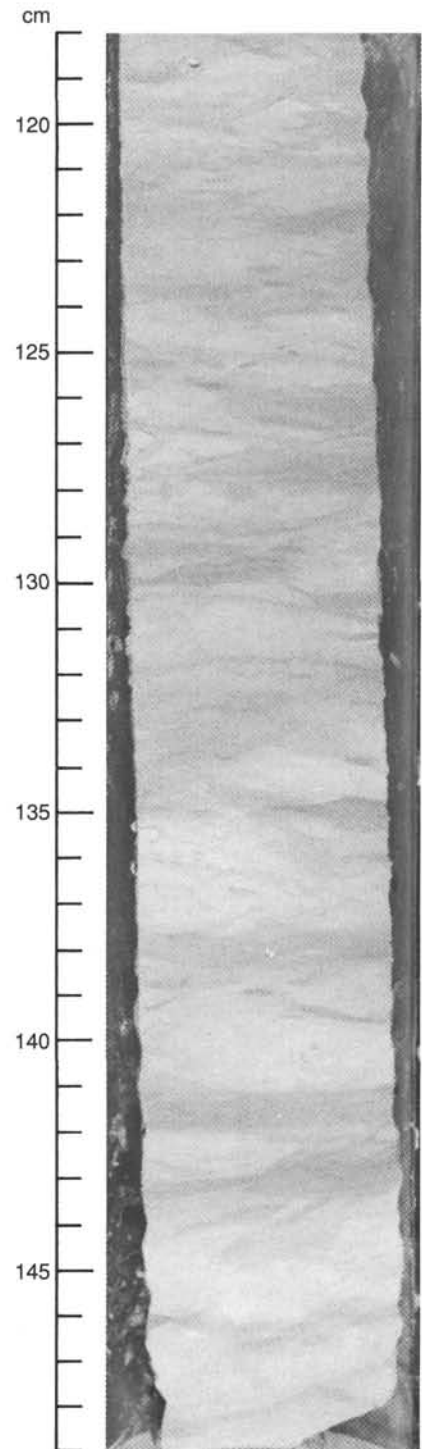


Figure 15. Fucoid structures in burrowed chalk of Subunit IIIA (Core 120-750B-4W-2, 118-149 cm).

Cretaceous section encountered appears to include a complete(?) Maestrichtian sequence, continuing downhole into the upper Campanian. Any doubt concerning the completeness of the Maestrichtian section relates to the possible absence of the youngest Maestrichtian, a question we cannot answer with the available material. This section is disconformably separated from an underlying unit of interbedded dark marly chalk and light chalk that yielded material containing poorly to moderately preserved calcareous microfossils of quality and diversity too low to allow

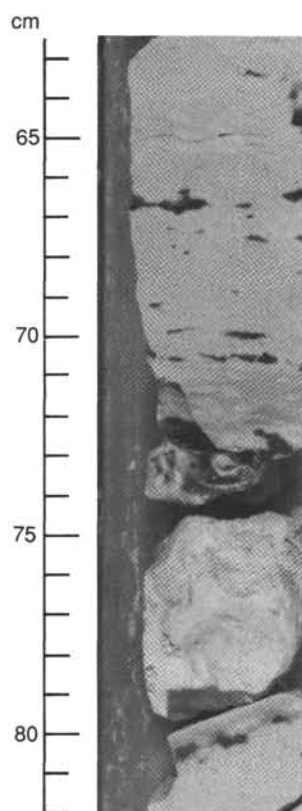


Figure 16. Campanian silicified limestone of Subunit IIIB with chert blebs (Core 120-750B-6W-1, 62.5–82 cm).

more refined subdivision. This sequence, in turn, lies disconformably on an earlier sequence of Cenomanian to lower Campanian pelagic sediment overlying Albian nonmarine sediments and basement.

All epochs within the Upper Cretaceous appear to be present, but it is suggested that there is a discontinuity within the Campanian and possibly in the Turonian-Santonian sequence.

Planktonic Foraminifers

Cenozoic

Hole 750A was drilled to a depth of 460.5 mbsf before loss of part of the bottom assembly forced its abandonment. Since the hole was partially cored and partially washed (in order to reach Cretaceous levels more rapidly), recovery, in general, was moderately good to poor. Cenozoic sediments were recovered in the interval of Cores 120-750A-1R to -15R; the Maestrichtian/Danian boundary was recovered toward the lower part of Section 120-750A-15R-3. Planktonic foraminifers are abundant and well preserved in almost all core-catcher samples examined (but see comments below regarding Core 120-750A-14R). Foraminifers have been examined from all core-catcher samples and/or specially selected samples where necessary.

Hole 750A began in middle Eocene sediments; a sample from the bottom of Section 120-750A-1R-3 contains a fauna dominated by *Globigerapsis index*, with less common *Acarinina primitiva*, *A. collactea*, *Subbotina linaperta*, and chiloguembelinids (common in the fine fraction). The overlap of *A. primitiva* and *Chiloguembelina cubensis* suggests a level correlative with Zone P14 of low latitudes, which is, in turn, correlative with magnetic polarity Anomaly Correlative 18 of the general polarity time scale (GPTS).

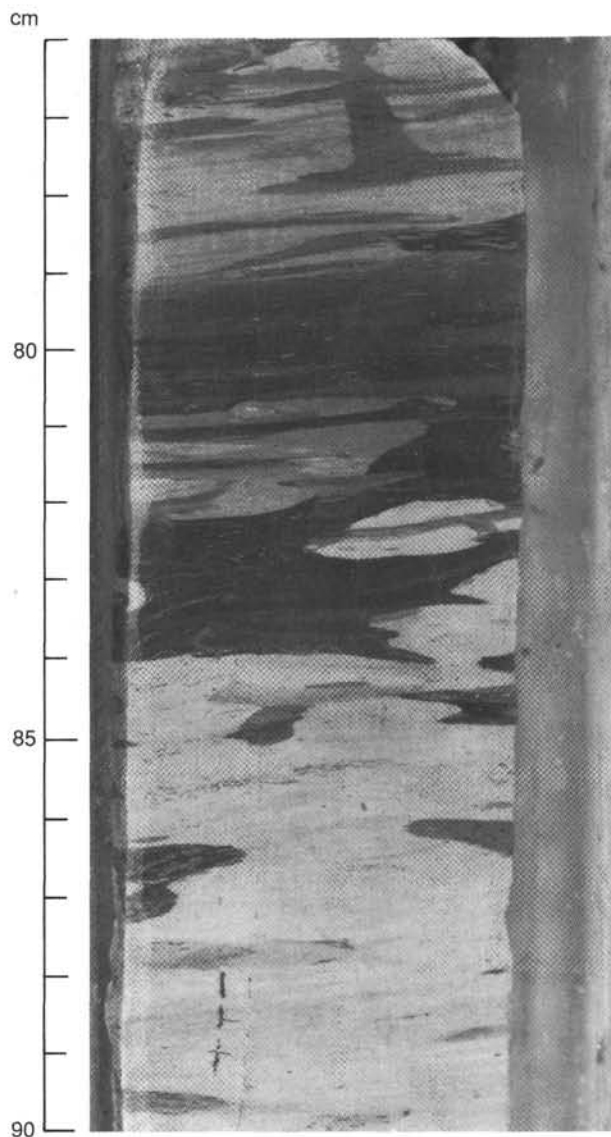


Figure 17. Burrowed clayey limestone, Subunit IIIC (Core 120-750B-11W-2, 76–90 cm).

Core 120-750A-2W was a wash core (7.9–56.4 mbsf), and no data are available from this interval. Core 120-750A-3R-CC (56.4–65.6 mbsf) recovered an early middle Eocene fauna with *G. index*, *A. primitiva*, *A. collactea*, *A. densa*, and *S. linaperta*, which places this in the *Globigerapsis index* Zone of the Austral zonal scheme (approximately equivalent to Zones P11–P12 of the low-latitude zonal scheme). Core 120-750A-4W was a wash core (to 143.3 mbsf), and core-catcher samples were not obtained. Core 120-750A-6R recovered only a piece of chert from which no age determination was possible. Core 120-750A-7W was a wash core (to 259.2 mbsf).

Core 120-750A-8R-CC contained an early Eocene (Ypresian) fauna characterized by relatively small acarininids (*A. primitiva*, *A. wilcoxensis*–*A. pseudotopilensis* group), *Subbotina patagonica*, and chiloguembelinids. Core 120-750A-9W was a wash core (to 297.8 mbsf), whereupon continuous coring was begun in the lower upper Paleocene. A sample from the bottom of Core 120-750A-9W yielded a middle Paleocene fauna with *Acarinina mckannai*, *Chiloguembelina midwayensis*, *C. morsei*, and *Subbotina triloculinoides*. In the absence of a core-catcher sam-

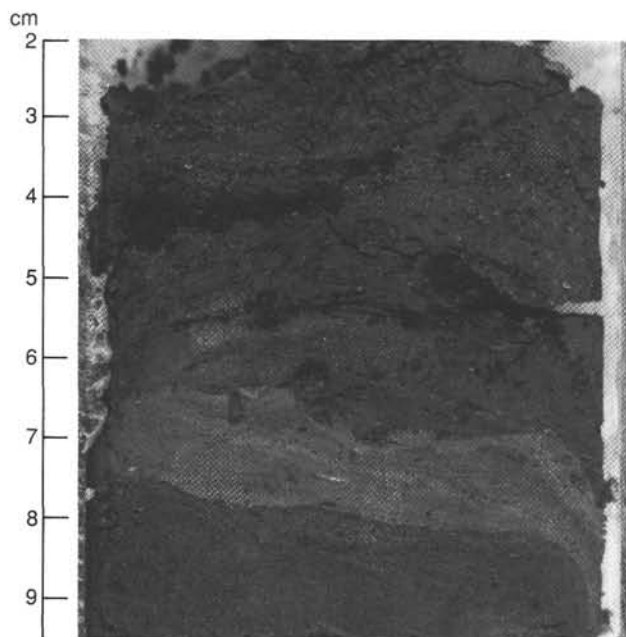


Figure 18. Dark brown clayey siltstone with coaly wood fragments in current-stratified deposits, Unit IV (Core 120-750B-12W-CC, 2-9.5 cm).

ple from Core 120-750A-10R, Sample 120-750A-10R-3, 1-3 cm, was taken. A diversified Zone P3B fauna is characterized by *Morozovella angulata*, *M. conicotruncata*, *M. praecursoria*, *S. triloculinoides*, *S. pseudobulloides*, and chiloguembelinids.

An anomalously thick (around 45 m) Danian section was recovered in Cores 120-750A-11R to -15R (around 317-355 m). It is not known yet whether the stratigraphic interval equivalent to Zones P3A and P2 is present in Cores 120-750A-11R as only core-catcher samples have been examined at this time. Sample 120-750A-11R-CC contains a late Danian fauna (Zone P1C) characterized by *Eoglobigerina appressa*, *E. edita*, *Subbotina trivialis*, and *S. pseudobulloides*.

Cores 120-750A-12R and 120-750A-13R-CC contain a similar late Danian fauna with the same taxa as listed above as well as *E. simplicissima*, *E. danica*-*E. moskvini* group, and *Morozovella inconstans*. Sample 120-750A-14R-CC is somewhat of an enigma at this time. Washed residues are extremely small, and planktonic specimens are relatively rare and are present essentially only in the fine ($> 63 \mu\text{m}$) fraction. In addition to Danian taxa (*E. edita*, *E. danica*, *E. appressa*, *Globoconusa daubjergensis*, and *S. pseudobulloides*), small reworked late Cretaceous forms (*Globigerinelloides*, *Heterohelix*) were also found.

The Danian/Maestrichtian boundary occurs within Section 120-750A-15R-3 (346.1-355.8 mbsf) at about 91 cm (about 350 mbsf). A preliminary examination of material immediately above the boundary suggests that elements of the *Eoglobigerina eugubina* (P1a) Zone may be present, but preservation is relatively poor. The boundary does not appear to be complete, however, at this site.

It should be mentioned at this point that parts of Anomaly Correlatives 27 and 28 appear to have been recovered in Cores 120-750A-12R and -14R, respectively, based on calcareous plankton biostratigraphy, providing valuable corroboration of sedimentation rate calculations (see "Sedimentation Rates" section, this chapter) and for magnetobiostratigraphic correlations. Anomaly Correlative 28 correlates with Zone P1b and Anomaly Correlative 27 with Zone P1c, supporting earlier suggested magnetobiostratigraphic correlations (see Berggren et al., 1985b, 1985c).

In summary, the main results of a preliminary study of the Cenozoic planktonic foraminifers of Site 750 include:

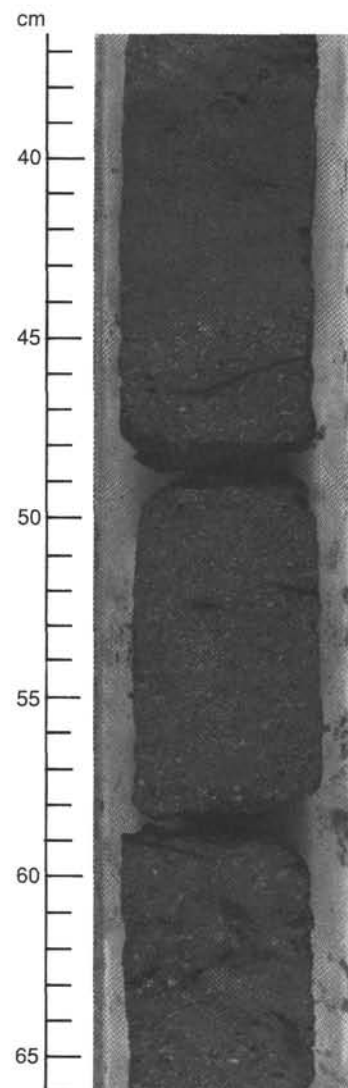


Figure 19. Multicolored red-brown, soft-pebble conglomerate with scattered centimeter-size coaly claystone clasts (Core 120-750B-13W-1, 36.5-66 cm).

1. Recovery of an early late Paleocene (Zone P3B) fauna that has not been observed previously on Leg 120 and that will enable us to fill in needed data on the biogeographic and stratigraphic distribution of taxa at this time in the austral region;

2. Recovery of a diversified and well-preserved Danian fauna over a stratigraphic interval of nearly 50 m that should yield important data on the taxonomy, early evolution, and paleobiogeography of Danian faunas following the terminal Cretaceous extinction event(s); and

3. The possibility of examination (at a relatively high resolution) of the series of events that characterize the Maestrichtian/Danian boundary. A series of integrated studies on stable isotopes, calcareous plankton taxonomy, biostratigraphy, evolution, paleobiogeography, magnetic polarity stratigraphy, and magnetic susceptibility is planned.

Cretaceous

In Samples 120-750A-14R-4, 89-91 cm, 120-750A-14R-CC, and 120-750A-15R-3, 91 cm, Cretaceous material is reworked into and dominated by the Danian component. *Inoceramus* prisms, *Globigerinelloides*, and *Abathomphalus* are present in minor quantities but are well preserved.

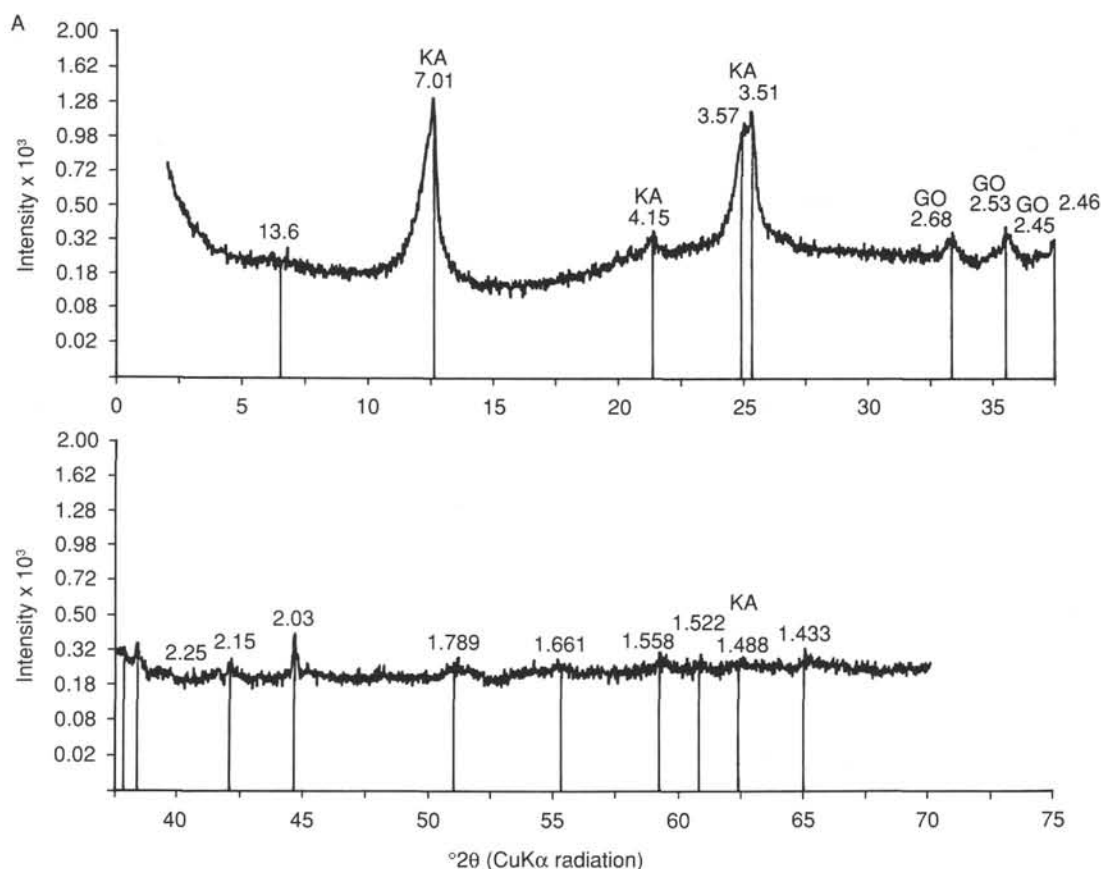


Figure 20. X-ray diffractograms of samples from Unit IV, Site 750. **A.** Calgon-treated clay fraction: kaolinite and goethite. Sample taken from Core 120-750B-12W-1, 54 cm. **B.** Bulk sample: apatite, halite, hematite, and kaolinite. Sample taken from Core 120-750B-12W-1, 109 cm. AP = apatite, GO = goethite, HA = halite, HE = hematite, KA = kaolinite, and ST = siderite.

Fully Cretaceous foraminifer faunas are abundant and well preserved from Sample 120-750A-15R-3, 112 cm, to the bottom of Hole 750A and include what appears to be a complete Maestrichtian sequence passing downhole without stratigraphic break into the Campanian in Hole 750B. The deepest core in Hole 750A (Sample 120-750A-25R-CC) is still in the Maestrichtian.

Faunal diversity, planktonic/benthic ratio, and specimen size vary markedly from sample to sample, suggesting that current activity was varying with time and that the fine, well-sorted, almost completely planktonic faunas at some levels may indicate deposition at this site of material winnowed from nearby. The variation is also due in part to variation in water temperature, which is reflected in faunal composition. In general, within the section encountered in Hole 750A, seawater temperature increased with time through the Maestrichtian. Depths of deposition vary from inner to outer continental shelf and upper slope depths.

The section penetrated in Hole 750B began downhole approximately where Hole 750A had ended and continued to Section 120-750B-11W-CC in dominantly pelagic oozes with additional but incomplete Campanian to Cenomanian sections. Inner and outer continental shelf depth deposits were drilled in Core 120-750B-11W, but sample control and quality were not as good as in Hole 750A.

Hole 750A

Samples 120-750A-14R-4, 89-91 cm, 120-750A-14R-CC, and 120-750A-15R-3, 91 cm, contain a Danian fauna with a few reworked small *Globigerinelloides* and *Heterohelix*, very rare *Abathomphalus*,

and some *Inoceramus* prisms. The Cretaceous element is well preserved and a minor component, suggesting a local erosion site or bioturbation.

Sample 120-750A-15R-CC contains a diverse, well-preserved, latest Maestrichtian fauna (latter half of the *Abathomphalus mayaroensis* Zone) as marked by the presence of *A. mayaroensis* (Bolli), *Globotruncanella citae* (Bolli), and *Gublerina* sp. cf. *G. ornatissima* (Cushman and Church). This fauna is the youngest Cretaceous recovered during Leg 120 (the latter half of the Maestrichtian or of the *A. mayaroensis* Zone was missing elsewhere) and reflects the warmest water conditions with a fauna that may possibly represent Sliter's (1976) Tethyan Faunal Province (FP). It is not a fully developed Tethyan fauna, but it is significantly more diverse and complex than the Transitional FP elements seen in other samples.

Sample 120-750A-16R-CC also belongs to the latter half of the *A. mayaroensis* Zone, containing the nominate species in addition to *Rugoglobigerina rugosa* (Plummer) s.s., and *Gublerina* sp. cf. *G. ornatissima*. Bivalve fragments (other than *Inoceramus*) occur in the coarse fraction. The fauna is neither as diverse nor as complex as that above and probably belongs to the Transitional FP. *Abathomphalus mayaroensis* Zone faunas continue downhole to Sample 120-750A-18R-CC, the lowest downhole occurrence of the nominate species. *Abathomphalus intermedius* (Bolli) accompanies it in Samples 120-750A-17R-CC and 120-750A-18R-CC showing that, in the *A. mayaroensis* Zone at least, early and late subzones can be recognized in this section. This is further support for the concept of allocating part of the section to the Tethyan FP, as noted above. Other

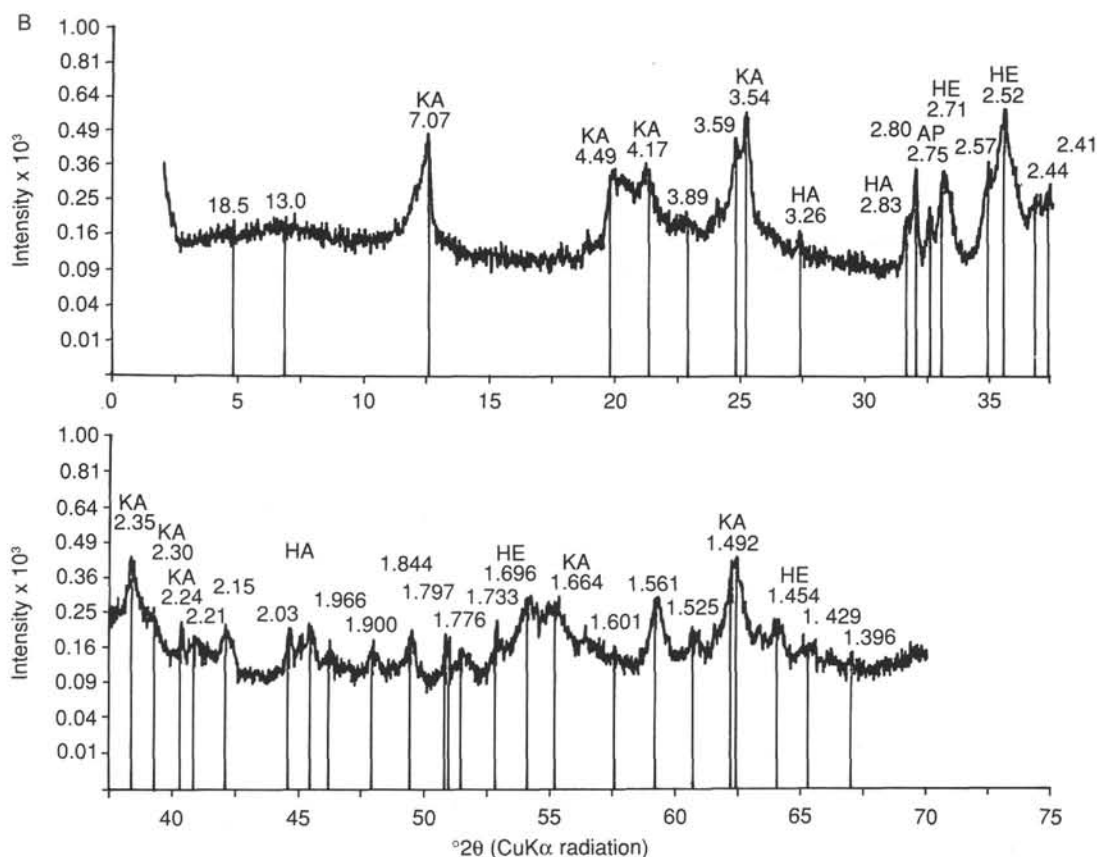


Figure 20 (continued).

forms present in the lower part of the *A. mayaroensis* Zone include *Rosita fornicata* (Plummer), *Rugotruncana* sp. (cf. *subpennyi*) and *Globotruncanella havanensis* (Voorwijk).

Abathomphalus intermedius is present in Samples 120-750A-19R-CC to 120-750A-21R-CC inclusively, suggesting correlation with the *Gansserina gansseri* Zone in the absence of the nominate taxon. Diversity decreases downhole and by the bottom sample, the faunas belong to the Austral FP. Samples 120-750A-19R-CC and 120-750A-20R-CC, although austral, are more diverse and include rare globotruncanids (e.g., *Rosita fornicata* and *Globotruncanella havanensis* in Sample 120-750A-19R-CC). All faunas are dominated by *Heterohelix-Globigerinelloides-Hedbergella* with rare *Rugoglobigerina* in support of the allocation to the Austral FP.

Samples 120-750A-22R-CC and 120-750A-23R-CC are lower Maestrichtian but cannot be allocated to either of the two recognized zones noted by Caron (1985) for this interval. Both samples are characterized by an abundance of small species (perhaps reflecting some deposition of faunas winnowed from elsewhere). Planktonic faunas are dominated by *Heterohelix-Globigerinelloides-Hedbergella* with *Guembelitra cretacea* Cushman in the upper sample. Highly rugose *Rugoglobigerina* are absent from Sample 120-750A-22R-CC but *R. rotundata* Brönnimann is present in Sample 120-750A-23R-CC. *Inoceramus* is common in the lower sample.

Sample 120-750A-24R-CC is taken as lower Maestrichtian, although definitive Maestrichtian foraminifers are lacking. Sample 120-750A-25R-CC contains *Globigerinelloides impensus* Sliiter, originally thought to be only of upper Campanian age but now recorded in the lower Maestrichtian (B. Huber, pers. comm.). Both faunas are restricted in diversity and globotruncan-

nids are rare (Sample 120-750A-24R-CC) or absent. Again, *Heterohelix-Globigerinelloides-Hedbergella* dominate and *Archeoglobigerina* becomes an important component.

Hole 750B

Core 120-750B-3W coincides in depth with the interval between Cores 120-750A-24R and -25R and contains a similar fauna of early Maestrichtian age. Core 120-750B-4W is lower than any from Hole 750A and contains *Globigerinelloides impensus*, here considered (as noted above) to range into the lower Maestrichtian.

Samples 120-750B-5W-CC to 120-750B-8W-1-CC are Campanian, a continuation (to 546.7 mbsf) of the Upper Cretaceous carbonate sequence initially encountered in Hole 750A. Samples yield results with some reluctance, and it is unlikely that further refinement can be made with the material available. Cores 120-750B-5W to -8W are difficult to date using foraminifers, and the results given below are based on calcareous nannoplankton for this interval.

Faunas are dominated by elements typical of the Austral FP to Section 120-750B-7W-1. Below that depth, globotruncanids appear and, generally speaking, become more numerous and diverse with depth. The Transitional FP influence in Sample 120-750B-8W-2, 10 cm, is weak, and this fauna is also taken as austral. Calcareous nannoplankton studies indicate a discontinuity within the Campanian sequence between Cores 120-750B-7W and -8W. Sample 120-750B-9W-1, 128 cm, has common, diverse globotruncanids and is Transitional or even warmer. Sample 120-750B-10W-1, 60 cm, is Transitional. Patterns of reworking established by calcareous nannoplankton studies are consistent

with the possibility that globotruncanids occurring in Core 120-750B-9W are recycled from the Turonian below.

Inoceramus usually is present, and radiolarians, sponge spicules, and calcispheres occur sporadically. Radiolarians are a dominant component of Sample 120-750B-6W-CC. Most samples reflect continental slope depths of deposition, but the basal sample (120-750B-11W) contains in part a continental shelf fauna.

Core 120-750B-11W has a Santonian (or even a Campanian?) aspect, but is considered here to be Turonian in age and represents, at least in part, the *Helvetoglobotruncana helvetica* Zone. Sample 120-750B-11W-2, 128 cm, contains a diverse, middle to outer continental shelf fauna. The foraminifers have a clearly defined middle Turonian element, but they also include Cenomanian elements (*Praeglobotruncana* sp. cf. *P. delrioensis*) and well-preserved, common specimens of *Dicarinella imbricata* (Mornod) and *Marginotruncana* sp. There is also a diverse benthic component.

Sample 120-750B-11W-CC was mainly of indurated rock similar to that containing the faunas described above. It also contained some plastic clayey nannofossil ooze clinging to the indurated rock. This plastic sediment was processed separately. Although dominated by Turonian species, it also produced very well-preserved, rare *Praeglobotruncana delrioensis* (Plummer) and its immediate successor "*Dicarinella*" *imbricata*. The former is an index for the Cenomanian and the latter for the Turonian.

Another species of *Praeglobotruncana* is present but not yet identified. Thus, there is present in the interval from 594.6 to 623.5 mbsf a thin Cenomanian-Turonian unit of soft, poorly sampled plastic clay similar in age to faunas described from the northeastern flank of the Southern Kerguelen Plateau by Quilty (1973). These two localities have yielded the oldest marine faunas overlying Kerguelen Plateau basement. Older material representing the time interval between the formation of basement and the deposition of the oldest recovered sediments may exist.

Core 120-750B-11W consists of two lithologies, a dark grey shale and a white to pale grey indurated chalk, in a complexly interdigitating relationship. The two were subsequently processed separately. The foraminiferal fauna in the dark shale is dominated by benthic species of a diverse, shallow-water aspect. The planktonic fauna is of a small species characteristic of the Austral FP. It appears to be an inner continental shelf deposit. The pale sediment has a dominantly planktonic fauna of relatively low diversity with many larger specimens. Although most of the fauna is consistent with a Turonian age (*Helvetoglobotruncana helvetica* Zone), there are older elements present (in particular, *Praeglobotruncana delrioensis*) that indicate reworking of Cenomanian species into Turonian sediment.

It seems that there is in the section, probably below the level sampled in Section 120-750B-11W-CC, a thin Cenomanian unit that has been eroded locally to yield material for reworking into the Turonian. Soft sediment of Cenomanian age probably occurs below Section 120-750B-11W-CC, but it has not been cored, although the scrapings from Core 120-750B-11W may be of this unit. If this is true, there is the possibility also of a thin lowermost Turonian *Whiteinella archeocretacea* Zone sequence below.

A preliminary, rough analysis of patterns of diversity and complexity in planktonic foraminifers suggests that Turonian to lower Santonian faunas are Transitional FP and that they are Austral throughout the rest of the Santonian through lower Maestrichtian, indicating cooler conditions. The upper Maestrichtian has increasing diversity and complexity with time, so that the latest Cretaceous in the section represents the warmest conditions, within the Transitional FP (perhaps even Tethyan) that were encountered in the Leg 120 sites.

Benthic Foraminifers

All core-catcher samples of Site 750 obtained by rotary drilling (Samples 120-750A-1R-CC, 120-750A-3R-CC, 120-750A-8R-CC, and 120-750A-10R-CC through 120-750A-14R-CC) were analyzed for their benthic foraminifer content. Benthic foraminifers are well preserved and abundant in all Cenozoic samples with the exception of Sample 120-750A-14R-CC. In this sample, almost all of the benthic foraminifers are physically damaged and broken. About 100 specimens in each sample were picked and mounted from the >125- μ m fraction.

The following benthic foraminifer assemblages were recognized in the Cenozoic sedimentary sequence of Hole 750A (the assemblages are defined and numbered according to the criteria and stratigraphic boundaries established for Sites 747, 748, and 749).

Assemblage 4a: Late to Middle Eocene

Faunas from Samples 120-750A-1R-CC and 120-750A-3R-CC belong to this assemblage. Planktonic foraminifers and calcareous nannofossils indicate an age of late middle Eocene for these samples (see "Sedimentation Rates" section, this chapter). The upper boundary of benthic foraminifer Assemblage 4a was defined by the last occurrences (LOs) of *Nuttallides truempyi* and *Bulimina elongata*.

As pointed out in the biostratigraphy reports for the other Leg 120 sites (this volume), *N. truempyi* is not expected in shallow-water sites during late and late middle Eocene. We were able to corroborate at Site 748 (present water depth, 1290 m), the worldwide last appearance datum (LAD) of this species, which is at the Eocene/Oligocene boundary except at sites off Antarctica. We did not find it, however, at Site 749 (present water depth, 1069.5 m) in the upper Eocene. As expected, however, Samples 120-750A-1R-CC and 120-750A-3R-CC, from a present water depth of 2030.5 m, include a characteristically high number of *N. truempyi* in the upper middle Eocene. On the other hand, *Bulimina elongata*, a common constituent of this assemblage at the previous middle to lower bathyal sites, are not found at the lower bathyal to abyssal Site 750.

Frequent additional components of this assemblage are *Cibicides* spp., *Stilostomella* spp., *Anomalina spissiformis*, *Pullenia eoacenaica*, *Oridorsalis umbonatus*, and *Hanzawaia cushmani*. Accessory constituents are *Alabama dissonata*, *Spiroplectammina spectabilis*, *Plectofrondicularia lirata*, *Uvigerina* cf. *hispidocostata*, *Karrierella chapopotensis*, *Anomalinoides semicribratus*, *Fissurina* spp., *Gyroidina* spp., *Dentalina* spp., *Lenticulina* spp., and *Nodosaria* spp.

Assemblage 4b: Middle Eocene–Middle Early Eocene

The upper boundary of this assemblage is defined by the LO of *Bulimina bradburyi*. Because there was either no recovery or only wash cores retrieved, this boundary is situated somewhere between Samples 120-750A-3R-CC and 120-750A-8R-CC. Benthic foraminifer Assemblage 4b is only present in Sample 120-750A-8R-CC. Common constituents in this sample are *Nuttallides truempyi*, *Cibicides subspiratus*, *Oridorsalis umbonatus*, and *Cibicides* spp., whereas *Bulimina bradburyi*, *Pullenia eoacenaica*, *Vulvulina spinosa*, *Anomalina spissiformis*, *Lenticulina* sp., and *Stilostomella* spp. are minor components.

Assemblage 5a: Late Paleocene–Late Early Paleocene

Benthic Assemblage 4c could not be detected probably because of the widely spaced sample intervals. Assemblage 4c was defined at the previous sites by the occurrence of *Bulimina trinitatis* following the disappearance of *Stensioina beccariiiformis* at the top of the Paleocene.

In Sample 120-750A-10R-CC the co-occurrence of *B. trinitatis* and *S. beccariiformis* indicates the late Paleocene Assemblage 5a. This agrees well with dating by means of planktonic foraminifers (Zone P3b) and calcareous nannofossils (Zone NP5). Sample 120-750A-11R-CC of late Danian age (Zone P1C) is tentatively placed in this assemblage, because we did not find *Coryphostoma midwayensis* and *Bolivinoidea delicatulus* at this site. The LO of these species were chosen at Site 748 to indicate the upper boundary of benthic foraminifer Assemblage 5b.

Assemblage 5a is dominated by *Stensioina beccariiformis* with *Nuttallides truempyi* as the most common additional component. Common accessory components are *Lenticulina whitei* and *Anomalinoidea cf. semicribratus*. In addition, these samples include *Oridorsalis umbonatus*, *Pullenia coryelli*, *Neoponides hillebrandti*, *N. cf. lunata*, *Spiroplectamina subhaeringensis*, *Bulimina trinitatis*, *Pyramidina rudita*, *Anomalina praeacuta*, *Lenticulina* spp., *Gyroidina* spp., *Cibicidoides* spp., *Pleurostomella* spp., and *Stilostomella* spp. A few specimens of *Neoflabellina semireticulata*, *Gaudryina pyramidata*, *Dorothia trochoides*, *Osangularia velascoensis*, *Bulimina midwayensis*, *Dentalina* sp., and *Nodosaria* sp. are identified in Sample 120-750A-11R-CC.

Assemblage 5b: Early Paleocene

This assemblage comprises Samples 120-750A-12R-CC through 120-750A-14R-CC. *Nuttallides truempyi* becomes the dominant species and clearly outnumbers *Stensioina beccariiformis* in the older samples. *Coryphostoma midwayensis* is very common in Sample 120-750A-12R-CC whereas *Bolivinoidea delicatulus* becomes common in Sample 120-750A-13R-CC. *Anomalina praeacuta*, *Pullenia coryelli*, *Bulimina trinitatis*, and *Neoponides hillebrandti* are characteristic species throughout the assemblage. Frequently found accessory species are *Tritaxia aspera*, *Cibicidoides dayi*, *Cibicidoides* spp., *Lenticulina* spp., and *Neoflabellina semireticulata*. Complementary species in most samples of this assemblage are *Dorothia trochoides*, *Anomalinoidea cf. semicribratus* (only in Sample 120-750A-12R-CC), *Bulimina midwayensis*, *Pyramidina* sp., *Oridorsalis velascoensis*, *Lenticulina whitei*, *Neoflabellina jarvisi*, *Allomorphina* sp., *Gyroidina* sp., and *Anomalinoidea capitatus*.

In summary, different environmental conditions seem to have been present in the Paleogene at Site 750 in comparison with the previous Leg 120 sites. This is indicated by the less common occurrence of *Bulimina* spp. throughout the Paleogene and the dominance of the lower bathyal to abyssal *Nuttallides truempyi* and *Stensioina beccariiformis*. This difference in the faunal composition is mainly a reflection of the deeper paleowater depth (about the same or somewhat deeper than present water depths throughout the investigated sequences) at Site 750 in comparison to the previous sites.

In addition, it might be an indication of a less productive area, because *Bulimina*-dominated faunas are known to prefer a low oxygen/high organic carbon environment with a high supply of particulate organic matter. In other words, Sites 747 through 749 might have been situated in a high productivity area throughout most of the Cenozoic.

The Cretaceous benthic faunas have not been studied in detail at this time, although preservation in the younger Cretaceous is excellent and the composite fauna from all samples is very diverse. Most of the benthic foraminifers are similar to those described from the Santonian-Campanian of Western Australia by Belford (1960), but many deeper-water elements are present that do not occur in the continental shelf faunas from Western Australia.

Bolivinoidea draco (Marsson) is a prominent component of the uppermost Maestrichtian sample (120-750A-15R-CC) and *B. delicatulus* Cushman occurs in Samples 120-750A-17R-CC and 120-750A-22R-CC. *Bolivina incrassata* Reuss is a notable

element in many Campanian-Maestrichtian faunas as are *Neoflabellina praereticulata* Hiltebert and *Quadriformina allomorphinoides* (Reuss). *Gyroidinoidea*, so important at other Leg 120 sites, is much less evident here and *Stensioina beccariiformis* (White), *Nuttallides truempyi* (Nuttall) and *N. florealis* (White) are more important, which suggests a deeper-water deposition, perhaps in bathyal depths.

In Hole 750B, deep water benthic indexes are less prominent at the base, and most deposition seems to have taken place initially in inner and outer continental shelf depths, becoming deeper as time progressed. Such forms as *Marssonella oxycona* (Reuss), *Globorotalites conicus* (Carsey), *G. umbilicatus* (Loetterle), and *Nuttallinella coronula* (Belford) occur with deeper-water forms like *Stensioina beccariiformis* down to Sample 120-750B-7W-CC. Stratigraphically below that sample, in Core 120-750B-11W, shallower-water forms, such as *Valvulineria erugatus* Belford and *Reussella szajnochae* (Grzybowski), become more important.

The dark shale facies in Core 120-750B-11W contains a significant fauna of agglutinated species, a fauna not seen elsewhere on Leg 120. In addition, many foraminifers have been crushed during compaction of the sediment.

Calcareous Nannofossils

Cenozoic

Two holes were drilled at Site 750. Nine washed and rotary cores were taken alternately in the upper 297.8 m of the sedimentary section penetrated in Hole 750A. Since lower upper Paleocene sediments were reached at 297.8 mbsf, we initiated continuous coring with the expectation that a continuous Danian-Maestrichtian section might be recovered. A thick Danian (over 40 m) to Maestrichtian (over 70 m) section was then penetrated, and the Cretaceous/Tertiary boundary was cored in Section 120-750A-15R-3 (around 350 mbsf). Recovery was irregular throughout the Cenozoic section and averages 50% in the Paleocene (Cores 120-750A-10R to -15R).

Hole 750B was washed down to 299 mbsf, at which level Core 120-750B-1W was taken. This is the single core taken in Cenozoic sediments from Hole 750B. Recovery was very poor and was restricted to a few fragments of chert, a piece of chalk, and small pebbles of chert and chalk.

Core 120-750A-1R (0–7.9 mbsf) contains a calcareous nannoflora representative of the middle Eocene and assignable to Zone NP16. Cores 120-750A-2W (7.9–56.4 mbsf) and 120-750A-3R (56.4–65.4 mbsf) also contain a rich, characteristic middle Eocene calcareous nannoflora, assignable to Zone NP15–NP16 (undifferentiated). There was no recovery of oozes from Cores 120-750A-4W (65.4–143.3 mbsf), -5R (143.30–153.0 mbsf), and -6R (153.0–162.6 mbsf). Chert fragments without calcareous crusts were recovered from Cores 120-750A-4W and -6R.

We recovered a characteristic lower Eocene (Zone NP12) calcareous nannoflora in Cores 120-750A-7W (162.6–259.2 mbsf) and -8R (259.2–268.9 mbsf). Core 120-750A-9W (268.9–297.8 mbsf) recovered lower upper Paleocene oozes (Zone NP6). A continuous lower upper through lower Paleocene sequence was recovered between 297.8 (Core 120-750A-10R) and approximately 350 mbsf (Sample 120-750A-15R-3, 91 cm). Sample 120-750A-10R-CC belongs to Zone NP5. The NP4/NP5 zonal boundary occurs between Samples 120-750A-11R-2, 55 cm, and 120-750A-11R-2, 77 cm. The NP2/NP3 zonal boundary occurs between Samples 120-750A-15R-1, 34 cm, and 120-750A-15R-1, 132 cm.

The Cretaceous/Tertiary boundary occurs at 91 cm within Section 120-750A-15R-3. The lowermost Paleocene Zone NP1 seems to be either extremely thin (0.5 cm) or absent. Dissolution on both sides of the boundary results in a stratigraphic uncertainty that only further detailed sampling and onshore studies

of the smallest taxa will resolve. Calcareous nannofloras are surprisingly rich a few centimeters above the boundary; they will be the object of a detailed onshore study.

Only one core (washed down to 299 mbsf) of Cenozoic sediments was taken from Hole 750B. The abundant, well-diversified, and well-preserved calcareous nannoflora in the ooze recovered from this core, either as worn pebbles or as encrustations on chert fragments, is of late early Eocene age (Zone NP13). These oozes originate from a level that was not cored in Hole 750A. Recovery in Hole 750B indicates extensive development of lower upper Eocene cherts. Considering the level at which Core 120-750B-1W was taken, it is clear in comparison with Hole 750A that lower horizons in the lower Eocene were sampled in the wash core, as well as possibly upper Paleocene intervals. Thus, it is not possible to resolve the question of the possible presence of a lower Eocene/lower upper Paleocene unconformity (see "Sedimentation Rates" section, this chapter).

In summary, Site 750 provided an extended, almost continuous section from lower upper Paleocene to Maestrichtian (discussed below) that will serve to illustrate in greater detail the paleontologic events associated with the Cretaceous/Tertiary boundary event. Although it is not possible to establish it clearly, the presence of a lower upper Paleocene/lower Eocene unconformity is suspected.

Cretaceous

Drilling at Site 750 recovered Upper Cretaceous nannofossils spanning the upper Turonian(?) through uppermost Maestrichtian. For logistical reasons (see "Operations" section, this chapter), much of the section was only discontinuously cored, preventing it from serving as an important reference section for the Southern Indian Ocean. Nevertheless, nannofossil preservation and abundance in the sediment is quite favorable for establishing a biostratigraphic framework, allowing paleoceanographic deductions and permitting correlation of this pelagic section with the more marginal marine section at Site 748.

The upper part of the Cretaceous section, cored mostly in Hole 750A, consists of cherts with interbedded nodular chert. The lower part of the Cretaceous section, discontinuously cored in Hole 750B, consists of harder, often silicified limestones and chert with only a few softer chalk horizons. Core-catcher samples from Hole 750B were often useless for biostratigraphic purposes. Much of the analysis was based on samples of softer lithologies chosen after the core was split.

Hole 750A

The uppermost Cretaceous lies in contact with the lowest Paleocene at Sample 120-750A-15R-3, 90–91 cm. Visual inspection of the core reveals that the contact is an artifact of rotary drilling procedures, since the Paleocene cherts lie on softer, disturbed Maestrichtian ooze and chalk with several chert fragments at the boundary. Preliminary examination of the Paleocene nannofossil biostratigraphy (discussed above) also suggests that much of the earliest Paleocene record (Zone NP1) is missing. Below the contact, the sediment contains moderately preserved assemblages that include *Nephrolithus frequens*, *Cribrosphaerella daniae*, and rare *Prediscosphaera grandis* without *Nephrolithus corystus*.

The presence of *N. frequens* without *N. corystus* is indicative (at this paleolatitude) of the uppermost Maestrichtian, following the stratigraphy of Huber et al. (1983). This uppermost Maestrichtian assemblage occurs within the interval from the Cretaceous/Tertiary contact through Sample 120-750A-16R-3, 21–22 cm (350–359.7 mbsf). Preservation improves from moderate to good downward through the interval.

Nephrolithus frequens is joined by *N. corystus* in Sample 120-750A-16R-CC. These two species co-occur throughout the

rest of the range of *N. frequens* (Sample 120-750A-16R-CC through Core 120-750A-19R; 365.3–394.4 mbsf), defining the lower part of the *N. frequens* Zone. The presence of *N. corystus* is also suggestive of the austral character of the assemblages, although other austral indicators are not common in the upper part of the interval. For example, *Monomarginatus quaternarius* does not appear in abundance until the lower portion of the interval (Cores 120-750A-18R and -19R). This may indicate progressive warming through the late Maestrichtian, although quantitative work will be necessary to examine this phenomenon.

Core 120-750A-20R and Sample 120-750A-21R-1, 32–33 cm (394.4–404.3 mbsf) contain *Reinhardtites levis* without *Tranolithus phacelosus*, indicating the *R. levis* Zone of early Maestrichtian age. The frequent occurrence of *Nephrolithus corystus*, *Monomarginatus* spp., and *Biscutum magnum* indicate the austral nature of the assemblages. The absence of assemblages that lack both *N. frequens* and *R. levis* (the combined *Arkhangelskiella cymbiformis/Lithraphidites quadratus* Zone) confirm the absence of such a "gap zone" at these high latitudes.

The interval from Sample 120-750A-21R-1, 114–115 cm, through Core 120-750A-25R (405.1–457.3 mbsf) contains *Tranolithus phacelosus* and *R. levis* without *Aspidolithus parvus*. This association indicates the earliest Maestrichtian part of the *T. phacelosus* Zone (CC23b). Austral taxa are common throughout the interval. *Nephrolithus corystus* has its first occurrence (FO) in Sample 120-750A-23R-CC and is common above this level. A single, reworked specimen of *A. parvus constrictus* occurs in Sample 120-750A-24R-CC. Preservation in Core 120-750A-25R is generally poor with abundant micrite diluting the nannofossils. Core recovery from Hole 750A ended at this point due to bit failure.

Hole 750B

Hole 750B was discontinuously cored using the strategy described in the biostratigraphy introduction (above). Cores 120-750B-2W through -11W recovered sediment containing Cretaceous nannofossils.

Core 120-750B-2W consists of chert fragments with a small quantity of adherent chalk. Scrapings of this chalk yielded a nannofossil assemblage containing *Nephrolithus frequens*, *Cribrosphaerella daniae*, and *Arkhangelskiella cymbiformis* (s.s.), indicating the late Maestrichtian *N. frequens* Zone. This material could have been derived from anywhere within the cored interval (299–450 mbsf), although results from Hole 750A suggest it was derived from approximately 350 to 400 mbsf.

Cores 120-750B-3R and -4W (450–478.9 mbsf) contain *Tranolithus phacelosus* and *Reinhardtites levis* without *Aspidolithus parvus*, indicating the lower Maestrichtian part of Zone CC23. This section is a continuation of the zone in which Hole 750A ended. Austral taxa (*Monomarginatus* spp., *Misceomarginatus pleniporus*) are common. A single specimen of *Aspidolithus parvus constrictus*, found in Sample 120-750B-3R-1, 43–44 cm, is considered to have been reworked.

The interval from Core 120-750B-5R through Sample 120-750B-6W-1, 90–91 cm, contains *Aspidolithus parvus expansus* and (sporadically) *A. parvus parvus* without *Reinhardtites anthophorus* and *Eiffelithus eximius*, indicating the upper Campanian part of Zone CC23. The lowest sample (120-750B-6W-1, 90–91 cm) contains rare reworked specimens of *Eiffelithus eximius* as well as numerous specimens of *Helicolithus trabeculatus* and *Broinsonia dentata*. The *E. eximius* specimens (in particular) exhibit distinctly greater diagenetic alteration (overgrowth) than the autochthonous assemblage. Based on the range of *E. eximius* and the local range of *H. trabeculatus* and *B. dentata*, the source of the reworked material is thought to be from the lower to lower upper Santonian (equivalent to that occurring in Core 120-750B-10W).

Samples 120-750B-6W-2, 30–31 cm, and 120-750B-7W-1, 0–1 cm, contain all three subspecies of *A. parvus* and *R. anthophorus* without *E. eximius*, indicating the uppermost part of the upper Campanian Zone CC22. As at Site 740, there is a significant stratigraphic interval between the last *R. anthophorus* and the last *E. eximius*.

The occurrence of *E. eximius* and *R. levis* in the interval from Sample 120-750B-7W-1, 45–47 cm, through 120-750B-7W-CC (508.3–527.3 mbsf) indicates the late Campanian Subzone CC22c. The genus *Monomarginatus* occurs throughout, indicating the austral nature of the assemblages. This upper Campanian interval lies disconformably on the underlying sequence, with much of the upper and lower Campanian missing across the unconformity.

Core 120-750B-8W contains assemblages of the early Campanian Zone CC18, as indicated by the occurrence of *A. parvus* and *Seribiscutum primitivum*. The common to frequent occurrence of the latter indicates the austral nature of these assemblages.

The late Santonian Zone CC17 is represented by sediment in Core 120-750B-9W and Sample 120-750B-10W-1, 36–38 cm (546.7–566.38 mbsf). Placement of the Santonian-Campanian boundary (between Cores 120-750B-8W and -9W) is based on the first appearance datum (FAD) of *A. parvus parvus*. *Biscutum coronum* has its FO at the base of this interval, at approximately the same level as the LO of *Eprolithus floralis*. *Seribiscutum primitivum* occurs throughout the interval, suggesting an austral affinity for these assemblages.

Eprolithus floralis occurs with *Lucianorhabdus cayeuxii* in the interval from Sample 120-750B-10W-1, 48–50 cm, through 120-750B-10W-1, 80–81 cm (566.5–566.8 mbsf), indicating the late Santonian Zone CC16. It is uncertain whether the thinness of this zone (<76 cm) is a true reflection of the sedimentary sequence or is an artifact of the drilling strategy.

Samples 120-750B-10W-1, 114–118 cm, and 120-750B-10W-CC contain *Micula decussata*, *Reinhardtites anthophorus*, and *Lithastrinus septenarius* without *Lucianorhabdus cayenxi*, indicating the early Santonian Zone CC15. *Seribiscutum primitivum* occurs commonly throughout the interval, indicating the austral character of the assemblages.

The nature of the drilling strategy makes it impossible to determine whether Cores 120-750B-10W and -11W are separated by an unconformity. At least one and a half zones are unrepresented between the material recovered at the base of Core 120-750B-10W and the top of Core 120-750B-11W. The latter contains *Eiffellithus eximius* without *M. decussata* or *R. anthophorus*, indicating Zones CC12–CC13a of late Turonian to early Coniacian age.

Radiolarians

Hole 750A

In Hole 750A, core-catcher samples were examined from Cores 120-750A-3R, -7W, -8R, -9W, -10R, -12R, -14R, -15R, -17R, -19R, -20R, -22R, and -25R. Sample 120-750A-3R-CC contains common, moderately preserved radiolarians. All other samples contain no radiolarians, except for Sample 120-750A-22R-CC, which includes very rare, poorly preserved radiolarians.

Sample 120-750A-3R-CC includes *Lychnocanoma amphitrite*, *Cyclampterium milowi*, *Lophocyrtis biaurita*, *Lophoconus titanothericeraos*, *Eusyringium fistuligerum*, *Sethochytris babylonis*, *Sethochytris* sp. of Chen (1975), and *Stylacanthium* sp. with robust spines. This assemblage indicates an Eocene age and is similar to the assemblages from the middle to upper Eocene of Sites 748 and 749.

Sample 120-750A-22R-CC contains *Dictyomitra* sp. and *Amphipyndax stocki*, which indicate a Cretaceous age.

Hole 750B

In Hole 750B, we examined the following samples: 120-750B-3R-CC; 120-750B-4W-CC; 120-750B-5R-CC; top of 120-750B-6W; 120-750B-6W-CC; 120-750B-7W-1, 10–12 cm; 120-750B-8W-2, 15–16 cm; 120-750B-9W-1, 46–47 cm; 120-750B-10W-1, 97–98; 120-750B-11W-CC; 120-750B-13W-CC; and 120-750B-14W-CC. Core-catcher samples from Cores 120-750B-3R, -4W, -13W, and -14W contain rare, very poorly preserved radiolarians or only fragments of radiolarians, rendering specific assignment impossible. The other samples include rare to few, poorly preserved radiolarians.

Samples from Cores 120-750B-3R to -9W include *Amphipyndax stocki* and/or *Dictyomitra* sp., which indicate a Cretaceous age. Sample 120-750B-6W-CC contains relatively well-preserved radiolarians including *Amphipyndax stocki*, *Dictyomitra* sp., *Stichomitra asymbatos*, *Spongosaturnalis?* spp., and some fragments of neosciadiocapsids(?).

Samples from Cores 120-750B-10W and -11W include relatively diversified radiolarians when compared with the above sections. These two samples contain *Amphipyndax stocki*, *Dictyomitra* sp., *Stichomitra asymbatos*, *Cryptamphorella conara?*, *Solenotryma?* sp., *Neosciadiocapsa?* sp., *Theocampe* sp., and *Pseudocrucella?* sp. Sample 120-750B-11W-CC also contains *Paronaella?* sp., *Acaeniotyle?* sp., and *Alievium?* sp. The occurrence of *C. conara?* suggests a late Cretaceous age, but a more detailed age determination is impossible because of the absence of other age-diagnostic taxa.

Diatoms

Pliocene-Pleistocene

Diatoms are present only in the upper three cores of Hole 750A. Core 120-750A-1R apparently double-punched the mud line, resulting in the recovery of Pliocene-Pleistocene sediments at the top (Core 120-750A-1R-1, 0–37 cm) and bottom (Core 120-750A-1R-6, 38–73 cm) of this core (see “Lithostratigraphy and Sedimentology” section, this chapter). Three distinct diatom assemblages, separated by two sandy lag-gravel horizons, are identified in the upper 37 cm of Section 120-750A-1R-1.

In this section, the youngest interval (0–10 cm) belongs to the lower Pleistocene *Coscinodiscus elliptopora/Actinocyclus ingens* Zone (0.62–1.58 Ma) based on the presence of *A. ingens* and an assemblage dominated by *Nitzschia kerguelensis* and *Thalassiosira lentiginosa*. A lag deposit of manganese-coated stones separates this diatom assemblage from the underlying mid-Pliocene diatom assemblage *Nitzschia interfrigidaria/Coscinodiscus vulnificus* Zone (2.8 to 3.1 Ma). The identification of this lower zone is based on the co-occurrence of *N. interfrigidaria* and *C. vulnificus*. This zone is noted in the interval between Samples 120-750A-1R-1, 12 cm, and 120-750A-1R-1, 22 cm. A major unconformity representing approximately 40 m.y. underlies this mid-Pliocene assemblage and is identified by a lag-gravel deposit resting on middle Eocene nannofossil ooze.

A thicker lower Pleistocene interval than the one present in Section 120-750A-1R-1 was recovered at the base of Section 120-750A-1R-6 due to the double spud-in during rough seas. Approximately 35 cm of the lower Pleistocene *C. elliptopora/A. ingens* Zone was recovered in Core 120-750A-1R-6, 38–73 cm. The upper one third of this lower Pleistocene interval in Section 120-750A-1R-6 is a diatom-bearing foraminifer ooze that was either not recovered or was disturbed in the upper part of Section 120-750A-1R-1. The lower two thirds of this interval from Core

120-750A-1R-6, 49–73 cm, is diatom-bearing gravel, equivalent to the upper 11 cm recovered in Section 120-750A-1R-1.

Middle Eocene

Rare and poorly preserved diatoms, including *Ethmodiscus rex* and *Pyxilla* spp. fragments are noted in the bottom of Section 120-750A-1R-3. Diatoms are better represented in Sample 120-750A-3R-CC, but they are still poorly preserved and occur in low number. Species in this sample include *Hemiaulus polymorphus*, *Melosira sulcata* var. *crenulata*, *Pseudotriceratium radiosoreticulatum*, *Pseudorutilaria monomembranacea*, *Sceptro-neis* spp., *Stephanopyxis* spp., *Triceratium inconspicuum* var. *trilobata*, and *Triceratium pulvinar*. All other core-catcher samples from Hole 750A were barren of siliceous microfossils.

Silicoflagellates, Ebridians, and Endoskeletal Dinoflagellates

Only samples from the base of Section 120-750A-1R-3 and 120-750A-3R-CC contain Cenozoic representatives of these siliceous microfossil groups. Diagenetic processes related to chert formation are most likely responsible for the absence of siliceous microfossils in samples below these intervals.

Silicoflagellates from the above samples belong to the middle Eocene *Mesocena apiculata* Subzone of the *Dictyocha grandis* Range Zone of Shaw and Ciesielski (1983). This assemblage includes the following taxa: *Cannopilus* spp., *Dictyocha fibula*, *D. grandis*, *Distephanus quinquangellus*, *Mesocena apiculata*, *M. occidentalis*, and *Naviculopsis constricta*.

Rare and poorly preserved Upper Cretaceous silicoflagellates *Lyrulula furcula*, *L. simplex*, and *Corbisema* spp. were encountered in Sample 120-750B-6W-CC.

Ebridians and endoskeletal dinoflagellates assemblages are not assignable to a zonal scheme, but they are similar in composition to that recovered in middle Eocene intervals from Holes 748B and 749B. Assemblages include the following taxa: *Ebriopsis antiqua*, *E. crenulata*, *Hovaserbia brevispinosa*, *Micromarsipium anceps*, *Pseudoammodochium sphaericum* (ebridians), and *Carduifolia onoporoides* and *C. gracilis* (endoskeletal dinoflagellates).

Calcspheres

Hole 750A

Calcspheres are a common constituent of all samples between Sections 120-750A-12R-CC and 120-750A-25R-CC, inclusive, and thus occur in Danian and Maestrichtian sediments. They were reported from Site 738 at approximately the same interval. Nothing appears to have been published on the Indian Ocean calcspheres since Bolli's (1974) review and his treatment of the Upper Jurassic–Lower Cretaceous forms. No satisfactory taxonomic analysis could be performed on board ship, but a study will be completed for the Leg 120 *Scientific Results* volume. Material studied here is that retained on a 63- μ m sieve, predominantly from core-catcher samples. Several different forms seem to be present, and there is a stratigraphic order to their occurrence.

Samples 120-750A-12R-CC and 120-750A-13R-CC (Danian) have the same two forms in common; these are much more abundant in Sample 120-750A-12R-CC. Neither is quite spherical, but both are of the same size (about 80 μ m). The two forms are distinguished on aperture size: one minute and not always visible, the other very large. Both appear to have very fine textured or smooth but not polished surfaces. However, surface details cannot be studied satisfactorily with the light microscope and must await shore-based scanning electron microscope (SEM) study.

Samples 120-750A-14R-CC to 120-750A-25R-CC contain a biota distinct from that above. Two species occur, both considerably larger than and easily differentiated from those in the higher samples. One species is spherical, about 110 μ m in diameter with an aperture intermediate between and not overlapping with those of the younger forms. The second species is elongate, typically 125 \times 80 μ m with a thick wall and narrow, parallel-sided internal cavity obvious through the wall. Both species have smooth (but not polished) surfaces. These species co-occur in all samples examined, but the ratio varies considerably.

Hole 750B

Calcspheres are also present in this hole, and the biota described above extends downhole to Section 120-750B-6W-CC. Cores 120-750B-7W through -10W appear to be barren of calcspheres. Section 120-750B-11W has a fauna of approximately spherical forms, intermediate in size between the spherical forms of the higher samples but with a minute aperture. There appears to be a potentially useful stratigraphic order to these forms.

Macroscopic Plant Material

Cores 120-750B-12W and -13W consist of nonmarine clays, silts, and coarse sands with abundant authigenic minerals; they possibly represent aqueous sedimentation and paleosols. They contain abundant clasts of carbonized wood up to 5 cm across, the diameter of the core suggesting that they are parts of even larger fragments. They should yield data on climate and nearby vegetation.

Palynology

A preliminary shore-based palynological study was conducted by B. Mohr (written comm., 1989) in order to provide an age determination for lithologic Unit IV, which contained no microfossils datable on board ship. Three samples examined from Core 120-750B-12W, Sections 1–3, were barren of palynomorphs. Three samples from Core 120-750B-13W, however, contained large amounts of organic matter, including well-preserved wood particles and cuticles and very well-preserved spores and pollen.

The assemblage is entirely terrestrial, and the following spore taxa are present: *Gleicheniidites* sp. (very common), *Stereisporites* sp., *Baculatisporites comaumensis*, *Foveogleicheniidites confossus*, *Aequitriradites spinulosus*, *Densosporites velatus*, and *Dictyotosporites complex*. Among the pollen taxa *Clavatipollenites hughesii* were identified. No other angiosperm pollen, except for this primitive one, were found. This occurrence, plus the presence of the *Dictyotosporites* complex (LO in approximately middle Albian), make an Albian age for this assemblage very probable. This age determination has been confirmed by D. Hos (written comm., 1989). For the purpose of this report, we adopt an Albian age for the unit.

Summary

Coring strategy at Site 750 resulted in a discontinuous record of sedimentation. Despite this, several conclusions can be reached based on the paleontological analysis of the sediments recovered at this site, as summarized below.

Neogene and Quaternary

Only a thin veneer of upper Cenozoic sediment exists at Site 750. Due to the rough sea conditions at the start of drilling operations, this thin sediment veneer was recovered twice in Core 120-750A-1R. Diatom biostratigraphy indicates two distinct ages for this sediment: a diatom-bearing foraminifer ooze of early Pleistocene age overlies a sandy gravel of mid-Pliocene age. The entire sequence is less than 1 m thick and lies disconformably over middle Eocene material.

Paleogene

The upper part of the Paleogene sequence at Site 750 was washed through in Holes 750A and 750B, with only a few spot cores. This upper part of the sequence began in middle Eocene nannofossil chalk and continued downward through upper Paleocene through middle Eocene chalk and chert. Spot coring revealed relatively good calcareous planktonic microfossil abundance and preservation, although siliceous microfossils were more poorly preserved and apparently restricted to the middle Eocene. Continuous coring began in the lower upper Paleocene and continued down through the Cretaceous/Tertiary boundary.

An apparently complete lower (but not lowermost) through lower upper Paleocene sequence was recovered in Hole 750A. This included an anomalously thick (around 45 m) Danian section with good calcareous fossil abundance and preservation. Two distinct assemblages of calcispheres are also evident in this section. The lowermost calcareous nannofossil zone (NP1) is either very thin or missing in the recovered sequence. This, and the obvious drilling disturbance at the boundary horizon, indicate that this sedimentary section (as recovered on Leg 120) will not be useful in investigations of the Cretaceous/Paleogene boundary crisis. However, the well-preserved calcareous fossil assemblages in the expanded Danian offer the potential for important studies on the early evolution of Cenozoic oceanic biotas as well as the history of the oceanic recovery following the catastrophic Cretaceous/Paleogene boundary event(s).

Four of the benthic foraminifer assemblages previously defined at other Leg 120 sites have been recognized in the Paleogene of Site 750. Preliminary investigation of the benthic foraminifer record suggests that Site 750 was consistently deeper during the Paleogene than the other Leg 120 sites and productivity at Site 750 was probably lower during the Paleogene than at the other Leg 120 sites.

Cretaceous

The combination of continuous coring in the upper part of the Cretaceous sequence (Hole 750A) and spot coring in the lower part of the sequence (Hole 750B) yielded a relatively good, albeit discontinuous, record of the history of Cretaceous sedimentation at Site 750.

A relatively complete record of the Maestrichtian exists at Site 750. Biostratigraphic control is based on calcareous plankton fossils, although the sporadic, moderately preserved radiolarian faunas may add additional information after further investigation.

A thick upper Campanian sequence was recovered at the site. Many of the biohorizons found useful at Sites 747 and 748 were well expressed in the pelagic record at Site 750 (especially true for the nannofossils). An examination of additional samples should provide a reliable, high-resolution correlation between these sites and greatly aid in interpreting the Late Cretaceous history of the Kerguelen Plateau as well as the Indian Ocean.

Beside the value of this relatively complete upper Campanian through Maestrichtian record to Southern and Indian ocean biostratigraphic studies, changes in assemblage composition suggest significant climatic variations at Site 750 during this time. The occurrence of numerous globotruncanids in the upper part of the sequence suggests relatively warm conditions at the site during the latest Maestrichtian. These assemblages suggest that Site 750 was in or near the Tethyan FP during the latest Maestrichtian.

Changes in planktonic foraminifer assemblage composition downsection suggest that the site was within the Transitional FP during the late (but not latest) Maestrichtian. The early and

middle Maestrichtian was apparently characterized by transitional to fully austral conditions at the site. The site was evidently part of the Austral FP during the late Campanian. The composition of the nannofossil assemblages appears to reflect, albeit to a lesser degree, a similar progressive warming in the late Maestrichtian.

In an effort to remind us of our limitations as mortals, the Kerguelen Plateau delivered, as our last bit of Cretaceous pelagic sediment, Core 120-750B-11W. The combined efforts of the planktonic foraminifer and calcareous nannofossil biostratigraphers have yielded four distinct age determinations for material in this core, not one of which is truly corroborated by the other fossil group. Investigations of the planktonic foraminifers indicate at first glance an age of Santonian or even Campanian for the bulk of the sediment in the core.

In addition, we observed well-preserved fossils in samples of drilling paste and as reworked specimens in the dominant (Campanian?) sediment, which indicated that additional material of late Cenomanian and early Turonian age exists at Site 750. Calcareous nannofossil biostratigraphy, on the other hand, dates the dominant sediment as late Turonian to early Coniacian, with the possibility that it could be as young as late Santonian if very unusual paleoecologic exclusion was operating at the site. In addition, very rare coccoliths similar to a species known to have become extinct in the latest Cenomanian were observed. Clearly, more work needs to be done on this enigmatic core before it can provide clues to the early oceanic history of the Kerguelen Plateau. For purposes of this report, however, we adopt a late Turonian to early Santonian age for the core.

The lowest sedimentary unit consists of reddish brown silty claystones and clayey siltstones with a few interbedded conglomerates. No marine fossils were observed in this sequence. The common occurrence of carbonized wood, in conjunction with the basic sedimentary features, suggests a terrestrial origin for this unit (see "Lithostratigraphy and Sedimentology" section, this chapter). The wood fragments are large enough that their examination may yield evidence about the paleoclimate existing on the Plateau during its deposition. Shore-based palynological investigations have yielded an Albian age determination for this unit, and future studies may provide additional information on the terrestrial flora of this ancient depositional environment.

PALEOMAGNETICS

Site 750 is located on the eastern margin of the Raggatt Basin (57°35.54' S, 81°14.42' E). At Hole 750A 5 cores were recovered by rotary coring, and the remaining cores were washed down for the first 298 mbsf. Therefore, the first 9 cores (0–298 mbsf) were unsuitable for determining magnetostratigraphy. The only continuous coring (with average recovery about 50%) was from Cores 120-750A-10R to -20R. These 11 cores (298–404 mbsf) were measured with the pass-through cryogenic magnetometer at 10 cm between measurements.

The rotary drilled cores consisted of undisturbed segments of consolidated sediment (drill biscuits) with very disturbed sections between them. This type of core cannot be expected to provide a continuous magnetostratigraphic record. The only way to identify some of the normal and reversed segments was with the help of the paleontologists by cross-correlation with biostratigraphic zones (see "Biostratigraphy" section, this chapter).

First, natural remanent magnetization (NRM) was measured on all cores that were not too badly disturbed (Fig. 21). Subsequently, each core was alternating-field (AF) demagnetized with a peak field of 9 mT and remeasured (Fig. 22). Because of the incomplete recovery, there are gaps between measurements from different cores, which results in blocks of data every 9.6 m. It is

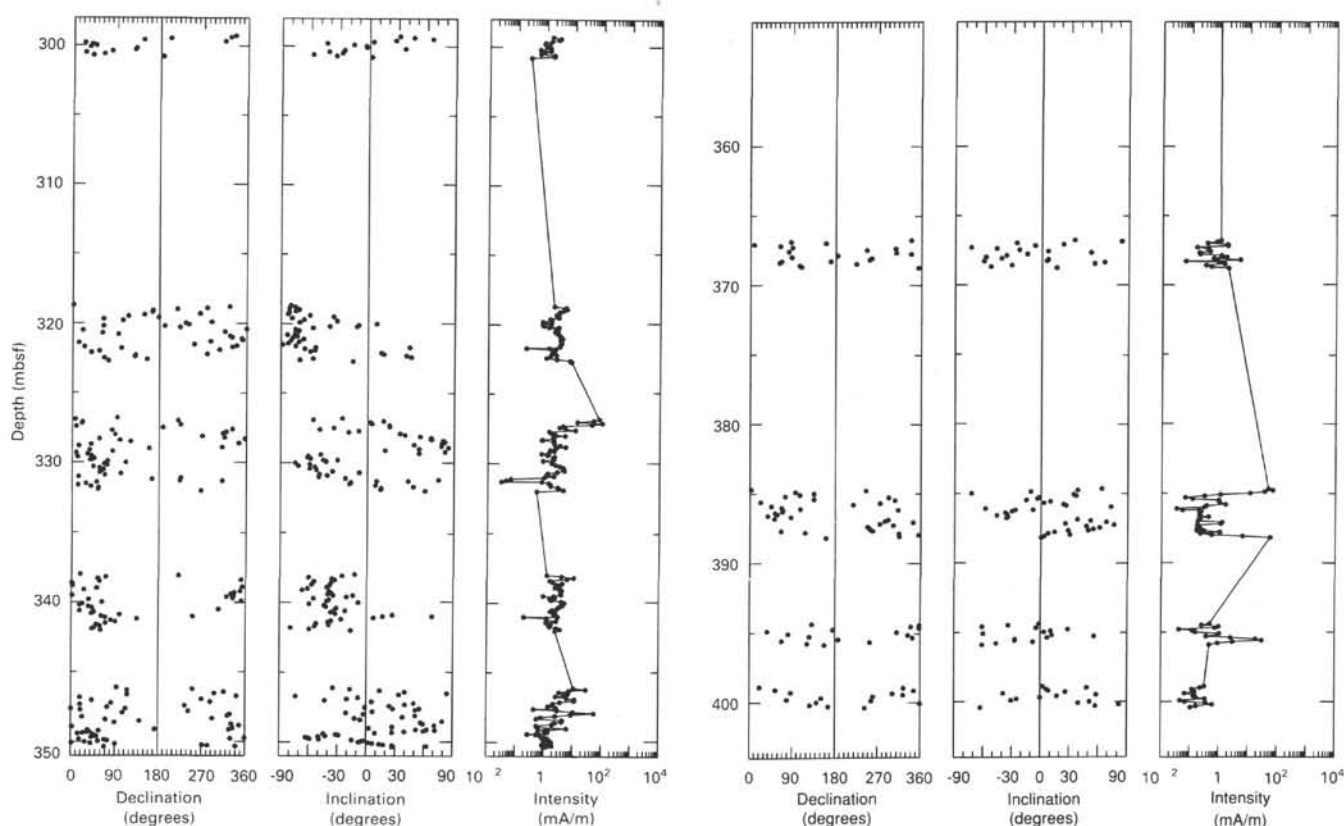


Figure 21. Declination, inclination, and intensity of natural remanent magnetization of Cores 120-750A-10R to -20R (297.8–404.0 mbsf). The archive halves of cores were measured with the pass-through cryogenic magnetometer. The data gaps in the declination and inclination plots are due to the incomplete recovery of rotary cores and the movement of all sections to the top of a core.

worthwhile to note that the declinations of the NRM's in Figure 21 are quite randomly distributed between 0° and 360° . After AF demagnetization at 9 mT, there seems to be a certain bias toward positive declination values between 20° and 120° (Fig. 22). This clustering of declinations could be possibly explained by the induction of a small anhysteretic remanent magnetization (ARM) by the demagnetization coils along the x - and y -axis.

Following the practice from the three previous sites, we interpreted the inclination record after AF demagnetization in terms of polarity intervals. The normal polarity sequence in Core 120-750A-12R (below 318 mbsf in Fig. 22) is interpreted as the lower part of Anomaly Correlative 27 in the early Paleocene. The normal period in Core 120-750A-14R (339 mbsf) occurs where Anomaly Correlative 28 should fall based on paleontologic evidence. The short normal-reversed-normal sequence at the top of Core 120-750A-20R (395 mbsf) is tentatively identified as part of Anomaly Correlative 32 in the early Maestrichtian. Measurements of the discrete samples might improve these results.

The remanence after AF demagnetization above and below the Cretaceous/Tertiary boundary (350 mbsf) is reversed (Fig. 22). These whole-core measurements were confirmed by measurements with the spinner magnetometer on eight discrete samples between 349.57 and 350.25 mbsf. A reversed magnetic polarity at the Cretaceous/Tertiary boundary was found at Deep Sea Drilling Project (DSDP) Site 577 (Wright et al., 1985) and is expected from the Berggren et al. (1985a) time scale. Therefore, we can correlate the reversed interval between 347.0 and 350.3 mbsf (Fig. 22) to the reversed Chron C29R.

We measured the magnetic susceptibility (K) with a 3-cm spacing on the archive half of Section 120-750A-15R-3, which

contained the Cretaceous/Tertiary boundary (see "Biostratigraphy" section, this chapter). We found a sevenfold increase in susceptibility from the top of the section until K reached its maximum at 94 cm down the section exactly at the bottom of the Danian sediments (Fig. 23). The rapid drop of K reflects the change in lithology (see "Lithostratigraphy and Sedimentology" section, this chapter). The detailed features of the susceptibility curve of Figure 23 have been confirmed by susceptibility measurements on discrete samples from Section 120-750A-15R-3.

A peak in initial susceptibility at the Cretaceous/Tertiary boundary has been observed previously in sections of DSDP cores (Worm and Banerjee, 1987). These authors identified the magnetic material causing this peak in K as small black spherules of magnetite. Another possible explanation for the increase in susceptibility could be an increase in iron-rich clay minerals above the Cretaceous/Tertiary boundary. The increase in K we observed may be an indicator for two magnetic phases. The broad maximum in K in Figure 23 could reflect the contribution from clay minerals, whereas the sharp maximum just above the boundary could be caused by a thin layer of black magnetite spherules. The abrupt decrease in K could be caused by an unconformity at the Cretaceous/Tertiary boundary.

Of the basement samples from Hole 750B, seven samples from two flows were investigated on board ship. Six basalt samples were stepwise AF demagnetized, and one sample was progressively thermally demagnetized up to its Curie temperature. The results of the demagnetization experiments are summarized in Table 5, where the boundary between the two flows is indicated by a line. The characteristic inclination (I) for each sample was determined by fitting a straight line through at least three data points on a Zijderveld plot. As an example, the AF demag-

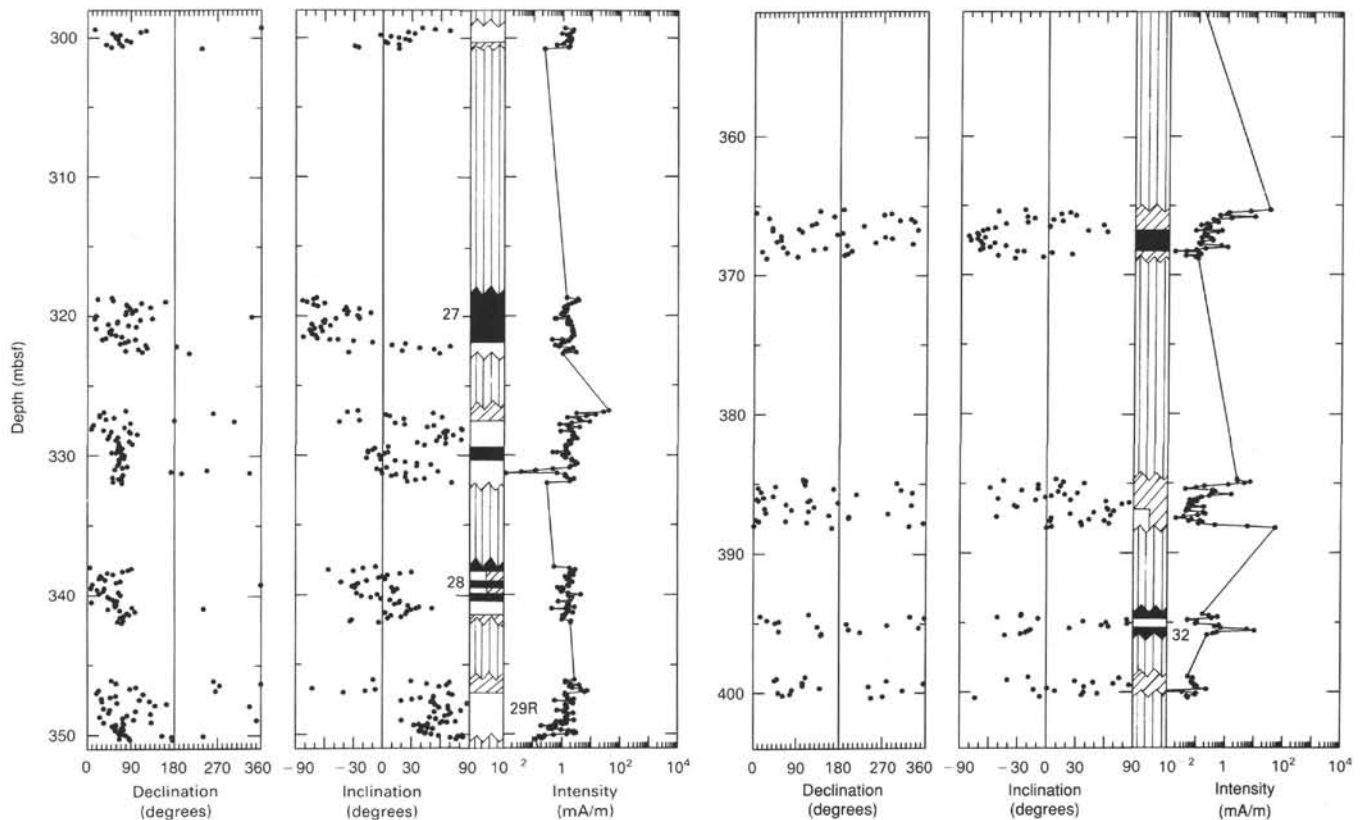


Figure 22. Declination, inclination, and intensity of Cores 120-750A-10R to -20R (297.8–404.0 mbsf) after peak alternating-field (AF) demagnetization at 9 mT. A preliminary identification of normal (black) and reversed (white) polarity chrons is shown to the right of the inclination record. Data gaps are indicated by vertical lines and uninterpretable data by diagonal lines. Polarity chrons, which are based on less reliable data, are drawn with one half appearing as diagonal lines.

netization properties for Sample 120-750B-16R-8, 34–36 cm, are plotted in Figure 24. The intensities of NRM (M_0) and the median destructive fields are also shown in Table 5.

The mean inclination and 95% confidence limit are calculated by Kono's (1980) method from the seven characteristic inclinations as 73° and 0.7° , respectively. The present inclination at Site 750 is 72° , assuming an axial geocentric dipole field. The mean basalt inclination and the present inclination are nearly the same. There are two possible explanations for these similar inclinations. The first, but less likely, explanation is that Sites 748 and 750 in the Raggatt Basin form one tectonic block and moved independently from Sites 747 and 749 (see "Paleomagnetism" section, Site 749 chapter).

The second (and in our opinion more probable) explanation is that the magnetic remanences of the basement at Site 750 are mainly present-field overprints. The results of thermal demagnetization indicate a bimodal distribution of blocking temperatures (Fig. 25). A bimodal distribution of blocking temperatures seems to occur in the highly altered basalts of Sites 748 and 750 (see "Igneous Petrology" sections, Sites 748 and 750 chapters). An investigation of the magnetic mineralogy and rock magnetic properties should help to distinguish between the two possible interpretations of our inclination.

SEDIMENTATION RATES

The poor recovery of material in Holes 750A and 750B precludes precise calculation of sedimentation rates over a large part of the recovered Upper Cretaceous and Paleogene section. Estimates for the Maestrichtian-Danian sedimentation rates are, however, based upon more reliable data.

Sedimentation rate estimates for Site 750 are based upon calcareous microfossil (nannofossils and planktonic foraminifers) data (Table 6) that are used to construct the age-depth curve shown in Figure 26.

There may be a hiatus within the washed interval of 269–298 mbsf (between Cores 120-750A-8R and -10R). Alternatively, a marked reduction in sedimentation rate may have occurred in the late Paleocene–early Eocene interval at this site.

Sedimentation rates in the late Maestrichtian and Danian are estimated to be about 11 m/m.y., and late early Eocene to late middle Eocene rates to be about 30 m/m.y. An admittedly inadequate data base yields an estimated rate of 90 m/m.y. in the late Campanian–early Maestrichtian, but this rate should be viewed with caution pending additional shore-based studies. It appears that the average sedimentation rate from late Campanian through middle Eocene is high (about 20 m/m.y.), which indicates high pelagic productivity as exemplified by the numerous chert beds in the sequence.

INORGANIC GEOCHEMISTRY

Introduction

Two holes were drilled into Cenozoic and Cretaceous sediments and the underlying basaltic basement at Site 750, located on the Southern Kerguelen Plateau about 15 nmi east of Site 751. As the objective of this site was to drill Paleogene and Cretaceous sediments and basalt, no continuous coring occurred and thus interstitial water (IW) samples are restricted.

We obtained a total of four samples from depths between 300.75 and 387.65 mbsf and took one sample with only 4-mL

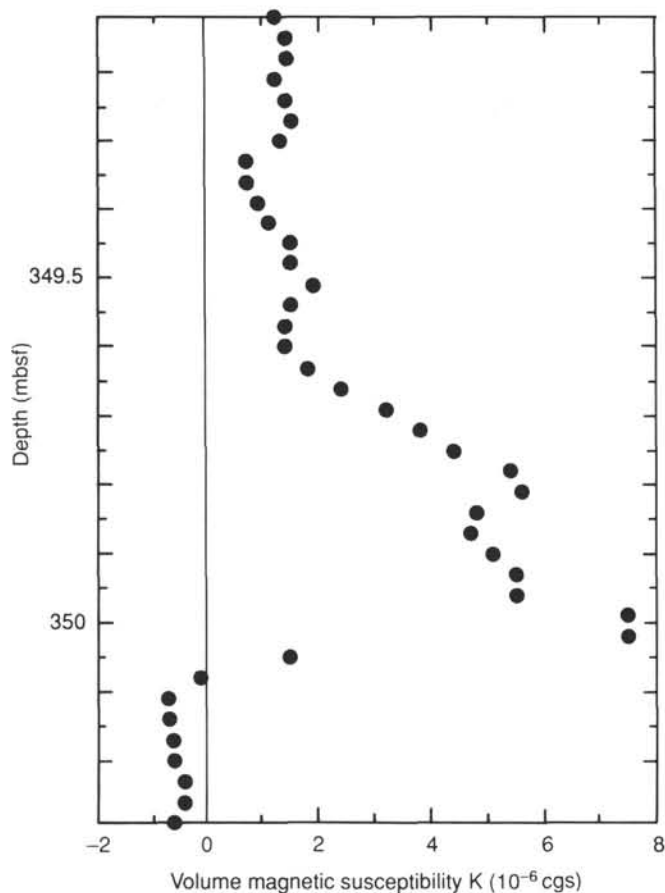


Figure 23. Low field susceptibility of Section 120-750A-15R-3 (349.1–350.6 mbsf) measured at 3-cm spacing across the Cretaceous/Tertiary contact. The susceptibility reaches a maximum at the bottom of the Danian and drops steeply at the contact with the Maestrichtian.

Table 5. Paleomagnetic results from demagnetization experiments on basalts from Hole 750B.

Core, section, interval (cm)	I (°)	M_0 (mA/m)	MDF (mT)	Demag
120-750B-				
15R-2, 78–80	-76	760	14	AF
15R-4, 126–128	-78	1704	—	Th
16R-3, 134–136	-73	2212	4	AF
16R-4, 98–100	-77	829	7	AF
16R-8, 34–36	-71	2768	14	AF
170-750B-				
17R-1, 49–51	-71	2253	17	AF
17R-2, 86–88	-69	2948	7	AF

Note: Six samples were stepwise demagnetized and one sample was thermally demagnetized to 590°C. The characteristic inclinations (I) were determined from orthogonal vector projections. M_0 is the NRM intensity and MDF is the median destructive field that is required to AF demagnetize one half of the NRM. The horizontal line represents the boundary between two flows.

squeezed fluid at 624.95 mbsf from clayey material supposed to represent altered basalt or volcanoclastic rocks. Shipboard analysis of pH, alkalinity, salinity, sulfate, chlorinity, magnesium, calcium, and silica were conducted according to the methods described by Gieskes and Peretsman (1986; see also “Explanatory Notes” chapter, this volume). Results of IW analyses are summarized in Table 7. All concentrations are given in millimoles per liter (mM) except for silica (μM).

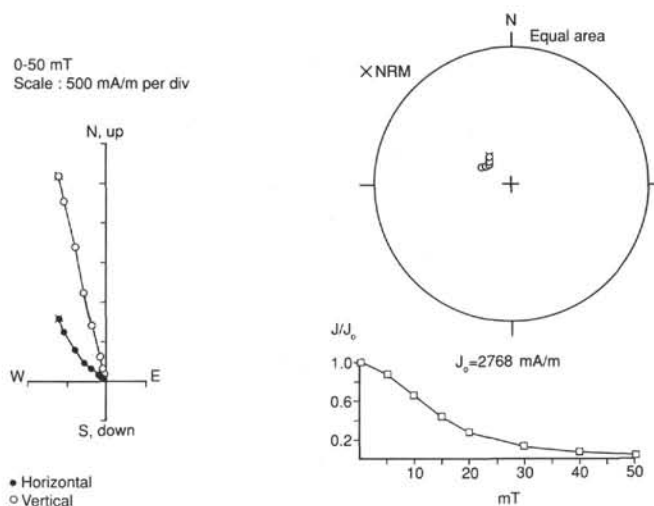


Figure 24. Alternating-field demagnetization of Sample 120-750B-16R-8, 34–36 cm. This sample possesses a stable single-component magnetization with a median destructive field of 12.5 mT.

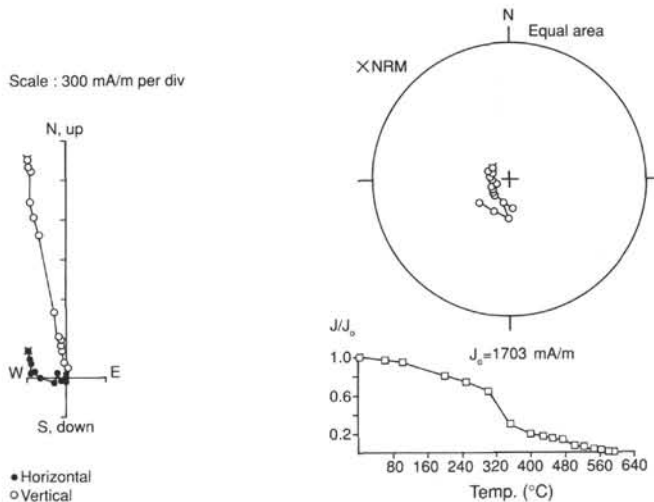


Figure 25. Stepwise thermal demagnetization of Sample 120-750B-15R-4, 126–128 cm. The remanence is unstable, especially above 400°C. The intensity decay curve suggests a bimodal blocking temperature distribution, possibly suggesting the presence of two magnetic phases.

Results

Salinity and Chlorinity

Salinity values for the upper four samples range from 36.2 to 36.4 g/kg and are on the average (36.25 g/kg) significantly higher than salinity values from the previous sites, where all the samples have been taken from depths above 300 mbsf (Fig. 27). Chlorinity values range from 559 to 566 mM.

The lowermost sample (120-750B-12W-1, 145–150 cm) has a high salinity of 38.3 g/kg, which is matched by a high concentration in Cl at 597 mM. Even with a terrigenous origin for the clayey material (see “Lithostratigraphy and Sedimentology” section, this chapter), subsequent burial in a marine environment as well as open-system water circulation account for the highly marine character of the IW.

Alkalinity and pH

The alkalinity values for the upper four samples range from 2.459 to 2.047 mM and decrease with depth (Fig. 27). The sharp-

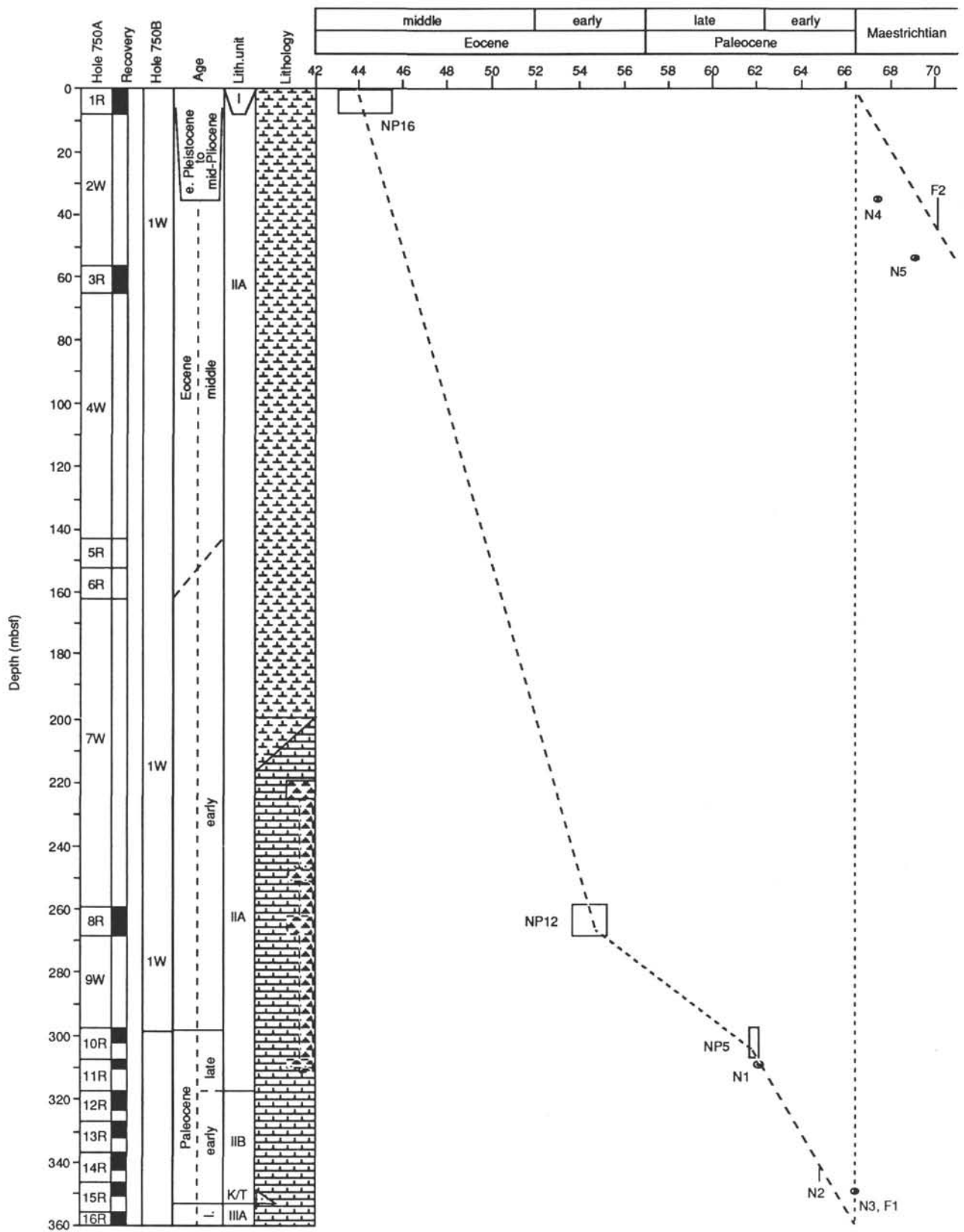


Figure 26. Estimated sedimentation rate curve for Site 750. Ages are as determined and described in the text. The biostratigraphic data is from the "Biostratigraphy" section (this chapter). The lithology is shown in the right-hand column at the left of the figure; for an explanation of the lithologic symbols, see "Lithostratigraphy and Sedimentology" section (this chapter) and the "Explanatory Notes" chapter (this volume). Biostratigraphic datum levels are from Table 6, which gives the age, depth, and name of each datum. Depth uncertainty in the placement of datum levels is shown by vertical lines, uncertainty in age calibration is shown by horizontal lines, and uncertainties in both depth and age, by hollow boxes. The dashed line of the age-depth curve denotes inadequacies in the data base to produce reliable rate estimates.

Table 6. Biostratigraphic data used to plot age-depth curve in Figure 26.

Biostratigraphic event			Core, section, interval (cm)	Depth (mbsf)	Age (Ma)
Calcareous nannofossils					
N1	<i>F. tympaniformis</i>	FAD	120-750A-11R-2, 55 120-750A-11R-2, 77	309.55 309.77	62.00
N2	<i>C. danicus</i>	FAD	120-750A-15R-01, 34 120-750A-15R-01, 132	346.44 342.42	64.80
N3	<i>N. frequens</i>	LAD	120-750A-15R-03, 91	350.00	66.40
N3	<i>N. frequens</i>	LAD	120-750A-15R-3, 91	350.0	66.4
N4	<i>R. levis</i>	LAD	120-750A-20R-1, 20	394.6 394.4	69 72
N5	<i>A. parvus</i>	LAD	120-750B-4W-2, 150 120-750B-5R-1, 12	462.6 478.4	73.5 74.5
N6	<i>R. anthophorus</i>	LAD	120-750B-6W-1, 90 120-750B-6W-2, 30	489.4 490.3	74.5 75.5
N7	<i>E. eximius</i>	LAD	120-750B-7W-1, 1 120-750B-7W-1, 45	507.9 508.4	75 76
N8	<i>R. levis</i>	FAD	120-750B-7W-2, 16 120-750B-8W-1, 115	509.6 528.5	75.5 76.5
N9	<i>A. parvus</i>	FAD	120-750B-8W-2, 12 120-750B-9W-1, 8	528.9 546.8	83 84
N10	<i>L. septenarius</i>	LAD	120-750B-10W-1, 80 120-750B-10W-1, 115	566.8 567.2	85 86
N11	<i>R. anthophorus</i>	FAD	120-750B-10W-1, 115 120-750B-11W-1, 63	567.2 595.23	86 87
N12	<i>L. septenarius</i>	FAD	120-750B-11W-2, 8 120-750B-11W-2, 76	596.2 596.8	88 88.5
Planktonic foraminifers					
F1	K/T boundary (LAD planktonic foraminifers) (LAD calcareous nannofossils)		120-750A-15R-03, 91	350.00	66.40
F2	<i>G. mayaroensis</i>	FAD	120-750A-19R-CC 120-750A-20R-CC	394.40 404.00	70.00
F2	Campanian/Maestrichtian boundary		120-750A-24R-CC 120-750A-25R-CC	452.30 457.30	74.00

Note: Biostratigraphic datums are numbered in descending order and identified by prefix. N = calcareous nannofossil and F = planktonic foraminifer. See "Explanatory Notes" chapter (this volume) and "Biostratigraphy" section (this chapter) for age and depth information. FAD = first appearance datum and LAD = last appearance datum.

Table 7. Interstitial water chemical data, Site 750.

Core, section, interval (cm)	Depth (mbsf)	Vol. (cm ³)	pH	Alk. (mM)	Sal. (g/kg)	Mg ²⁺ (mM)	Ca ²⁺ (mM)	Cl ⁻ (mM)	SO ₄ ²⁻ (mM)	SiO ₂ (μM)	Mg ²⁺ /Ca ²⁺
120-750A-10R-2, 145-150	300.75	23	7.09	2.353	36.2	47.91	16.96	561.00	26.46	503	2.83
120-750A-13R-3, 145-150	331.25	15	7.15	2.459	36.4	47.91	16.96	559.00	25.25	505	2.83
120-750A-16R-2, 145-150	358.75	18	7.31	2.417	36.2	46.81	18.08	559.00	26.11	457	2.59
120-750A-19R-2, 145-150	387.65	22	7.42	2.047	36.2	48.17	16.38	566.00	26.28	344	2.94
120-750B-12W-1, 145-150	624.95	4	7.22	1.721	38.3	36.45	55.50	597.00	24.62	195	0.66

est drop (from 2.417 to 2.047) occurs between 358.75 and 387.65 mbsf and may reflect distinct IW behavior shortly below the Cretaceous/Tertiary boundary. We observed an overall increase in pH from 7.09 to 7.42.

The lowermost sample from the clayey material has a pH of 7.22 and a low alkalinity of 1.721 (Fig. 27). It cannot yet be concluded whether carbonate precipitation (siderite) is the reason for this low alkalinity value. Nevertheless, this value is the lowest one measured and is obtained from the deepest sample recovered during Leg 120.

Sulfate

No regular pattern can be deduced from the sulfate concentrations, which range from 25.25 to 26.46 mM in the upper four samples (Fig. 27). A significant low at 331.25 mbsf may be due to local organic carbon or sulfide matter. But conditions overall are still highly oxidizing, which can also be seen from the low

organic carbon contents in the respective intervals (see "Organic Geochemistry" section, this chapter).

A surprisingly high sulfate concentration is reported for the lowermost sample, as fossil wood chips and pyrite formation are reported from this interval. Again, caution must be taken as only one sample was analyzed, and micro-milieus may have developed due to the poor permeability of the clayey material.

Magnesium and Calcium

The uppermost samples show corresponding magnesium (46.81-48.17 mM) and calcium (16.38-18.08 mM) concentrations (Fig. 27). Their cation sums all range between 64.55 mM and 64.89 mM, which is within 1% deviation of the standard seawater value (IAPSO has 64.55 mM for total alkaline earth cations). The Ca and Mg concentrations again reflect the conservative cation exchange for these two elements and furthermore indicate their strong interdependence on seawater. This

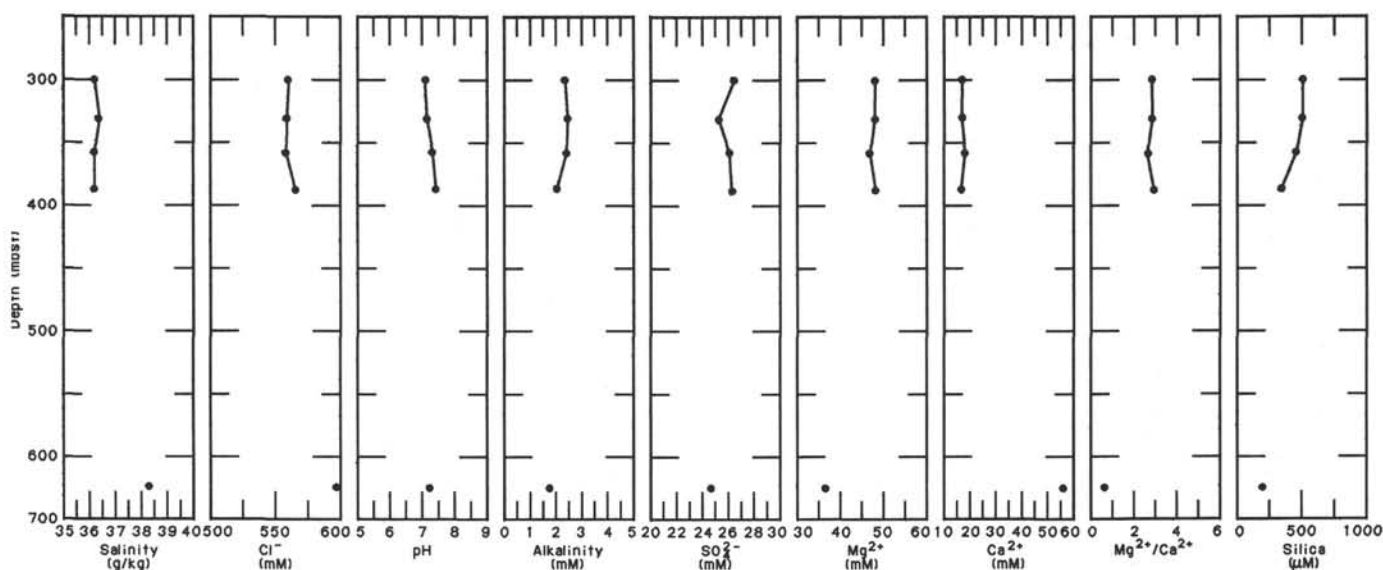


Figure 27. Summary of interstitial water analyses, Site 750, as a function of depth.

observation also reflects the open-system character of the IW column for the alkaline earths. The main factor controlling the alkaline earth system of IW in a rather homogeneous calcareous environment seems to be the depth-dependent calcium undersaturation of the IW.

The uppermost two samples show equal concentrations of magnesium and calcium and represent IW from Paleocene sediments. A downhole decrease in magnesium and an increase in calcium marks the transition from Paleocene to Maestrichtian sediments.

The lowermost sample has 36.45 mM of Mg-cations and 55.50 mM of Ca-cations in solution. The alkaline earth cation sum is 91.95 mM, which is greater than seawater values. If primary seawater infiltrated the clayey material or its precursor, then distinct cation exchange processes different from those observed in the calcareous and siliceous oozes have taken place. The source for the calcium input is the alteration of basalts (or perhaps Ca-plagioclase and Ca-pyroxene and glass in the basalt). Magnesium values are still rather high, so the formation of magnesium-rich clay minerals is evidently not a consequence of the alteration of the basaltic material.

To keep the charge balance, it is assumed that alkali metals are removed from the IW together with Si to form authigenic clay minerals. Therefore, mineral formation and particularly clay mineral formation are thought to reduce concentrations of silica, potassium, sodium, and probably magnesium in IW. The contemporary processes of alteration, devitrification, and hydration of basaltic material supplies calcium and removes some of the pore water. These processes may account for the high calcium concentrations and the high salinity of the IW.

Silica

Silica concentrations for the uppermost two samples are virtually the same (503 and 505 μM , respectively), then drop to 457 μM at 358.75 mbsf, and 344 μM at 387.65 mbsf, marking the transition from Paleocene to Maestrichtian sediments. Clay mineral formation or siliceous cementation can account for the decrease in dissolved silica.

The most significant drop, however, is observed for the lowermost sample from the clayey material, where dissolved silica is drastically reduced to 195 μM . If we consider open-system conditions for the IW (which means continuous exchange with overlying IW with high silica concentrations), it is assumed that clay

mineral formation served as a sink for some silica from IW. On the other hand, the low abundance of soluble silica in the basalt and its alteration products can equally account for the low silica concentration of the lowermost sample.

Summary

The upper four IW samples do not show pronounced changes in salinity and chlorinity. However, for the remaining concentrations measured, there is a significant change from the uppermost two samples (Paleocene) to the lowermost two samples (Maestrichtian). Drops in alkalinity, a decrease in magnesium and an increase in calcium, a decrease in silica, and an increase in sulfate herald the peculiar composition of IW within the Cretaceous sediments. Apart from the possibility that contamination has caused the observed IW compositions, it appears that the unusual properties of the Tertiary and Cretaceous sediments of Site 750 are even reflected in IW characteristics.

The lowermost sample from the clayey material is very different in its IW composition from the IW of the siliceous and calcareous sediments analyzed throughout Leg 120. The particularly high calcium concentration of the IW is related to the alteration of the basaltic material assumed to be the source rock of the clay. Low silica concentrations and apparent (on the basis of charge balance) potassium and sodium losses from the IW can be attributed to clay mineral formation.

Magnesium concentration values remain high, weakening evidence for Mg removal from IW due to Mg incorporation into clay minerals. This is in clear contrast to the idea that the alteration of basaltic basement rock provides the sink for Mg from the IW and therefore is responsible for the gradient in Mg concentration seen in the IW column. One explanation, however, might be that the original alteration of the basaltic material did not occur in the marine environment but occurred subaerially. Thus, at the time of final subsidence and infiltration of marine water, the altered basaltic material was already being transformed into clayey material.

ORGANIC GEOCHEMISTRY

Inorganic and Organic Carbon

Total inorganic carbon content was determined for 120 samples from Holes 750A and 750B (Table 8 and Fig. 28). The downhole resolution is extremely poor as a result of the selective

Table 8. Total carbon, inorganic and organic carbon, and carbonate contents of samples from Holes 750A and 750B.

Core, section, interval (cm)	Depth (mbsf)	Total carbon (%)	Inorganic carbon (%)	Organic carbon (%)	CaCO ₃ (%)
120-750A-					
1R-1, 22-24	0.22		0.37		3.1
1R-1, 80-84	0.80	11.07	11.06	0.01	92.1
1R-1, 80-82	0.80		11.09		92.4
1R-3, 13-15	2.99		11.16		93.0
1R-6, 18-20	7.04		11.13		92.7
3R-1, 126-130	57.66	11.39	11.39	0	94.9
3R-1, 127-129	57.67		10.92		91.0
7W-1, 78-80	163.38		11.56		96.3
7W-1, 79-80	163.39		11.48		95.6
8R-1, 52-56	259.72	11.46	11.45	0.01	95.4
8R-1, 52-56	259.72		11.45		95.4
10R-1, 80-84	298.60		11.45		95.4
10R-1, 116-118	298.96		11.30		94.1
10R-1, 126-130	299.06	11.46	11.46	0	95.5
10R-2, 26-30	299.56		11.44		95.3
10R-2, 80-84	300.10		11.45		95.4
10R-2, 116-118	300.46		11.40		95.0
10R-3, 21-23	301.01		11.37		94.7
10R-3, 50-54	301.30		11.27		93.9
10R-3, 80-84	301.60		11.49		95.7
11R-1, 20-24	307.70	11.53	11.53	0	96.0
11R-1, 80-84	308.30		11.50		95.8
11R-1, 116-118	308.66		11.39		94.9
11R-2, 20-24	309.20		11.49		95.7
11R-2, 43-45	309.43		11.37		94.7
11R-2, 80-84	309.80		11.54		96.1
12R-1, 20-24	317.40	11.56	11.56	0	96.3
12R-1, 80-84	318.00		11.57		96.4
12R-1, 135-137	318.55		11.30		94.1
12R-2, 20-24	318.90		11.44		95.3
12R-2, 80-84	319.50		11.50		95.8
12R-2, 144-146	320.14		11.25		93.7
12R-3, 20-24	320.40		11.45		95.4
12R-3, 80-84	321.00		11.39		94.9
12R-3, 118-120	321.38		11.28		94.0
12R-4, 20-24	321.90		11.52		96.0
12R-4, 80-84	322.50		11.47		95.6
13R-1, 24-28	327.04		11.35		94.6
13R-1, 80-84	327.60	11.41	11.28	0.13	94.0
13R-2, 24-28	328.54		11.36		94.6
13R-2, 80-84	329.10		11.35		94.6
13R-2, 141-143	329.71	11.36	11.21	0.15	93.4
13R-3, 24-28	330.04		11.41		95.1
13R-3, 80-84	330.60	11.24	11.11	0.13	92.6
13R-3, 118-120	330.98		10.87		90.6
13R-4, 24-28	331.54		11.48		95.6
14R-1, 80-84	337.30	11.37	11.36	0.01	94.6
14R-2, 14-18	338.14		11.49		95.7
14R-2, 79-81	338.79		11.06		92.1
14R-3, 14-18	339.64		11.46		95.5
14R-3, 80-84	340.30		11.40		95.0
14R-4, 14-18	341.14	11.36	11.35	0.01	94.6
14R-4, 80-84	341.80		11.50		95.8
14R-4, 86-88	341.86		11.20		93.3
15R-2, 104-106	348.64	11.38	11.37	0.01	94.7
15R-3, 72-74	349.82	10.81	10.65	0.16	88.7
16R-1, 20-22	356.00	11.36	11.35	0.01	94.6
16R-2, 79-82	358.09		11.49		95.7
16R-2, 102-104	358.32		11.23		93.6
16R-2, 103-106	358.33		11.39		94.9
16R-3, 17-20	358.97	11.41	11.38	0.03	94.8
16R-3, 118-121	359.98		11.40		95.0
16R-4, 12-14	360.42		11.11		92.6
17R-1, 32-36	365.62	11.46	11.46	0	95.5
17R-1, 47-49	365.77	11.47	11.20	0.27	93.3
17R-1, 106-110	366.36		11.62		96.8
17R-2, 28-32	367.08		11.51		95.9
17R-2, 79-83	367.59		11.51		95.9
17R-3, 23-27	368.53		11.51		95.9
17R-3, 54-56	368.84		11.29		94.1
18R-1, 14-18	375.14		11.46		95.5
18R-1, 32-34	375.32	0.08	0.04	0.04	0.3
18R-2, 22-26	376.72		10.85		90.4
18R-2, 34-36	376.84	11.39	11.35	0.04	94.6
19R-1, 79-81	385.49	11.43	11.25	0.18	93.7

Table 8 (continued).

Core, section, interval (cm)	Depth (mbsf)	Total carbon (%)	Inorganic carbon (%)	Organic carbon (%)	CaCO ₃ (%)
120-750A- (Cont.)					
19R-1, 83-87	385.53		11.39		94.9
19R-2, 26-30	386.46		11.46		95.5
19R-2, 88-92	387.08	11.18	11.30	0	94.1
19R-3, 54-56	388.24		11.21		93.4
20R-1, 18-20	394.58		11.39		94.9
20R-1, 80-84	395.20		11.19		93.2
20R-4, 13-15	399.03	10.53	10.52	0.01	87.6
20R-4, 89-93	399.79		11.27		93.9
20R-5, 16-18	400.56		11.31		94.2
20R-5, 81-85	401.21		11.55		96.2
21R-1, 63-65	404.63		11.50		95.8
21R-1, 80-84	404.80	11.50	11.50	0	95.8
22R-1, 39-42	413.99	11.62	11.62	0	96.8
25R-1, 6-8	452.36	10.55	10.55	0	87.9
120-750B-					
4W-1, 65-67	460.25	7.90	7.90	0	65.8
4W-2, 108-110	462.18	4.74	4.69	0.05	39.1
4W-3, 11-13	462.71		5.99		49.9
5R-1, 33-35	479.23	10.65	10.92	0	91.0
6W-1, 65-67	489.15		2.02		16.8
6W-1, 115-117	489.65	10.66	10.68	0	89.0
7W-1, 98-100	508.88	10.85	10.85	0	90.4
7W-2, 68-70	510.08		4.94		41.2
8W-1, 71-73	528.01	5.58	5.58	0	46.5
8W-2, 37-38	529.17		10.75		89.6
9W-1, 62-64	547.32	5.22	5.10	0.12	42.5
9W-2, 87-89	549.07		5.35		44.6
10W-1, 41-43	566.41	10.91	10.91	0	90.9
10W-1, 75-77	566.75		2.64		22.0
11W-1, 60-62	595.20	2.32	2.30	0.02	19.2
11W-2, 64-66	596.74		10.33		86.1
12W-1, 47-49	623.97	1.11	0.90	0.21	7.5
12W-1, 90-92	624.40		1.45		12.1
12W-2, 21-23	625.21	1.06	0.38	0.68	3.2
12W-3, 22-24	626.72	1.43	0.34	1.09	2.8
13W-1, 25-27	643.05	6.79	0.03	6.76	0.3
13W-2, 25-27	644.55	10.54	0.01	10.53	0.1
13W-2, 84-86	645.14	5.78	0.01	5.77	0.1
13W-2, 131-133	645.61	6.88	0.04	6.84	0.3
13W-3, 18-20	645.98	2.41	0.01	2.40	0.1
13W-3, 30-32	646.10	2.18	0.03	2.15	0.3

spot-coring technique that was employed during the drilling of this site. A higher sampling resolution was available over the late Maestrichtian and Danian (289-425 mbsf), the only continuously cored portion of the sequence.

Total inorganic carbon, expressed here as weight percent calcium carbonate, ranges from 0% to 95% at Site 750. The upper 250-m Eocene section, which was cored at 50-m intervals, is characterized by high carbonate contents of 90%-95%. The sediment from this interval consists mainly of calcareous nanofossils and, to a lesser extent, foraminifers (see "Lithostratigraphy and Sedimentology" section, this chapter). Similar carbonate contents were encountered in the continuously cored Paleocene and Maestrichtian portion (317.7-450 mbsf) of the sequence as well.

From 450 to 623 mbsf (Subunits IIIB and IIIC), carbonate contents display extreme variability, ranging from 10% to 90%. This reflects the alternating chalk and silicified chalk lithology observed in cores from these subunits. From the base of Unit III to basement, carbonate contents are generally less than 5%-10% (Cores 120-750-12W and -13W). The carbonate in Core 120-750-12W is predominantly composed of authigenic siderite (see "Lithostratigraphy and Sedimentology" section, this chapter).

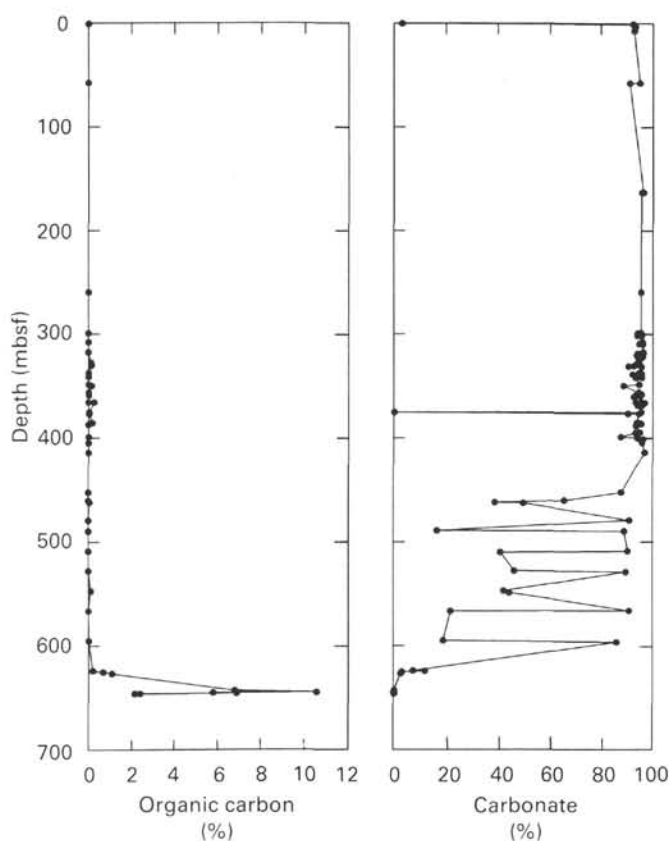


Figure 28. Total organic carbon and carbonate contents plotted vs. depth at Site 750.

With the exception of samples from lowermost Unit IV, total organic carbon (TOC) contents are relatively low at Site 750. From the top of the hole to 625 mbsf, TOC values never exceed 0.27%. These values are similar to those recorded at Sites 747 and 748 in sediments of the same age (see "Organic Geochemistry" section, Sites 747 and 748 chapters, this volume). In contrast, high TOC values in the range of 0.68%–10.0% were encountered in lowermost Unit IV (625–675 mbsf) at Site 750. The highest concentrations occur in the darker portions of the brown claystones from Core 120-750B-13W.

The bulk of the TOC in this unit is associated with beds rich in coal-like fragments. The structure of the organic matter (OM) suggests that they may have originated from woody material. In addition to the Site 750 samples, two samples from the base of Site 748, a red-brown claystone, were analyzed and yielded enriched TOC values of 2.65% and 1.88%. This and the lithologic resemblance would indicate that these sediments were deposited in a similar environment as the Site 750 Unit IV sediments.

Rock-Eval

In order to assess the source character and thermal maturation of organic matter deposited on Kerguelen Plateau further, a total of 16 samples from Site 750 were evaluated on board ship by Rock-Eval pyrolysis. Representative samples were selected from lithologic Subunits IIB (317.7–357 mbsf), IIIA (357–450 mbsf), and IIIB (450–594.6 mbsf) and from Unit IV (623.5–675.5 mbsf) (see "Lithostratigraphy and Sedimentology" section, this chapter). Only those samples containing greater than 0.1% TOC were selected from the carbonate-rich units (IIB, IIIA, and IIIB).

In addition, the two organic-rich samples from the base of Site 748 reported above were included in the analyses (all data are reported in Table 9). Because the Rock-Eval TOC apparatus was not functioning during Leg 120, the TOC values obtained

Table 9. Results of Rock-Eval analyses of organic-carbon-rich samples from Site 750 and of two samples from Site 748.

Core, section, interval (cm)	Depth (mbsf)	T _{max} (°C)	S ₁	S ₂	S ₃	PI	S ₂ /S ₃	PC	TOC (%)	HI	OI
120-750A-											
13R-1, 80–84	327.60	421	0.01	0	0	1.00	0	0	0.13	0	0
13R-2, 141–143	329.71	283	0.05	0	0.22	1.00	0	0	0.15	0	147
13R-3, 80–84	330.60	384	0.09	0.04	0.29	0.69	0.14	0.01	0.13	31	223
15R-3, 72–74	349.82	345	0.07	0.05	0.76	0.58	0.07	0.01	0.16	31	475
17R-1, 47–49	365.77	309	0.04	0	0.10	1.00	0	0	0.27	0	37
19R-1, 79–81	385.49	378	0.12	0.05	0.32	0.71	0.16	0.01	0.18	28	178
120-750B-											
4W-2, 108–110	462.18	378	0.02	0.07	0.47	0.22	0.15	0.01	0.05	140	940
9W-1, 62–64	547.32	337	0.05	0.02	0.42	0.71	0.05	0.01	0.12	17	350
12W-2, 21–23	625.21	480	0.10	2.73	3.23	0.04	0.85	0.23	0.68	401	475
12W-2, 21–23	625.21	507	0.08	2.41	4.00	0.03	0.60	0.21	0.68	354	588
12W-3, 22–24	626.72	461	0	2.61	4.58	0	0.57	0.22	1.09	239	420
13W-1, 25–27	643.05	465	0.04	2.84	1.69	0.01	1.68	0.24	6.76	42	25
13W-2, 25–27	644.55	434	0.31	8.25	2.18	0.04	3.78	0.71	10.53	78	21
13W-2, 25–27	644.55	419	0.26	8.39	2.08	0.03	4.03	0.72	10.53	80	20
13W-2, 84–86	645.14	467	0.01	3.83	1.30	0	2.95	0.32	5.77	66	23
13W-2, 131–133	645.61	455	0.07	3.53	1.71	0.02	2.06	0.30	6.84	52	25
13W-2, 131–133	645.61	482	0.14	3.90	1.88	0.03	2.07	0.34	6.84	57	27
13W-3, 18–20	645.98	493	0.02	2.59	0.97	0.01	2.67	0.22	2.40	108	40
13W-3, 30–32	646.10	492	0.14	2.61	1.02	0.05	2.56	0.23	2.15	121	47
120-748C-											
87R-CC, 1–3	934.00	427	0.03	1.69	0.54	0.02	3.13	0.14	1.65	102	33
87R-CC, 4–6	934.03	437	0	1.64	3.44	0	0.48	0.14	2.55	64	135

Note: PC = pyrolyzable carbon, TOC = total organic carbon, HI = hydrogen index, and OI = oxygen index. The TOC values were obtained by coulometric analyses. Included are values from duplicate analyses.

from the coulometric analyses were used to calculate the hydrogen and oxygen indexes. This method, however, may provide unreliable hydrogen and oxygen indexes for samples high in carbonate and relatively low in TOC (<1.0%).

The results of Rock-Eval analyses reveal at least three distinct types of organic matter at Site 750. The upper carbonate-rich Subunits IIB, IIIA, and IIIB (317–594 mbsf) are characterized by samples with a low T_{max} (<400°C), low pyrolyzable carbon (<0.01 mgC/g), and low S_2/S_3 ratios (0–0.16) and with high productivity indexes (0.2–1.0). In contrast, samples from the TOC-rich Unit IV are characterized by a high T_{max} (>420°C), high pyrolyzable carbon (0.23–0.72 mgC/g), and high S_2/S_3 ratios (0.6–4.03) and by a low productivity index (<0.01). In addition, the hydrogen and oxygen indexes show three clusters of data (Fig. 29) when plotted on a modified Van Krevelen diagram (Tissot and Welte, 1984).

The samples from the upper carbonate-rich units possess low hydrogen and high oxygen contents and fall along the Type III field, which indicates highly oxidized marine OM. Alternatively, the high oxygen concentrations may be an artifact of the high carbonate content, which can produce mineral matrix effects during pyrolysis (Katz, 1983). The samples from Unit IV fall into two distinct clusters. The OM from Core 120-750B-13W yields low hydrogen and oxygen values, whereas the OM from Core 120-750B-12W possess much higher values.

The low values recorded in Core 120-750B-13W are similar to values obtained for mature humic coals (Durand and Monin, 1980), reflecting the gradual loss of hydrogen and oxygen and enrichment of carbon during maturation. The maturity is also reflected by the high temperature of maximum hydrocarbon cracking (T_{max}) and pyrolyzable carbon values reported above. The samples from Core 120-750B-12W are unusual in that they possess high oxygen and carbon concentrations. Specifically, im-

mature terrestrial OM normally tends to be high in oxygen and depleted in hydrogen (Espitalie et al., 1977).

During maturation, dehydrogenation and oxidation occur in a manner such that the residual kerogen follows the Type III path toward low oxygen and hydrogen indexes. Conversely, marine OM initially contains high hydrogen and low oxygen contents and during maturation follows the Type II path. However, the values obtained for the samples from Core 120-750B-12W do not fall into either category. There are several potential possibilities to explain the discrepancy, such as (1) the Core 120-750B-12W OM represents immature boghead or swampwood coals relatively rich in hydrogen; (2) the OM is an admixture of hydrogen-rich immature marine OM and reworked terrestrial OM; or (3) the oxygen values are spurious as a result of carbonate mineral matrix effects. Core 120-750B-12W contains 10%–15% authigenic siderite, which has the lowest combustion temperature for carbonate minerals of just under 400°C.

Hydrocarbon Gases

Hydrocarbon gases were extracted by headspace techniques from core material on a routine basis at Site 750. Analytical methods are outlined in the “Explanatory Notes” chapter (this volume). Only traces of C_1 and C_2 gases were encountered at this site.

PHYSICAL PROPERTIES

Introduction

The objective of the physical properties program at Site 750 was to aid in the interpretation of stratigraphic and geophysical data from the Raggatt Basin. Holes 750A and 750B were completed to 460.5 and 709.7 mbsf, respectively, with the RCB technique. Measurements were made in order to determine the physical properties of the sediment and rock that composed the lithologic column at Site 750. Because the overall primary objectives at Site 750 were recovery of Mesozoic sediment and igneous basement rock, the two holes were only cored intermittently, with the exception of the Cretaceous/Tertiary boundary and the igneous basement.

Many of the samples used for physical properties determinations came from wash cores, and their stratigraphic position is imprecisely known. This factor, combined with sparse spot coring in the upper 300 m of both holes, precluded an analysis of geotechnical stratigraphy at Site 750. However, the data below 300 mbsf are sufficiently dense to allow an analysis of trends.

At Site 750 the physical properties determined were: (1) index properties (wet- and dry-bulk density, grain density, water content, and porosity, all in discrete samples) (Fig. 30 and Table 10); (2) compressional wave velocity in discrete samples (Hamilton Frame) (Fig. 31 and Table 11); and (3) thermal conductivity (Table 12). Because of sediment disturbance resulting from the RCB technique, the gamma ray attenuation evaluator (GRAPE) and P -wave logger (PWL) were not used at this site. No down-hole temperatures were obtained due to time constraints.

The methods employed in the determination of physical properties during Leg 120 are described in the “Explanatory Notes” chapter (this volume). A more detailed discussion of these measurements can be found in Lambe and Whitman (1969) and Boyce (1976, 1977).

Index Properties

Values for index properties determined from Site 750 samples appear in Table 10 and are plotted in Figure 30. For discrete samples, a Scientec balance was employed for weight determinations, a Penta pycnometer for volume measurements, and a Labconco freeze-dry apparatus for drying. No technique was available for index property determinations at *in-situ* pressure-

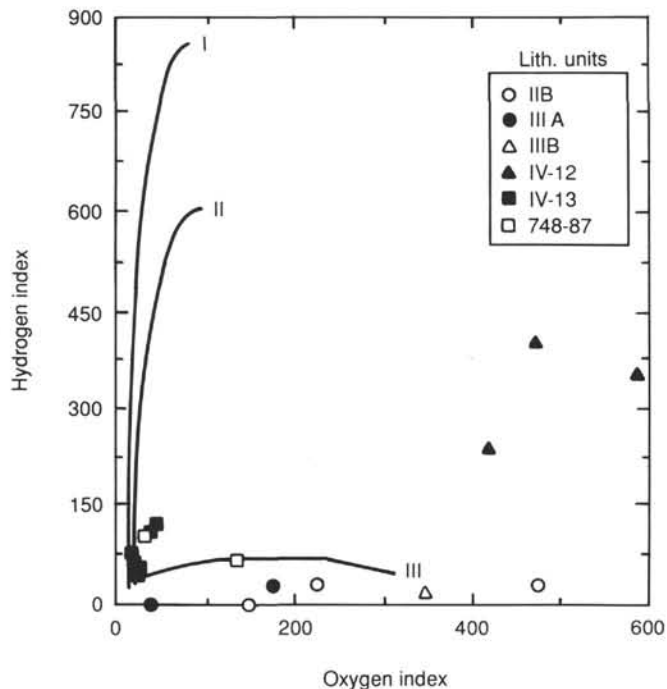


Figure 29. Van Krevelen plot of hydrogen (mg HC/g C_{org}) and oxygen (mg CO_2 /g C_{org}) indexes of organic matter determined from Rock-Eval analyses of samples from Sites 750 and 748. See “Explanatory Notes” chapter (this volume) for a more detailed explanation of the various parameters.

Table 10. Index property determinations, Site 750.

Core, section, interval (cm)	Depth (mbsf)	Water content (%)	Porosity (%)	Wet-bulk density (%)	Dry-bulk density (%)	Grain density (%)
120-750A-1R-1, 22	0.22	36.96	60.60	1.72	19.0	2.66
120-750A-1R-1, 80	0.80	39.18	63.76	1.66	11.0	2.77
120-750A-1R-3, 13	2.99	39.38	64.65	1.70	1.03	2.85
120-750A-1R-6, 18	7.04	36.90	59.91	1.69	1.07	2.59
120-750A-3R-1, 127	57.67	36.42	60.84	1.73	1.10	2.75
120-750A-7W-1, 71	163.31	2.26	5.41	2.62	2.56	2.52
120-750A-7W-1, 78	163.38	27.17	50.03	1.91	1.39	2.72
120-750A-10R-1, 116	298.96	26.02	49.08	2.01	1.49	2.78
120-750A-10R-2, 116	300.46	24.52	47.97	2.01	1.51	2.88
120-750A-10R-3, 21	301.01	26.44	49.22	1.95	1.43	2.74
120-750A-11R-1, 116	308.66	27.67	51.71	1.94	1.40	2.84
120-750A-11R-2, 43	309.43	28.75	51.69	1.93	1.37	2.69
120-750A-12R-1, 135	318.55	26.08	49.93	2.09	1.55	2.87
120-750A-12R-2, 144	320.14	29.87	52.55	1.84	1.29	2.64
120-750A-12R-3, 118	321.38	27.77	50.24	1.94	1.40	2.66
120-750A-13R-2, 141	329.71	26.32	49.49	1.94	1.43	2.78
120-750A-13R-3, 118	330.98	26.19	48.92	1.97	1.45	2.74
120-750A-14R-2, 79	338.79	26.83	50.77	1.97	1.44	2.85
120-750A-14R-4, 86	341.86	28.05	50.52	1.90	1.36	2.66
120-750A-15R-2, 105	348.65	26.59	49.45	1.94	1.43	2.74
120-750A-15R-3, 73	349.83	26.40	50.19	2.05	1.51	2.85
120-750A-15R-3, 91	350.01	26.07	49.10	2.37	1.75	2.78
120-750A-16R-1, 21	356.01	30.91	54.61	1.86	1.29	2.73
120-750A-16R-1, 89	356.69	26.84	50.16	1.92	1.41	2.78
120-750A-16R-2, 102	358.32	25.98	48.40	1.95	1.45	2.71
120-750A-16R-4, 12	360.42	28.37	50.95	1.87	1.34	2.66
120-750A-17R-1, 4	365.34	1.07	2.67	2.72	2.69	2.58
120-750A-17R-1, 47	365.77	26.57	50.40	2.00	1.47	2.85
120-750A-17R-3, 54	368.84	28.12	51.96	1.94	1.39	2.80
120-750A-18R-1, 32	375.32	0.48	1.20	2.70	2.68	2.54
120-750A-18R-2, 34	376.84	27.94	52.22	1.99	1.44	2.86
120-750A-19R-1, 79	385.49	29.31	53.68	1.92	1.36	2.84
120-750A-19R-3, 54	388.24	29.17	53.29	1.93	1.37	2.81
120-750A-20R-1, 18	394.58	26.19	47.58	1.94	1.43	2.59
120-750A-20R-4, 13	399.03	20.24	40.81	1.93	1.54	2.76
120-750A-20R-5, 16	400.56	32.13	55.80	1.94	1.32	2.70
120-750A-21R-1, 63	404.63	26.11	47.73	1.96	1.45	2.62
120-750A-23W-1, 4	423.34	26.05	49.82	2.01	1.48	2.86
120-750B-3R-1, 63	450.63	18.76	32.25	2.05	1.67	2.09
120-750A-25R-1, 6	452.36	25.14	45.81	1.91	1.43	2.55
120-750B-4W-1, 65	460.25	20.77	41.02	2.13	1.69	2.69
120-750B-4W-2, 48	461.58	22.13	44.51	2.20	1.72	2.87
120-750B-4W-2, 108	462.18	9.60	21.52	2.46	2.22	2.62
120-750B-4W-3, 11	462.71	11.53	23.36	2.19	1.94	2.38
120-750B-4W-C, 44	464.00	7.75	17.57	2.41	2.23	2.58
120-750B-5R-1, 33	479.23	23.28	45.97	2.09	1.60	2.85
120-750B-6W-1, 65	489.15	16.64	32.55	2.07	1.73	2.45
120-750B-6W-1, 115	489.65	22.72	43.05	2.07	1.60	2.61
120-750B-7W-1, 98	508.88	24.12	46.18	2.02	1.53	2.74
120-750B-7W-2, 53	509.93	14.93	29.27	2.20	1.88	2.39
120-750B-7W-2, 68	510.08	15.01	28.74	2.04	1.74	2.32
120-750B-8W-1, 34	527.64	0.13	0.32	2.62	2.62	2.53
120-750B-3R-1, 63	450.63	18.76	32.25	2.05	1.67	2.09
120-750B-4W-1, 44	460.04	7.75	17.57	2.41	2.23	2.58
120-750B-4W-1, 65	460.25	20.77	41.02	2.13	1.69	2.69
120-750B-4W-2, 48	461.58	22.13	44.51	2.20	1.72	2.87
120-750B-4W-2, 108	462.18	9.60	21.52	2.46	2.22	2.62
120-750B-4W-3, 11	462.71	11.53	23.36	2.19	1.94	2.38
120-750B-5R-1, 33	479.23	23.28	45.97	2.09	1.60	2.85
120-750B-6W-1, 65	489.15	16.64	32.55	2.07	1.73	2.45
120-750B-6W-1, 115	489.65	22.72	43.05	2.07	1.60	2.61
120-750B-7W-1, 98	508.88	24.12	46.18	2.02	1.53	2.74
120-750B-7W-2, 53	509.93	14.93	29.27	2.20	1.88	2.39
120-750B-7W-2, 68	510.08	15.01	28.74	2.04	1.74	2.32
120-750B-8W-1, 34	527.64	0.13	0.32	2.62	2.62	2.53
120-750B-8W-1, 71	528.01	11.28	23.52	2.30	2.04	2.46
120-750B-8W-2, 37	529.17	9.46	20.98	2.37	2.15	2.58
120-750B-9W-1, 37	547.07	7.06	14.48	2.45	2.27	2.26
120-750B-9W-1, 62	547.32	17.68	36.44	2.18	1.79	2.71
120-750B-9W-1, 124	547.94	10.62	21.85	2.30	2.05	2.39
120-750B-9W-2, 16	548.36	14.24	29.56	2.24	1.92	2.57
120-750B-9W-2, 48	548.68	17.12	36.22	2.22	1.84	2.79
120-750B-9W-2, 87	549.07	12.11	23.84	2.22	1.95	2.31
120-750B-10W-1, 41	566.41	17.02	36.26	2.22	1.84	2.82
120-750B-10W-1, 75	566.75	13.14	24.66	2.06	1.79	2.20
120-750B-10W-1, 105	567.05	0.38	0.99	2.73	2.72	2.68
120-750B-11W-1, 13	594.73	12.41	28.81	2.53	2.22	2.90
120-750B-11W-1, 47	595.07	16.49	33.18	2.27	1.89	2.55
120-750B-11W-1, 60	595.20	16.82	32.62	2.07	1.72	2.43
120-750B-11W-1, 147	596.07	20.49	40.22	2.10	1.67	2.65
120-750B-11W-2, 12	596.22	21.85	29.57	1.97	1.54	1.51
120-750B-11W-2, 64	596.74	18.89	37.59	2.13	1.73	2.63
120-750B-12W-1, 47	623.97	24.50	47.84	2.08	1.57	2.87
120-750B-12W-1, 90	624.40	22.97	46.87	2.17	1.67	3.00
120-750B-12W-2, 21	625.21	28.19	52.50	1.98	1.42	2.86
120-750B-12W-2, 78	625.78	26.08	50.34	2.06	1.52	2.92

Table 10 (continued).

Core, section, interval (cm)	Depth (mbsf)	Water content (%)	Porosity (%)	Wet-bulk density (%)	Dry-bulk density (%)	Grain density (%)
120-750B-12W-2, 121	626.21	24.01	49.35	2.10	1.59	3.13
120-750B-12W-3, 22	626.72	22.54	45.94	2.20	1.70	2.96
120-750B-12W-3, 59	627.09	26.06	50.18	1.94	1.44	2.90
120-750B-13W-1, 36	643.16	26.87	47.73	1.91	1.39	2.52
120-750B-13W-1, 41	643.21	22.79	45.02	2.17	1.68	2.82
120-750B-13W-1, 67	643.47	25.35	48.66	2.00	1.49	2.83
120-750B-13W-1, 116	643.96	23.33	43.98	1.96	1.51	2.62
120-750B-13W-2, 25	644.55	35.41	54.92	1.66	1.07	2.25
120-750B-13W-2, 78	645.08	25.09	45.96	1.94	1.45	2.58
120-750B-13W-2, 132	645.62	29.97	50.97	1.82	1.27	2.46
120-750B-13W-3, 31	646.11	27.54	50.39	1.91	1.38	2.71
120-750B-13W-CC, 1	646.61	26.58	47.12	1.91	1.40	2.49
120-750B-14R-1, 79	672.29	22.19	45.87	2.28	1.77	3.02
120-750B-14R-2, 85	673.85	3.37	8.67	3.00	2.90	2.77
120-750B-15R-1, 40	681.60	1.84	4.99	2.90	2.84	2.85
120-750B-15R-2, 37	683.07	3.58	9.58	2.89	2.78	2.90
120-750B-15R-2, 80	683.50	2.97	8.08	2.91	2.82	2.92
120-750B-15R-3, 38	684.48	2.35	6.91	3.28	3.20	3.14
120-750B-15R-4, 69	686.08	2.42	6.45	3.13	3.06	2.83
120-750B-15R-5, 45	687.14	2.40	6.53	3.09	3.02	2.90
120-750B-16R-1, 37	690.87	1.17	3.37	3.07	3.04	3.00
120-750B-16R-2, 41	692.41	1.11	3.14	3.07	3.04	2.95
120-750B-16R-3, 67	694.07	1.92	5.20	2.95	2.89	2.84
120-750B-16R-4, 97	695.73	1.40	4.03	3.06	3.02	3.01
120-750B-16R-5, 82	696.97	3.07	8.31	2.94	2.85	2.91
120-750B-16R-6, 100	698.58	2.02	5.61	3.03	2.97	2.93
120-750B-16R-7, 111	699.99	1.06	2.93	2.91	2.88	2.87
120-750B-17R-1, 15	700.35	3.26	10.01	3.40	3.29	3.36
120-750B-17R-3, 11	703.31	5.01	11.94	2.59	2.46	2.61

temperature conditions, making correlation with logging data sometimes difficult. Acoustic impedance calculations to produce synthetic seismograms for comparison with site survey multichannel seismic (MCS) data also suffer from a lack of the capability to determine *in-situ* sediment and rock densities.

Downhole variations in index properties commonly correlate with changes in sediment lithology (see "Lithostratigraphy and Sedimentology" section, this chapter) and carbonate content (see "Organic Geochemistry" section, this chapter). Overall downhole trends in index properties indicate a general inverse relation between wet-bulk density and water content (Fig. 30). An inverse relation also appears between wet-bulk density and porosity (Fig. 30). Porosity commonly correlates with carbonate content (Fig. 30).

Below 300 mbsf four distinct trends are observed in index properties. Between ~300 and ~450 mbsf, wet-bulk density, grain density, water content, porosity, and carbonate content are uniform with limited scatter. The lithologies in the interval are nannofossil chalk and chert. Between ~450 and ~575 mbsf, wet-bulk density increases and water content, porosity, and carbonate content decrease. In this interval the dominant lithologies are silicified limestone and calcareous chalk, with some chert.

Between ~575 and ~670 mbsf, wet-bulk density and carbonate content decreases, whereas water content and porosity increase. Calcareous chalk with marl and silty claystone with coal make up the interval. A sharp break in all index properties occurs near ~670 mbsf, below which basalt dominates. Wet-bulk density increases downhole, and water content and porosity decrease.

Compressional Wave Velocity

At Site 750 compressional wave velocities were calculated from discrete Hamilton Frame (HF) measurements to a depth of ~703 mbsf (Table 11 and Fig. 30). Measurements were generally made parallel to bedding, although some samples were oriented perpendicular to bedding to investigate for velocity anisotropy. The HF technique does not allow for velocity determination at *in-situ* pressure-temperature conditions, making correlation with logging and site survey MCS data difficult.

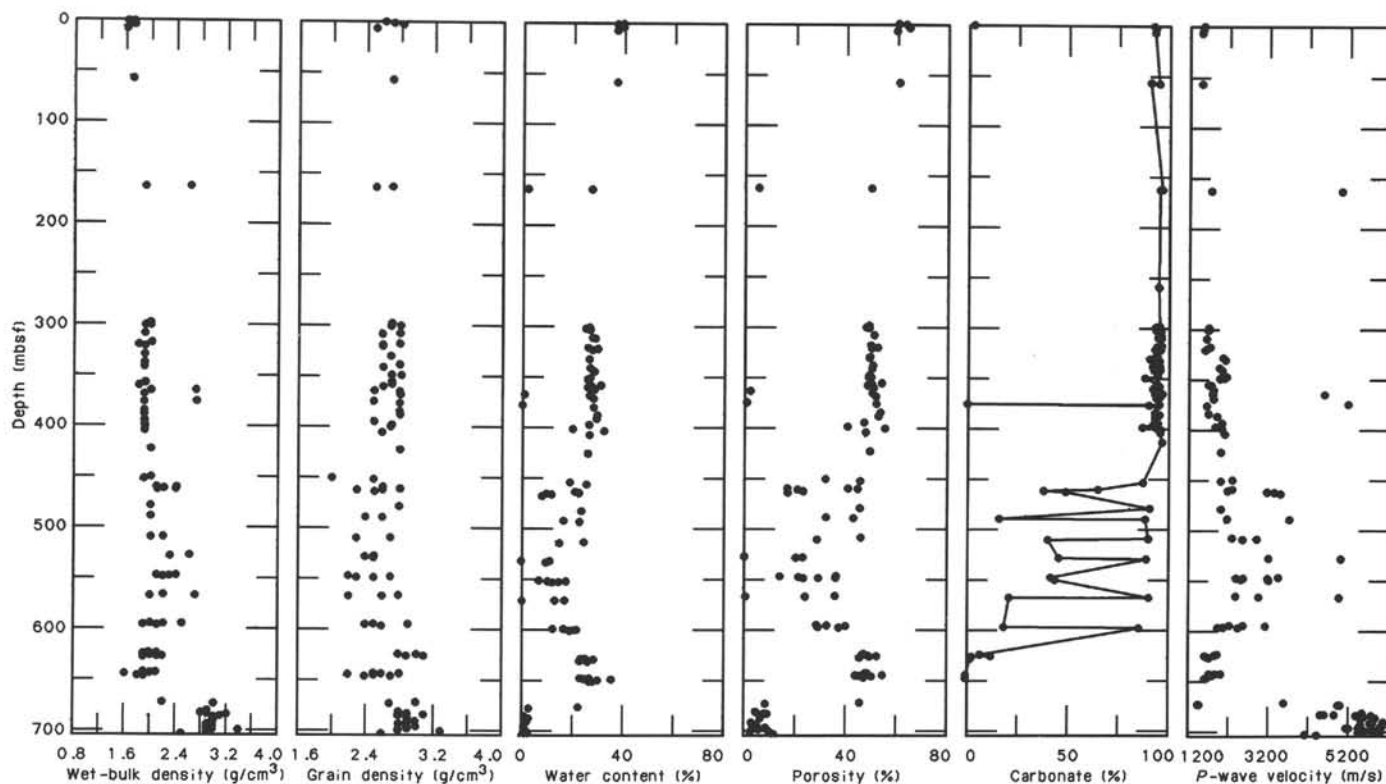


Figure 30. Downhole summary of index properties (wet-bulk density, grain density, water content, porosity, carbonate percentage, and P -wave velocity), Site 750.

The variations in compressional wave velocity downhole commonly correlate with changes in sediment lithology (see "Lithostratigraphy and Sedimentology" section, this chapter). In general, compressional wave velocity bears a direct relation to wet-bulk density (and grain density to a lesser extent) and is inversely related to water content and porosity.

The compressional wave velocity data show a fair degree of scatter beneath ~300 mbsf. A marked velocity contrast occurs in the vicinity of the Cretaceous/Tertiary boundary at ~355 mbsf (see "Biostratigraphy" section, this chapter). Above ~325 mbsf velocities are typically less than 1700 m/s. Between ~330 and ~350 mbsf, values are commonly greater than 2000 m/s. Beneath the boundary values are less than 1800 m/s. The lithology is nanofossil chalk above and below the boundary, with some chert present beneath. Between ~375 and ~575 mbsf, velocity increases gradually.

The lithologies encountered in this interval are nanofossil chalk, calcareous chalk, intermittently silicified limestone, and chert; the latter two are responsible for the scattered high velocity points. From ~575 to ~670 mbsf, velocity decreases in calcareous chalk with marl and in silty claystone with coal. This inversion reaches a minimum of ~1430 m/s in highly altered basalt (see "Igneous Petrology" section, this chapter). Within the igneous rock, velocities typically exceed 5500 m/s.

Thermal Conductivity

The uppermost core from Hole 750A was measured for thermal conductivity using a needle probe technique (Von Herzen and Maxwell, 1959). A probe was inserted and heated; measurements were then made over a 6-min interval. Only needle runs displaying a temperature drift rate of less than 0.04°C/min were retained. Because no downhole temperatures were to be determined at Site 750, thermal conductivity was measured solely in the sediment section reachable by conventional piston cores and temperature probes. The values appear in Table 12.

Concluding Discussion

The individual contributions of several interrelated variables, such as sediment lithology, depth of burial, and diagenesis, are likely responsible for the physical state of the sediment and rock recovered at Site 750. Three salient aspects are observed in the physical properties data.

1. Abrupt changes in velocity occur in the vicinity of the Cretaceous/Tertiary boundary. At the boundary itself, water content, porosity, and carbonate content reach very low values.

2. A velocity inversion is present between ~575 and ~670 mbsf. This inversion corresponds to relative decreases in wet-bulk density and carbonate content as well as to increases in water content and porosity.

3. Compressional wave velocity in the igneous rock is unusually high when compared with laboratory and field velocity determinations in shallow (less than 1–2 km) oceanic crust (e.g., Fox and Stroup, 1981). This may result from a different petrographic character and/or a deeper emplacement level.

IGNEOUS PETROLOGY

Introduction

Basalt was encountered at 675.5 mbsf and cored to a depth of 709.7 mbsf with 66.9% recovery (Cores 120-750B-14R to -17R). The basaltic basement is overlain by an Albian ferruginous calcareous claystone rich in wood fragments. The actual basement/sediment contact was not recovered.

Macroscopic Core Description

The basalts are composed of a moderate to highly altered upper section (Core 120-750B-14R-1, 23 cm, to Core 120-750B-14R-2, 113 cm) and a slightly to moderately altered lower section (Cores 120-750B-15R-1 to -17R). The basalts have been

Table 11. Compressional wave velocity determined from Hamilton Frame data, Site 750.

Core, section, interval (cm)	Depth (mbsf)	DIR	Velocity (m/s)
120-750A-1R-1, 22	0.22	C	1562.1
120-750A-1R-1, 80	0.80	C	1534.2
120-750A-1R-3, 13	2.99	C	1524.9
120-750A-1R-6, 18	7.04	C	1525.9
120-750A-3R-1, 127	57.67	C	1517.7
120-750A-7W-1, 71	163.31	A	4966.1
120-750A-7W-1, 78	163.38	A	1735.0
120-750A-10R-1, 116	298.96	C	1679.0
120-750A-10R-2, 116	300.46	C	1702.1
120-750A-10R-3, 21	301.01	C	1674.3
120-750A-11R-1, 116	308.66	C	1617.3
120-750A-11R-2, 43	309.43	C	1618.0
120-750A-12R-1, 135	318.55	C	1715.4
120-750A-12R-2, 144	320.14	C	1625.9
120-750A-12R-3, 118	321.38	C	1616.1
120-750A-13R-2, 141	329.71	C	2048.9
120-750A-13R-3, 118	330.98	C	2099.6
120-750A-14R-2, 79	338.79	C	1948.2
120-750A-14R-4, 86	341.86	C	2023.9
120-750A-15R-2, 105	348.65	C	2126.5
120-750A-15R-3, 73	349.83	C	2058.1
120-750A-15R-3, 91	350.01	C	1949.4
120-750A-16R-1, 21	356.01	C	1696.0
120-750A-16R-1, 89	356.69	C	1744.3
120-750A-16R-2, 102	358.32	C	1760.3
120-750A-16R-4, 12	360.42	C	1790.9
120-750A-17R-1, 4	365.34	C	4556.5
120-750A-17R-1, 47	365.77	C	1775.5
120-750A-17R-3, 54	368.84	C	1796.2
120-750A-18R-1, 32	375.32	C	5163.7
120-750A-18R-2, 34	376.84	C	1636.6
120-750A-19R-1, 79	385.49	C	1677.2
120-750A-19R-3, 54	388.24	C	1892.3
120-750A-20R-1, 18	394.58	C	2021.8
120-750A-20R-4, 13	399.03	A	1851.1
120-750A-20R-5, 16	400.56	C	2025.1
120-750A-21R-1, 63	404.63	A	2079.5
120-750A-23W-1, 4	423.34	A	1982.2
120-750B-3R-1, 63	450.63	C	2280.3
120-750A-25R-1, 6	452.36	C	1982.5
120-750B-4W-1, 66	460.26	A	2275.3
120-750B-4W-2, 49	461.59	A	2151.8
120-750B-4W-2, 109	462.19	A	3314.6
120-750B-4W-3, 12	462.72	A	3130.2
120-750B-4W-CC, 45	464.00	A	3471.4
120-750B-5R-1, 34	479.24	A	1987.1
120-750B-6W-1, 66	489.16	A	3709.6
120-750B-6W-1, 116	489.66	A	2148.2
120-750B-7W-1, 99	508.89	A	2281.3
120-750B-7W-2, 54	509.94	A	2886.3
120-750B-7W-2, 69	510.09	A	2539.4
120-750B-8W-1, 35	527.65	A	4978.9
120-750B-8W-1, 72	528.02	A	3173.7
120-750B-8W-2, 37	529.17	A	3174.6
120-750B-9W-1, 37	547.07	A	3420.0
120-750B-9W-1, 62	547.32	A	2380.6
120-750B-9W-1, 124	547.94	A	3142.1
120-750B-9W-2, 16	548.36	A	2553.5
120-750B-9W-2, 48	548.68	A	2497.1
120-750B-9W-2, 87	549.07	A	3161.6
120-750B-10W-1, 41	566.41	A	2376.5
120-750B-10W-1, 75	566.75	A	2935.0
120-750B-10W-1, 105	567.05	A	4932.1
120-750B-11W-1, 13	594.73	A	2230.3
120-750B-11W-1, 47	595.07	A	2558.1
120-750B-11W-1, 60	595.20	A	3087.6
120-750B-11W-1, 147	596.07	A	2066.9
120-750B-11W-2, 12	596.22	A	1927.8
120-750B-11W-2, 64	596.74	A	2441.7
120-750B-12W-1, 47	623.97	A	1883.5
120-750B-12W-1, 90	624.40	A	1843.3
120-750B-12W-2, 21	625.21	A	1605.9
120-750B-12W-2, 78	625.78	A	1649.8
120-750B-12W-2, 121	626.21	A	1611.0
120-750B-12W-3, 22	626.72	A	1684.2
120-750B-12W-3, 59	627.09	A	1660.0
120-750B-13W-1, 36	643.16	A	1737.9
120-750B-13W-1, 41	643.21	A	1977.8

Table 11 (continued).

Core, section, interval (cm)	Depth (mbsf)	DIR	Velocity (m/s)
120-750B-13W-1, 57	643.37	A	1945.1
120-750B-13W-1, 67	643.47	A	1716.2
120-750B-13W-1, 116	643.96	A	1843.1
120-750B-13W-2, 25	644.55	A	1770.8
120-750B-13W-2, 78	645.08	A	1798.6
120-750B-13W-2, 132	645.62	A	1705.4
120-750B-13W-3, 31	646.11	A	1663.3
120-750B-13W-CC, 3	646.63	A	1614.2
120-750B-14R-1, 35	671.85	A	3569.0
120-750B-14R-1, 79	672.29	C	1464.4
120-750B-14R-1, 79	672.29	A	1431.0
120-750B-14R-2, 85	673.85	C	4987.3
120-750B-14R-2, 85	673.85	A	4922.6
120-750B-15R-1, 40	681.60	C	5542.2
120-750B-15R-1, 40	681.60	A	5544.9
120-750B-15R-2, 37	683.07	C	4572.2
120-750B-15R-2, 37	683.07	A	4495.3
120-750B-15R-2, 80	683.50	C	4491.3
120-750B-15R-2, 80	683.50	A	4834.8
120-750B-15R-3, 38	684.48	C	5398.1
120-750B-15R-3, 38	684.48	A	5766.6
120-750B-15R-4, 69	686.08	C	5571.3
120-750B-15R-4, 69	686.08	A	5866.7
120-750B-15R-5, 45	687.14	C	5525.9
120-750B-15R-5, 45	687.14	A	5523.6
120-750B-16R-1, 37	690.87	C	5815.6
120-750B-16R-1, 37	690.87	A	6054.8
120-750B-16R-2, 41	692.41	C	5730.9
120-750B-16R-2, 41	692.41	A	6211.9
120-750B-16R-3, 67	694.07	C	5506.7
120-750B-16R-3, 67	694.07	A	6037.6
120-750B-16R-3, 135	694.75	A	6025.8
120-750B-16R-4, 97	695.73	C	5452.2
120-750B-16R-4, 97	695.73	A	5995.6
120-750B-16R-5, 82	696.97	C	5140.2
120-750B-16R-5, 82	696.97	A	5178.7
120-750B-16R-6, 100	698.58	C	5500.0
120-750B-16R-6, 100	698.58	A	5805.8
120-750B-16R-7, 111	699.99	C	5464.6
120-750B-16R-7, 111	699.99	A	5996.7
120-750B-17R-1, 15	700.35	C	5623.4
120-750B-17R-1, 15	700.35	A	5863.5
120-750B-16R-8, 34	700.49	A	5789.5
120-750B-17R-3, 11	703.31	C	4091.9
120-750B-17R-3, 11	703.31	A	4385.7

Note: DIR = direction of wave propagation; A = perpendicular to bedding; and C = perpendicular to split face of core.

Table 12. Thermal conductivity determinations, Hole 750A.

Core, section, interval (cm)	Depth (mbsf)	Thermal conductivity (W/m·K)
120-750A-		
1R-1, 80	0.80	1.3610
1R-3, 25	3.11	1.3310
1R-6, 20	7.06	1.4270

subdivided into five units (Units 2–6 based on mineralogy, textures, and degree of alteration [see core descriptions, this chapter]). Unit 1 is a ferruginous claystone that occurs at the top of Core 120-750B-14R-1, 0–23 cm.

The upper section has a minimum thickness of 2.9 m and contains at least two flows. The first flow consists of a moderately altered, fine-grained, gray-green colored, sparsely plagioclase phyrlic basalt (Unit 2; Core 120-750B-14R-1, 23–57 cm; see core descriptions, this chapter). The basalt is massive and contains a few vesicles filled with calcite and minor green clays. It overlies a highly altered, partly decomposed green-colored basalt

(Unit 3; Core 120-750B-14R-1, 67 cm, to Core 120-750B-14R-2, 62 cm). The degree of alteration varies from pronounced replacement of the groundmass by green clays (the texture of the basalt can still be recognized) to complete decomposition of basalt to soft and friable, green clay-rich aggregates (Fig. 31).

Underlying this highly altered basalt is a moderately altered, fine-grained, sparsely plagioclase phyric basalt (Unit 4; Core 120-750B-14R-2, 62–112 cm). This basalt is locally crosscut by numerous subhorizontal calcite veins (1–4 mm wide; Fig. 32) and commonly contains irregular-shaped vesicles (up to 1 cm) mainly filled by green clays and surrounded by dark halos (Fig. 33). Units 3 and 4 may belong to a single flow.

The lower section consists of two basalt flows (Units 5 and 6) separated by a chilled margin (Core 120-750B-17R-2, 35–54 cm). The contact between Units 4 and 5 is not observed, although they were differentiated by their mineralogical composition and texture. Unit 5 consists of a moderately altered massive plagioclase-clinopyroxene phyric basalt with a thickness of 11.5 m. It

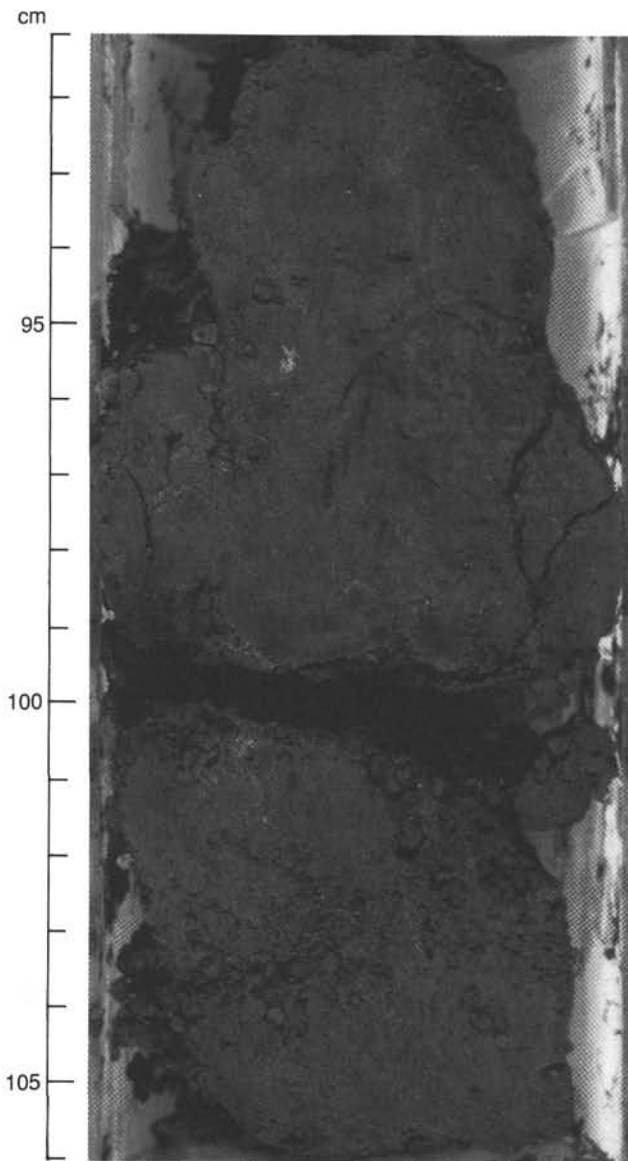


Figure 31. Complete decomposition of basalt into a soft and friable green clay (Core 120-750B-14R-1, 91–106 cm).

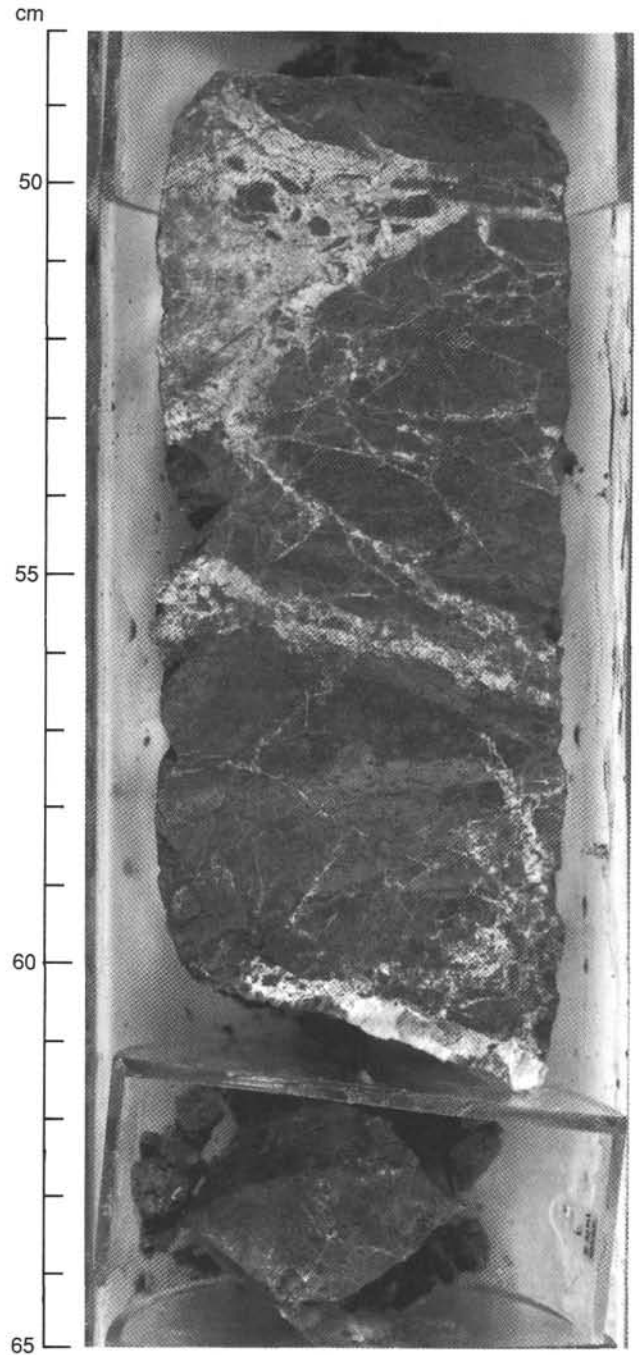


Figure 32. Calcite veins and veinlets crosscutting basalt (Core 120-750B-14R-2, 48–65 cm).

is gray to gray-green in color, is very fine to fine grained, and contains sparse euhedral to subeuhedral plagioclase and clinopyroxene phenocrysts (0.5–2 mm). The clinopyroxene phenocrysts locally cluster together.

The most distinctive textural feature of this basalt, more common in the lower part of the flow, is the occurrence of coarser and darker colored bands and clots up to a few centimeters in width or diameter (Fig. 34). They are phenocryst rich and show some signs of grading. These could be clumps of dislodged cumulates or represent mechanical segregation structures produced during flow. Alternatively, the texture may be a product of

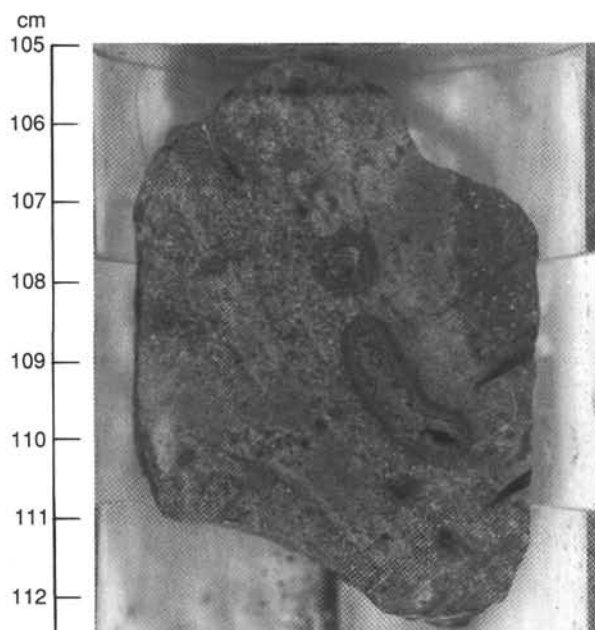


Figure 33. Irregular-shaped vesicle filled with green clay and surrounded by a dark halo (Core 120-750B-14R-2, 105–112.5 cm).

magma mixing. Irregularly shaped to subround vesicles (1–15 mm), filled mainly with green smectite (Fig. 35), calcite, and occasional rust-colored zeolites are common.

A zone of intense veining was observed in Core 120-750B-16R-3, 38–47 cm (Fig. 36). The veins (1–10 mm) consist mainly of green smectite with some calcite, but they may also have a minor component of quartz and iron hydroxides. Locally, some diffuse iron hydroxides can also be observed in the groundmass (Core 120-750B-15R-2, 0–32 cm). The base of the flow is cut by numerous nearly vertical veins (2–8 mm) lined by calcite and filled by green clays and occasional quartz (Core 120-750B-17R-1, 60–150 cm; Core 120-750B-17R-2, 0–34 cm).

The top of the lava flow of Unit 6 is marked by a chilled margin (Core 120-750B-17R-2, 35–54 cm), now altered glass. Unit 6 is composed of an aphyric, nonvesicular green-gray colored, microcrystalline basalt. Subvertical veins up to 10 mm in width consisting of clays and calcite are present throughout most of this unit.

Petrography

The basalts from Hole 750B are sparsely phyrlic. The basalts of Unit 2 and Unit 4 contain euhedral phenocrysts of plagioclase (1–1.5 mm) that are altered to zeolites. Unit 2 is distinguished by the presence of subhedral iddingsite pseudomorphs of olivine (0.7–1 mm). The groundmass is microcrystalline and contains plagioclase and Fe-Ti oxides. No thin sections were made of Unit 3 because the basalt is decomposed.

Unit 5 consists of a massive, plagioclase-clinopyroxene phyrlic basalt. This unit shows alternations (on the scale of a few centimeters) between two different textures: medium- to coarse-grained subophitic bands or clots separated by microcrystalline, intersertal basalt (Fig. 34). The plagioclase phenocrysts (An_{60-75}) form euhedral laths (up to 3 mm) and are often associated in radial aggregates. The groundmass is essentially composed of a network of small (0.05–0.5 mm) euhedral plagioclase laths (An_{55-65}). In the subophitic basalts, subhedral to anhedral clinopyroxene (up to 2 mm) poikilolitically enclose plagioclase crystals. The clinopyroxene often occurs in local clusters. Interstitial groundmass minerals consist of Fe-Ti oxides (0.05–0.1 mm) and clays.

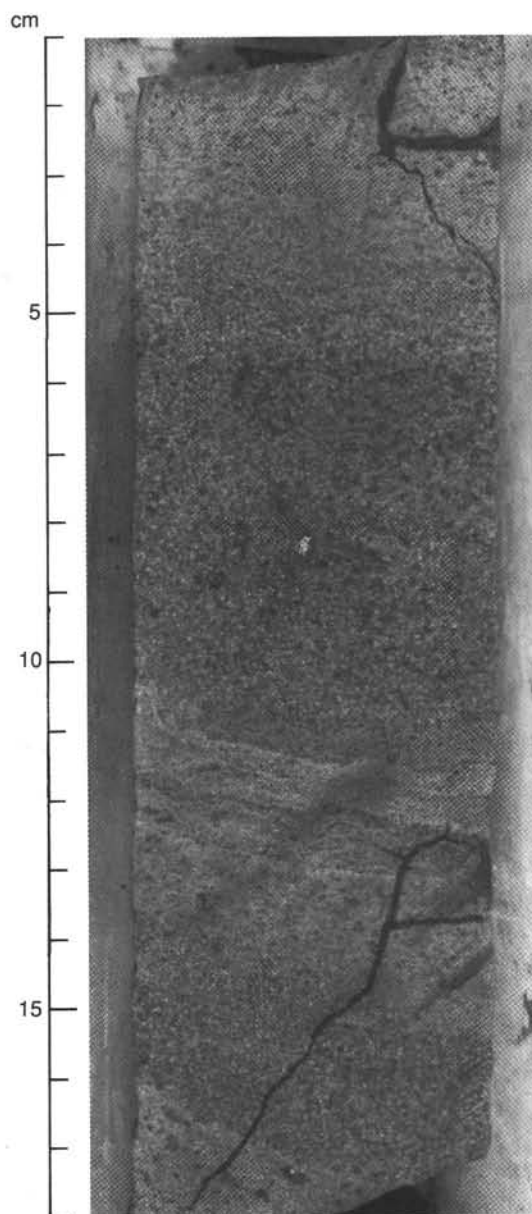


Figure 34. Graded bands of lighter, fine-grained and darker, medium-grained basalt of Unit 5. Note graded tops and sharply truncated bases (Core 120-750B-16R-6, 1–18 cm).

The microcrystalline basalts contain clinopyroxene, Fe-Ti oxides, and clays in the groundmass.

Unit 6 is a highly altered plagioclase-clinopyroxene phyrlic basalt with an intergranular texture. Euhedral plagioclase laths (0.5–0.7 mm) of undetermined composition are associated with subhedral clinopyroxene phenocrysts. The groundmass is composed of plagioclase, clinopyroxene (0.05–0.1 mm), and up to 50% clay.

Alteration

The basalts exhibit different degrees of alteration ranging from highly altered Units 3 and 6 and slightly to moderately altered Units 3, 4, and 5. The secondary minerals consist of green and colorless clays, calcite, and minor zeolites and quartz. The X-ray diffraction (XRD) patterns showed that the clay minerals are smectites. The green-colored smectite probably corresponds

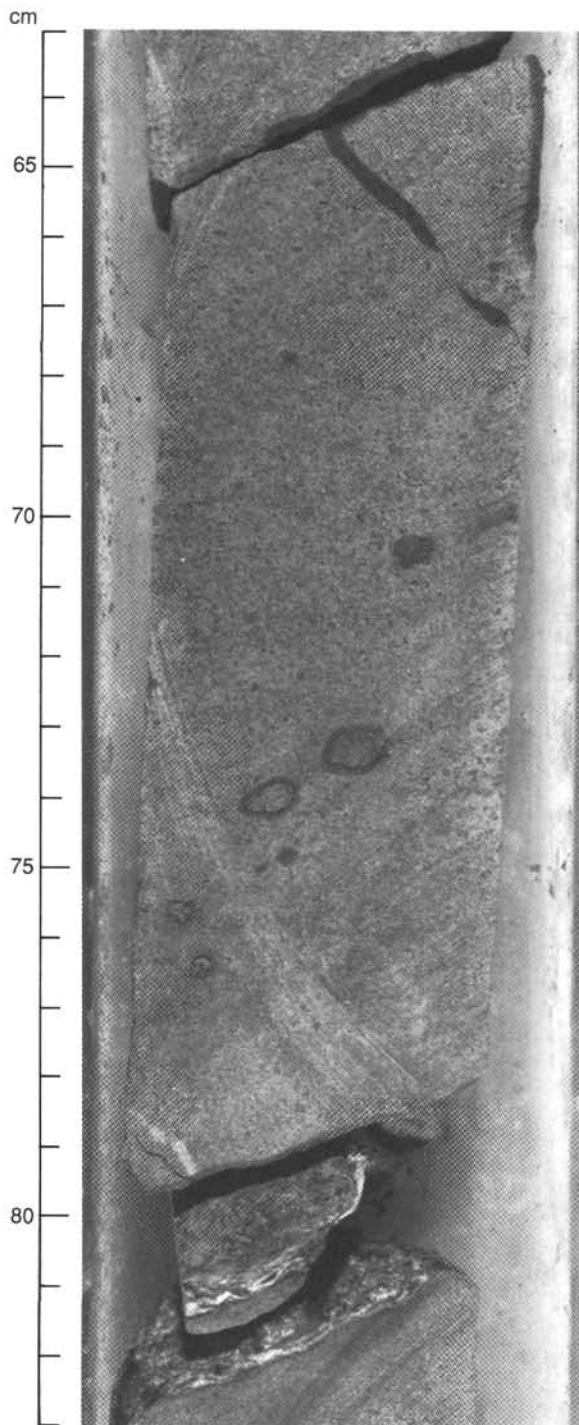


Figure 35. Round to subround vesicles filled with clay in Unit 5 basalt (Core 120-750B-16R-3, 63-83 cm).

to the iron-rich clay. The zeolite was identified as heulandite-clinoptilolite.

The secondary minerals within the groundmass consist of green smectite and, locally, calcite. A red-brown iron hydroxide is associated with groundmass smectite in Unit 5 (see "Macroscopic Core Description" section, above). In the highly altered basalts, green clays with interlayered smectites (XRD identification) have completely replaced the groundmass as well as clinopyroxene phenocrysts. The vesicles are largely infilled by clay minerals. Green smectite occurs as vesicle wall linings, with col-

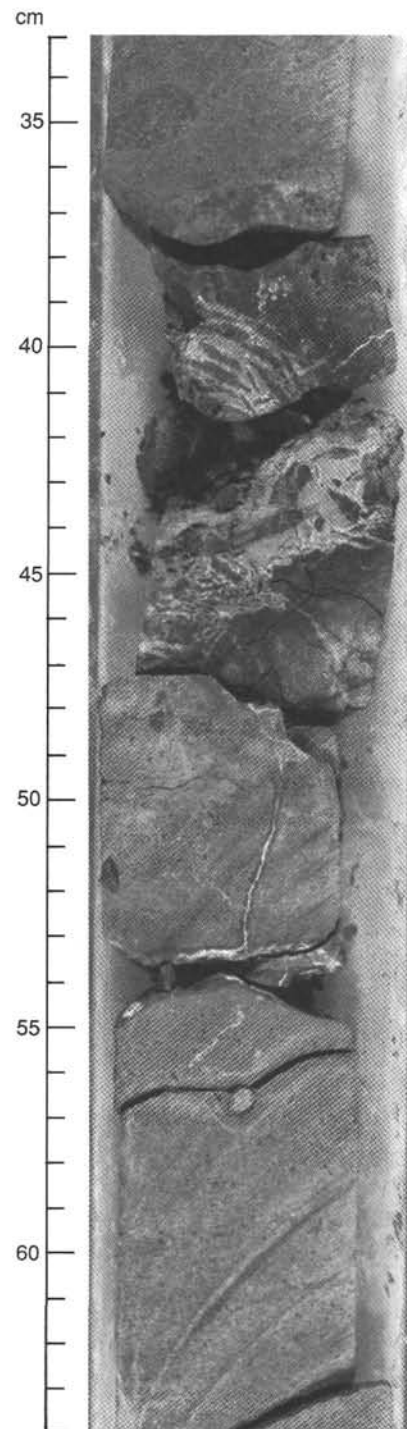


Figure 36. Zone of intense smectite and calcite veining in massive basalt of Unit 5 (Core 120-750B-16R-3, 33-64 cm).

orless smectite showing fibroradiated forms within the vesicle interior. In some vesicles, instead of colorless smectite, heulandite-clinoptilolite, calcite, and/or quartz occur in association with green smectite. Veins consist mainly of green smectite along the walls, with calcite in the interior associated in some cases with fibroradiated zeolites of undetermined composition. Within Unit 5, some thin veins of iron hydroxide occur.

The presence of interlayered smectite together with heulandite-clinoptilolite indicates that basalts from Hole 750B were metamorphosed in the intermediate- to high-temperature zone of the

zeolite facies. The presence of iron hydroxides and iron-rich smectites indicates an oxidizing environment during hydrothermal alteration. The crystallization of smectites is normally favored by higher Eh and lower pH compared to zeolites and calcite.

Geochemistry

Whole-rock major and trace element analyses of representative samples are presented in Tables 13 and 14. The recovered basalts are olivine-hypersthene normative tholeiites. They have high and variable loss on ignition values (3.1–10.0 wt%), reflecting the pervasive alteration observed macroscopically. Since basalts are altered, only elements considered largely immobile during secondary processes (e.g., Ni, Cr, Ti, P, Y, Nb, and Zr) will be considered in the following discussion on their geochemistry.

The lava flows analyzed from Hole 750B are compositionally similar and show only limited variations in Mg# (59.0–51.9), Ni (97–113 ppm), and Cr (105–173 ppm) contents. Compared with basalts from other sites on the Kerguelen Plateau recovered during Leg 120, samples from Hole 750B have lower Cr contents for comparable Mg#'s, indicating a more pronounced role for clinopyroxene fractionation. In terms of incompatible trace element abundances, basalts from Hole 750B are more depleted than samples from other sites on the Kerguelen Plateau (Fig. 37).

Table 13. Major element analyses and normative mineral proportions of basalts from Hole 750B.

Core, section, interval (cm)	14R-1 34–36	15R-2 78–80	16R-3 134–136	16R-4 98–99	16R-8 34–36	17R-1 49–50	17R-2 86–88
SiO ₂	42.85	49.94	49.54	49.34	49.76	49.42	49.24
TiO ₂	0.87	0.68	0.71	0.73	0.69	0.73	1.08
Al ₂ O ₃	17.83	15.61	15.49	15.81	15.36	14.88	14.72
Fe ₂ O ₃	26.45	11.35	11.56	11.07	11.75	12.63	15.31
MnO	0.07	0.15	0.16	0.16	0.17	0.19	0.26
MgO	6.99	9.31	8.74	8.92	8.07	9.43	9.44
CaO	4.43	10.65	11.01	11.07	11.47	10.47	9.12
Na ₂ O	0.89	2.46	2.47	2.80	2.60	2.28	2.34
K ₂ O	4.49	0.11	0.10	0.11	0.06	0.08	0.19
P ₂ O ₅	0.07	0.05	0.05	0.05	0.16	0.05	0.09
Total	100.94	100.31	99.85	100.05	100.10	100.16	100.79
LOI	8.42	10.00	3.90	3.11	9.70	4.18	7.70
Mg#	NC	59.03	57.03	58.56	54.64	56.68	51.88
Or	26.91	0.65	0.60	0.66	0.36	0.48	1.13
Ab	7.62	20.93	21.12	23.88	22.18	19.45	19.88
An	1.75	31.40	31.21	30.48	30.31	30.37	29.22
Di	0	17.50	19.39	20.07	21.43	17.77	12.93
Hy	27.76	17.26	15.23	7.11	13.84	19.57	18.59
Ol	17.79	8.57	8.64	14.08	7.85	8.32	12.95
Ap	0.15	0.11	0.11	0.11	0.35	0.11	0.20
Il	1.68	1.30	1.36	1.40	1.32	1.40	2.04
Mt	5.33	2.27	2.33	2.22	2.36	2.54	3.06
Co	11.01	0	0	0	0	0	0

Note: LOI = loss on ignition and NC = not calculated.

Table 14. Trace element analyses of basalts from Hole 750B.

Core, section, interval (cm)	Rb	Ba	Nb	Sr	Zr	Y	Zn	V	Cu	Ni	Cr
120-750B-											
14R-1, 34–36	17	248	3.5	43	33	13	109	332	152	113	139
15R-2, 78–80	1.3	60	2.3	123	32	17	81	254	111	106	109
16R-3, 134–136	1.4	63	3.0	121	33	18	84	280	149	109	105
16R-4, 98–99	2.0	55	4.6	123	33	18	86	277	149	98	113
16R-8, 34–36	0.4	56	3.5	121	33	18	79	270	146	97	111
17R-1, 49–50	1.1	53	3.3	110	32	18	126	274	126	101	110
17R-2, 86–88	4.1	49	4.5	112	50	26	101	293	62	106	173

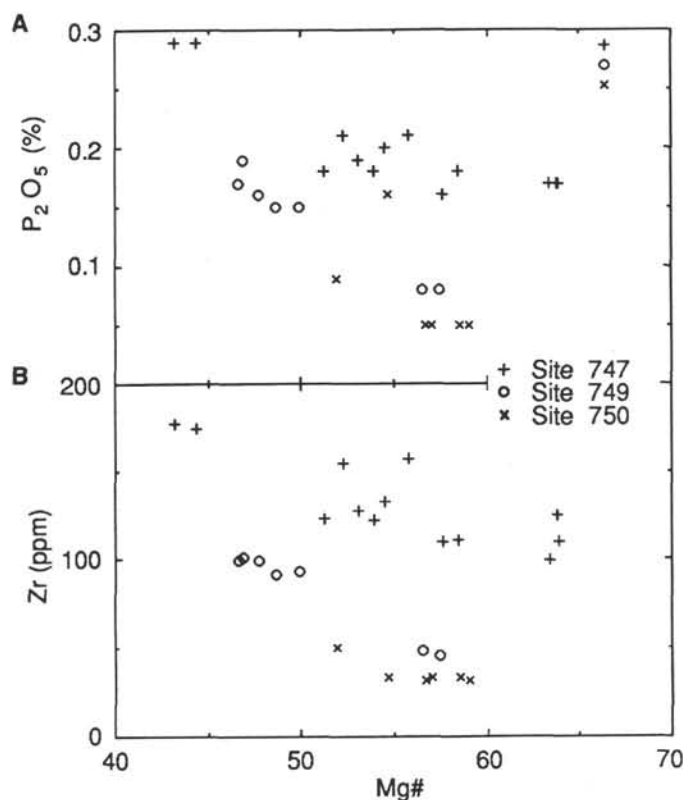


Figure 37. Plots of (A) Mg# vs. P₂O₅ and (B) Mg# vs. Zr for the basalts from Sites 747, 749, and 750.

On a Zr vs. Nb diagram, basalts from Hole 750B extend the trend defined by Site 747 and Site 749 basalts (Fig. 38). Hole 750B basalts have, on average, slightly lower P/Y and Zr/Nb ratios than those from Sites 747 and 749 (Fig. 39). This could reflect slight heterogeneities among the basalt mantle sources for the different sites. The variation in actual incompatible element abundances between the various sites may be caused by differences in the degree of partial melting.

Summary

Basement recovered at Site 750 consists of a minimum of four basalt lava flows. The top of the section consists of highly altered volcanics. All the basalts are olivine-hypersthene normative tholeiites. The basalts contain phenocrysts of plagioclase, clinopyroxene, and sporadic olivine. Clinopyroxene is more abundant in basalts from Hole 750B than those from Sites 747 and 749. The basalts are slightly to highly altered, the secondary mineral assemblage consisting of smectites and calcite, with minor heulandite-clinoptilolite, quartz, and iron hydroxides. These mineral assemblages suggest alteration occurred under oxidizing

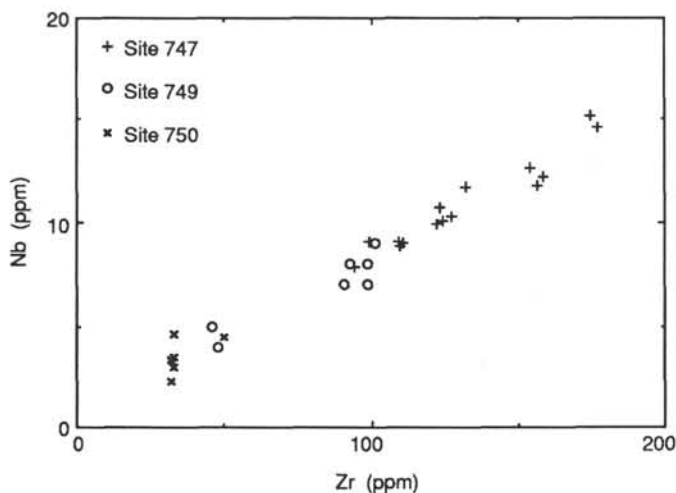


Figure 38. Zr vs. Nb diagram for the basalts from Sites 747, 749, and 750.

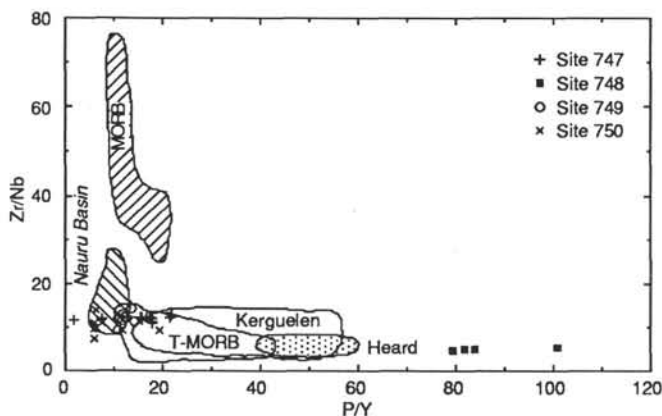


Figure 39. P/Y vs. Zr/Nb diagram showing the interelement variation for basalts for all Leg 120 sites with respect to MORB, Kerguelen Island, T-MORB, and Heard Island fields. Fields of oceanic basalts from the Indian Ocean from Nauru Basin (Saunders, 1985), MORB (Price et al., 1986), Kerguelen and Heard (Storey et al., 1988), and T-MORB (le Roex et al., 1983). T-MORB = transitional basalts from the Southwest Indian Ridge.

conditions corresponding to the intermediate- to high-temperature zone of the zeolite facies.

Basalts from Site 750 are more depleted in incompatible trace elements than any of the other basalts recovered on Leg 120. This may indicate that basalts from Hole 750B were produced by higher degrees of melting than those of Sites 747 and 749. Excluding the single (OIB) basalt flow drilled at Site 748, Leg 120 basalts show some intersite variations in incompatible element ratios, possibly indicating source heterogeneities.

Compositionally, Hole 750B basalts show affinities with Nauru Basin basalts (Saunders, 1985) and transitional basalts from the Southwest Indian Ridge (le Roex et al., 1983). The alkaline basalt lava from Hole 748C is quite distinctive, being extremely enriched in incompatible elements with compositional characteristics typical of OIB-type magmatism.

LOGGING

The initial logging program in Hole 750A called for three Schlumberger runs: seismic/stratigraphic, lithoporosity, and geochemical. Due to time constraints and problems encountered

when entering the hole with the second tool string, only one logging run (SDT/DITE/NGT) was completed.

The seismic/stratigraphic tool string run in Hole 750A was comprised of AMS (auxiliary measurement sonde), TCCB (telemetry cartridge), NGT (natural gamma ray spectroscopy tool), MCD (caliper), SDT (multichannel sonic), DITE (phasor induction/resistivity), and VSTP (Lamont-Doherty temperature tool). A more detailed explanation of the logging tools successfully used on Leg 120 can be found in the "Explanatory Notes" chapter (this volume).

Prior to logging, the hole was conditioned and displaced to 9.8 lb/gal freshwater mud. The bit was mechanically released, and the pipe pulled to leave approximately 70 m of BHA below the seafloor.

Schlumberger commenced rigging up at 1000 hr (LT), 17 April 1988. The first tool string (DITE/SDT/NGT) started in the hole at 1200 hr (LT); however, shortly after running in hole (at a depth of 200 m) the DITE malfunctioned. The tool string was pulled to the surface and the faulty DITE sonde replaced with a backup. Schlumberger ran down to TD with this tool string. A single bridge was found, and successfully punched through, at 2180 m below rig floor (mbrf; 140 mbsf); no further problems were encountered while running to bottom.

A downlog was recorded while running down to TD; TD for this hole was found at 2493 mbrf (453 mbsf). The open-hole section was successfully uplogged at 800 ft/hr from TD back into the drill pipe. The drill pipe was pulled up an additional 20 m when logging the upper section of the hole to allow more open hole to be logged. A repeat section was logged over the interval from 350 to 420 mbsf. This interval was expected to contain the Cretaceous/Tertiary boundary, and it showed some interesting characteristics on the main log. Schlumberger was out of the hole with the first tool string at 2130 hr (LT), 17 April 1988.

Deteriorating weather conditions made it necessary to run an extra 50 m of drill pipe in the hole before running the second tool string. This positioned the end of the drill pipe/BHA at 120 mbsf. Schlumberger started in the hole with the second tool string (LDT/CNT/NGT) at 2330 hr (LT), 17 April 1988. All tools operated successfully while running down through the drill pipe, although the logging cable shorted out immediately after the tool string exited the drill pipe and entered the open hole, and no log was recorded. The tool was pulled back to the surface.

Once at the surface, the head of the logging cable was found to be severely kinked just above the tool head. The damage sustained by the logging tool suggests that it may have impacted with the end of the drill pipe/BHA. This could have resulted from a combination of excessive pipe heave while exiting from the drill pipe into the open hole and the tool hitting a bridge just below the end of the drill pipe. Time restrictions precluded the repair and rerunning of this tool string. The second run was abandoned, and Schlumberger was rigged down at 0645 hr (LT), 18 April 1988.

Log Quality/Interpretation

All depths quoted in this report are wireline loggers' depths. When a borehole is logged in rough weather with considerable ship heave (as in Hole 750A), there is no fixed formation datum into which the logger can tie his depths. The drill pipe is suspended, uncompensated, in the borehole; consequently, it moves with ship heave relative to the formation. In Hole 750A the logger found the end of the drill pipe at 2092 mbrf, whereas the driller placed the length of drill pipe in the hole at 2088 mbrf, a discrepancy of 4 m.

In situations of no heave, log depths may be adjusted to agree with drillers' depths and therefore coring depths. Considerable ship heave was experienced while logging Hole 750A. At-

tempting to tie wireline log depths to coring (formation) depths by correcting to an uncompensated drill pipe depth is difficult. Loggers' depths are used throughout the report.

Logging at Site 750 was performed under more favorable weather conditions than at the previously logged site (Site 747). The wireline heave motion compensator was used for the initial 100 m of the main uplog. Sea conditions deteriorated throughout the logging run and caused the compensator to trip out. The heave compensator was not used for the remainder of the logging runs. Although the logs were primarily recorded without using the compensator, they do not appear to be affected by ship motion.

The caliper log shows that the hole exhibits frequent wash-out zones, particularly over the upper section of the hole where the formation is less competent (see Fig. 40). The resistivity (DITE) and gamma ray (SGR) logs were unaffected by the poor borehole conditions, and they recovered good quality data over the complete hole section. The sonic (SDT) log is, however, badly affected by the poor borehole conditions. These data have been reprocessed by Schlumberger, Houston; the reprocessed data is presented in Figure 41. More sophisticated post-cruise reprocessing of the sonic waveform data may yield further useful information.

The resistivity curves show an interesting change in log character below 357 mbsf (see Fig. 40). The shallow-reading SFLU curve begins to read higher than both the medium (ILM) and deep (ILD) induction resistivity curves. In the upper hole section (230–357 mbsf), all three resistivity curves overlay. The separation of the resistivity curves, the resistivity profile, is a classic example of mud filtrate invasion into the formation. In this particular case, the invading fluid is the freshwater mud used to condition the hole prior to logging. The invading low-salinity (5,000 ppm NaCl) freshwater filtrate displaces the higher-salinity (36,000 ppm NaCl) formation water from around the wellbore and creates an invaded zone of higher resistivity around the borehole.

The SFLU, which has the shallowest depth of investigation, is most affected by the higher resistivity invaded zone close to the wellbore. Both induction logs have a much greater depth of investigation and take the greater proportion of their resistivity measurement from the lower resistivity uninvaded zone further away from the wellbore. The observed resistivity/invasion profile is a function of formation permeability, contrasting fluid salinities, and the differing depths of investigation of the three resistivity tools.

The auxiliary measurement sonde (AMS), run in combination with the SFLU, continuously records downhole temperature and borehole fluid (mud) resistivity. Figure 42 shows the comparison of mud resistivity with the three recorded formation resistivities. The mud resistivity is relatively constant above 350 mbsf, but below 350 mbsf the mud resistivity increases rapidly. This response is consistent with the presence of freshwater in the lower section of the hole but not above 350 mbsf. The evidence suggests that the freshwater mud used to condition the hole did not fill the hole as expected but leaked off into the formation below 357 mbsf.

The volume of the borehole from TD to 357 mbsf is estimated from the caliper log to be approximately 50 bbl. A total of 115 bbl of freshwater mud was pumped during the conditioning process; this implies 65 bbl of freshwater must have leaked off into the formation. It is calculated, assuming a formation porosity of 40%, that the depth of fluid invasion would be approximately 7 in.

Sonic and resistivity porosities have been calculated throughout the hole section (Fig. 41). Sonic porosities were calculated from the reprocessed sonic transit times using a Raymer-Hunt transform applicable to "soft" formations. Resistivity porosi-

ties were calculated from the deep induction (ILD) resistivity curve, assuming a basic "soft sediment" Archie relationship. In general, both sonic- and resistivity-derived porosities are in good agreement and show an expected gradual decrease in porosity with increasing depth.

Log-Derived Lithologic Horizons

The whole of the logged interval for Site 750 shows very few major changes in log character that can be attributed to significant lithologic boundaries. These uniform log responses are to be expected as the whole interval consisted of a rather homogeneous calcareous ooze/chalk section. However, the logs reveal subtle changes in lithology through the interval and have provided useful stratigraphic control for core-derived lithologies.

For the purpose of this analysis, the total logged interval has been divided into three separate units (log Units 1, 2, and 3). These divisions were primarily based on changes in character of the resistivity logs. In general, the sonic and gamma rays were not helpful in providing any stratigraphic control. The gamma ray curve records very low levels of radioactivity throughout the logged interval. A slight increase in the gamma ray is seen with increasing depth, this is due to the slight increase in clay content. The sonic log, as previously mentioned, contains many intervals of spurious data. The reprocessed sonic log (Fig. 41) does show a gradual decrease of transit time with depth. However, it cannot be used with confidence to detect subtle changes in lithology.

Log Unit 1

Both the resistivity and gamma ray curves are relatively featureless over this uppermost log unit (51.5–223 mbsf). The lack of character is consistent with the homogeneous, calcareous soft sediments and oozes recovered from this interval. Low resistivities and high sonic transit times (in intervals of valid data) are indicative of a highly porous, unconsolidated formation. The very low gamma ray response suggests virtually a complete absence of clays or other radioactive material in this unit.

Log Unit 2

This log unit (223–357 mbsf) is characterized by a slight increase in the resistivity at the top of the unit. Both an increase in resistivity and a decrease in sonic transit time suggest that the sediments become firmer and better cemented with depth. The caliper log (HD) shows that there are fewer washouts in this unit and is another indication of increasing lithification. The resistivity logs do show some very minor character changes throughout the unit. The low-amplitude SFLU spikes (<2.0 ohm) may identify thin chert stringers.

Lithologic data from cores suggest this unit contained an abundance of chert stringers. A series of low-amplitude peaks on the SFLU (317–327 mbsf) would appear to correlate with a significant increase in chert recovery at this depth. A slight increase in all three resistivity curves is noted toward the base of Log Unit 2 (338–345 mbsf). This is correlatable with increasing clay content, hardening of the sediment, and the presence of solution seams at this depth (see "Lithostratigraphy and Sedimentology" section, this chapter).

Log Unit 3

The most prominent feature of this unit (357–450 mbsf) is the invasion profile shown by the three resistivity curves; the nature of the invasion profile has been explained earlier in this report. The invasion profile has been generated by fluid invasion, not lithology contrasts; however, it can be used to infer certain physical properties of the sediments. The very fact that fluid invasion has occurred below 357 mbsf suggests that the formation

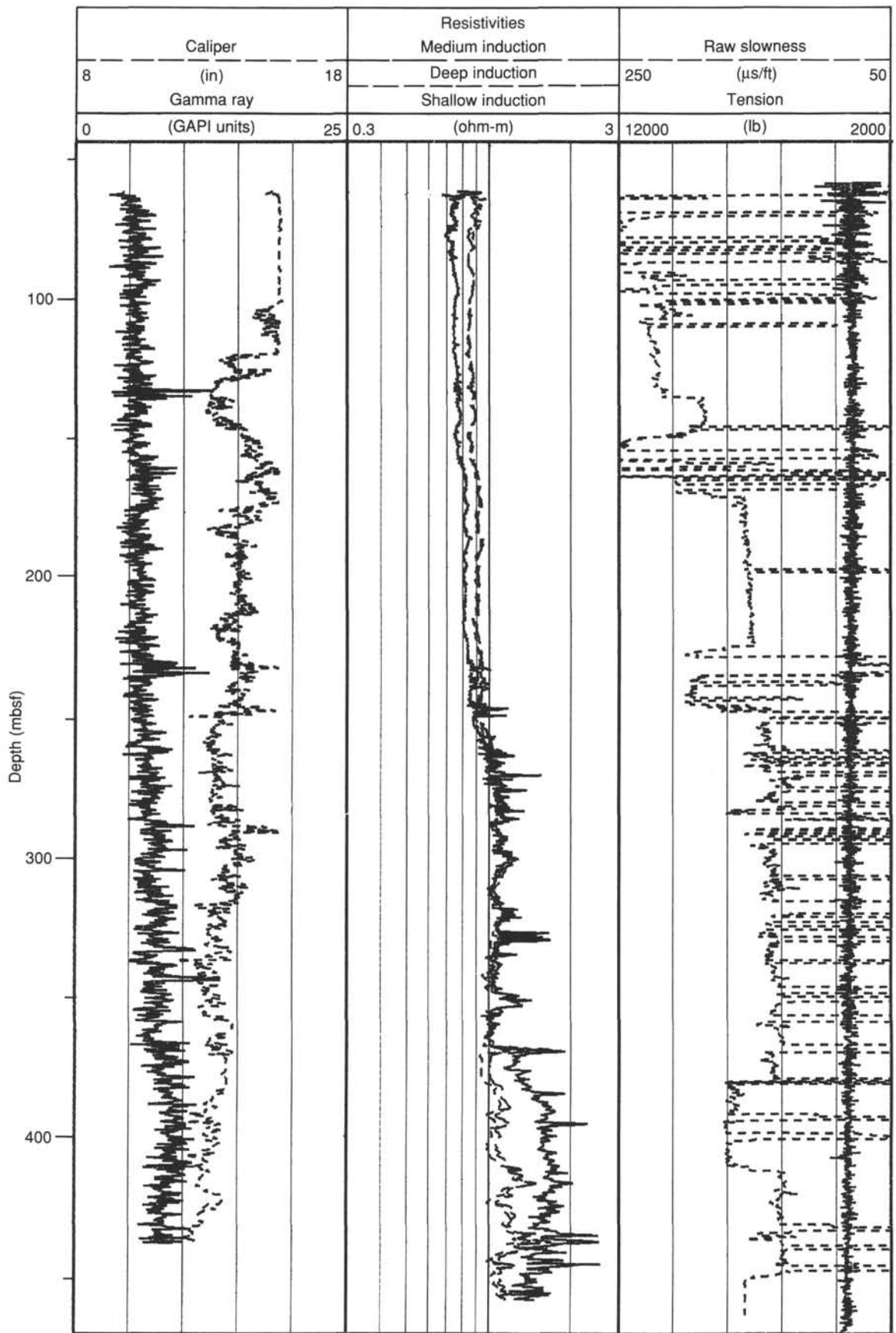


Figure 40. Raw DITE/SDT/NGT/MCD log data for Hole 750A.

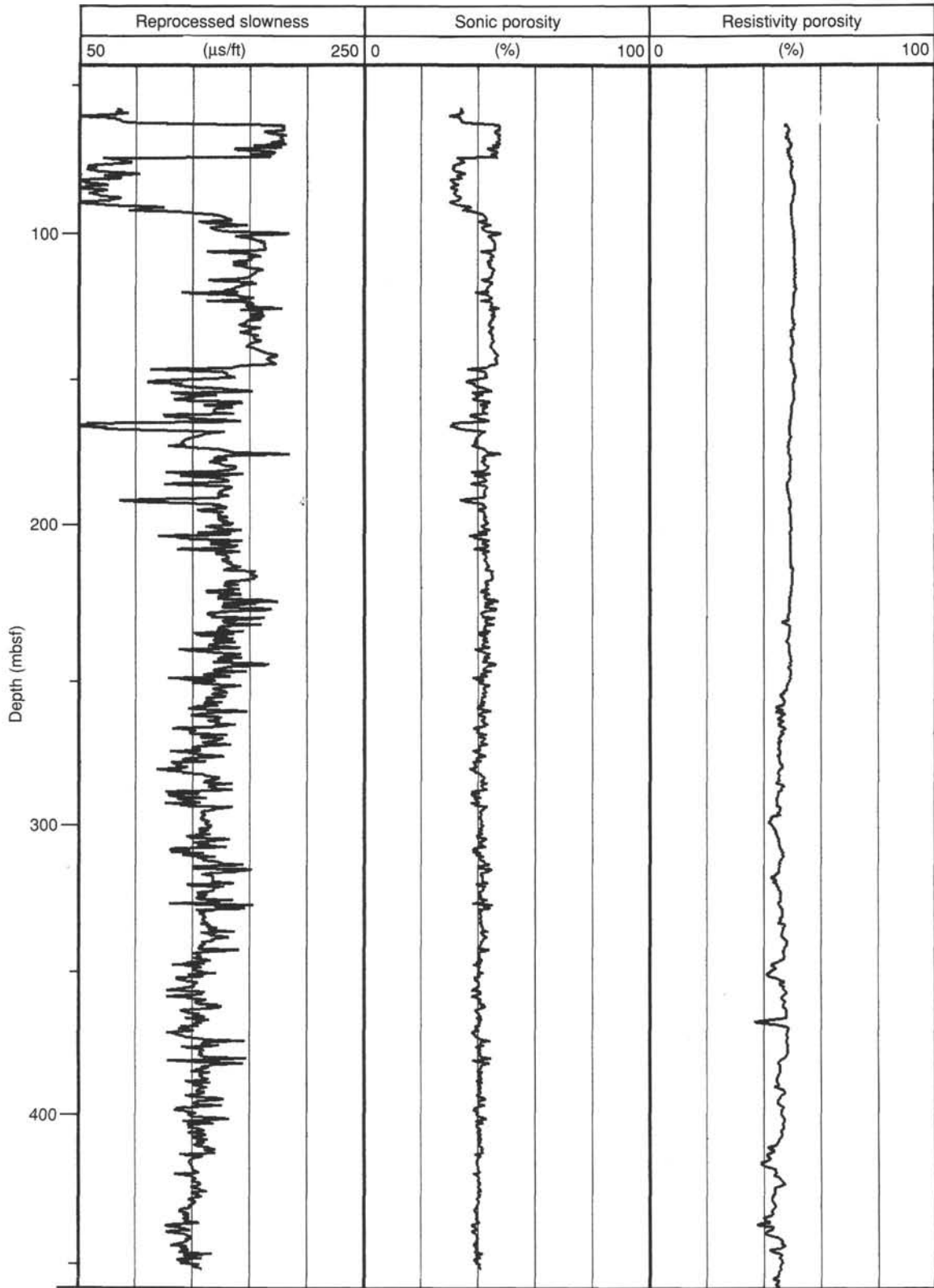


Figure 41. Plot of reprocessed sonic, Raymer-Hunt sonic, and resistivity (Archie-derived) porosities, Hole 750A.

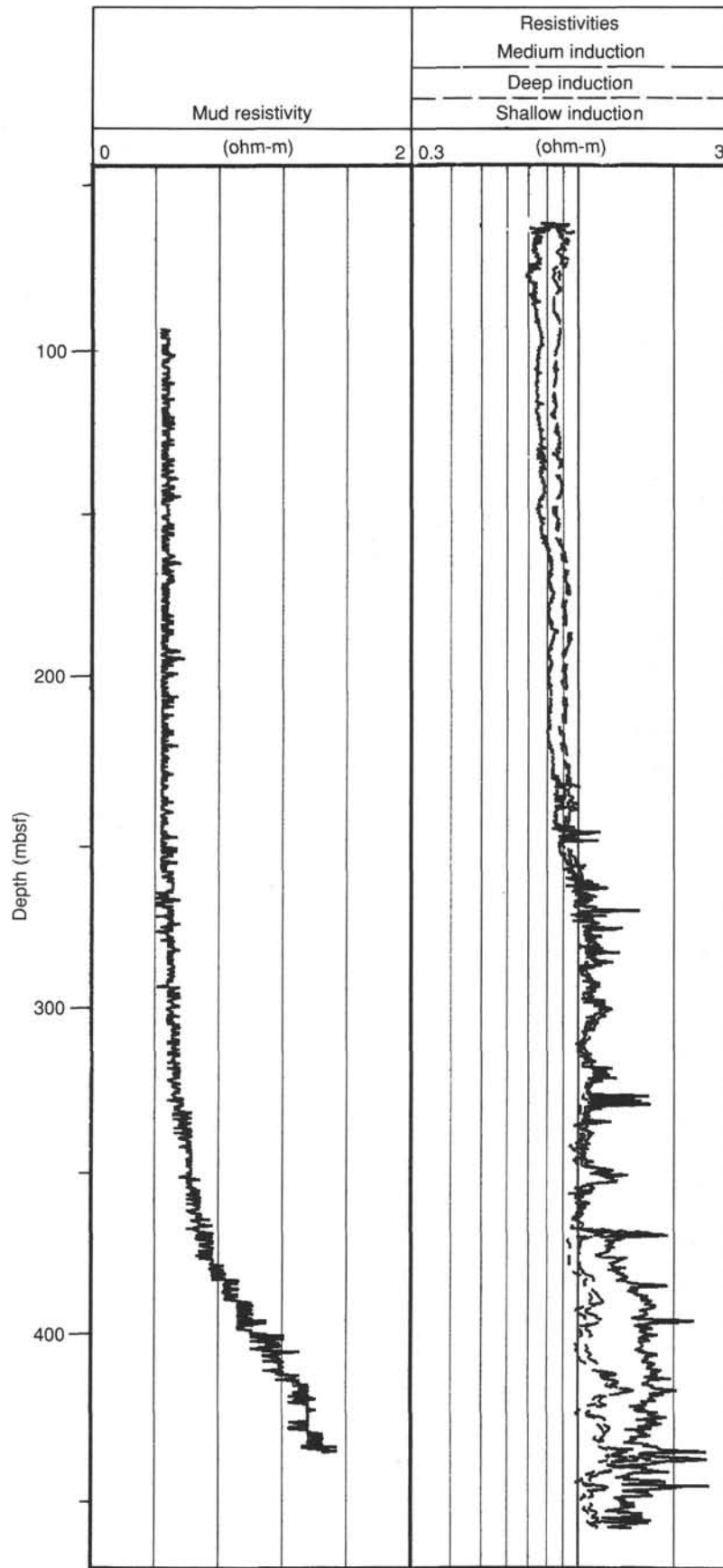


Figure 42. Plot of mud resistivity and formation curves, Hole 750A.

is rather permeable. A marked cut off of the profile at 357 mbsf would suggest a sudden reduction in permeability at this depth.

The deep (ILD) and medium (ILM) induction resistivities are used to identify minor lithology changes in this unit. These tools read beyond the invaded zone and should reflect variations in the true formation resistivity. The Cretaceous/Tertiary boundary is picked at 359.5 mbsf to coincide with the base of the resistivity peak seen on the logs. An undisturbed core was recovered across the Cretaceous/Tertiary boundary. Core lithology indicated a sharp increase in clay content immediately above the boundary, with little or no clay below. An increase in clay content could account for the increase in formation resistivity at this depth.

Plugging of the matrix pore spaces with clay would significantly decrease formation permeability and may explain why the invasion profile is restricted to below the Cretaceous/Tertiary boundary. Immediately below the Cretaceous/Tertiary boundary (at 359.5 mbsf), there is a 20-m-thick interval of slightly lower resistivity. This correlates well with a very soft chalk section recovered below the Cretaceous/Tertiary boundary.

Intervals of higher induction resistivity (401–408 and 423–457 mbsf) correspond to a firming and/or increase in cementation of the formation. The caliper log generally indicates smaller hole diameter opposite intervals of higher resistivity. A smaller diameter (in-gauge) hole would normally indicate a more competent formation. Core samples recovered from the above intervals show an increase in calcareous cementation, silicification, and solution seams (stylolites). The gamma ray shows a slight increase in formation radioactivity within the unit. This is probably due to a minor increase in clay content with depth.

Synthetic Seismogram

A synthetic seismogram was not generated for this site; this will be attempted after further post-cruise reprocessing of the sonic data.

Summary

The seismic/stratigraphic tool string run in Hole 750A showed few major changes in log character; this is consistent with a rather homogeneous calcareous ooze/chalk formation. The Cretaceous/Tertiary boundary was identified at a depth of 359.5 mbsf. Minor downhole changes in lithology—predominantly sediment lithification and increasing clay content—were successfully identified throughout the section and provided valuable stratigraphic control for the core-derived lithologies.

SEISMIC STRATIGRAPHY

The seismic profiles in the eastern Raggatt Basin across Site 750 (Figs. 2, 7, and 8) are dominated by a clear reflector that corresponds, as already observed at Site 748 in the western Raggatt Basin, to the boundary between Sequences K3 and P1. At Site 750 this reflector can easily be traced on the *Rig Seismic* and the *JOIDES Resolution* seismic records at 0.46 s TWT (Fig. 8). Basement lies at 0.69 s TWT and can only be resolved precisely on the *Rig Seismic* multichannel seismic reflection profile (Fig. 8).

The other reflectors at 0.59 and 0.31 s TWT, which were deduced from seismic stratigraphy interpretation, cannot be scaled on the *JOIDES Resolution* seismic line. These two reflectors correspond to the boundary between Sequences K2 and K3 and to the top of Sequence P1, respectively (see “Site Geophysics” section, this chapter). The reflectors traced at 0.69, 0.59, 0.46, and 0.31 s TWT on the seismic records at Site 750 are related to major changes in the lithology and physical properties.

Core descriptions revealed several clear lithologic events. Described from top to bottom, the first subdivision corresponds to the boundary between Subunits IIA and IIB at 317.2 mbsf. Subunit IIA consists of middle Eocene to Paleocene white nannofossil ooze, chalk, and chert; Subunit IIB consists of Danian white nannofossil chalk. Farther down two important changes are recorded in Unit III. The first occurs at the boundary between Subunits IIIA and IIIB at 450.0 mbsf; the second lies at the top of Subunit IIIC at 594.6 mbsf. Subunit IIIA consists of Maestrichtian to upper Campanian nannofossil chalk and minor chert, Subunit IIIB of upper Campanian intermittently silicified limestone and calcareous chalk, and Subunit IIIC of Cenomanian and Turonian chalk with dark clayey interlayers. The lowermost event recorded in the sedimentary column corresponds to the boundary between Units IV and V. Unit IV consists of Albian red to dark grey-brown silty claystone with charcoal and minor conglomerate; Unit V corresponds to the basaltic basement (see “Lithostratigraphy and Sedimentology” section, this chapter).

The physical properties (index properties, compressional wave velocities, and thermal conductivity) measured at Site 750 roughly follow the lithologic subdivisions already discussed (see “Physical Properties” section, this chapter). We cored Holes 750A and 750B intermittently with the exception of the Cretaceous/Tertiary boundary and the basaltic basement; thus, physical properties measurements are sparse and only available below 300 mbsf. Below this depth, major changes were recorded at 317.2, 450.0, 594.6, and 675.5 mbsf; these are directly correlated with the tops of Subunits IIB, IIIB, and IIIC and Unit V, respectively.

Preliminary processing of the seismic stratigraphic logging data allows us to distinguish two distinct events. The first lies in lithologic Subunit IIA at about 200–220 mbsf and probably corresponds to the first occurrence of porcellanite and chert. The second event corresponds to a clear change in the trend of the sonic curve at 290 mbsf; the velocity continuously increases from 1.81 km/s (100 mbsf) to 2.29 km/s (290 mbsf) and remains constant between 290 and 450 mbsf (see “Logging” section, this chapter).

From the seismic data, lithology, physical properties, and logging data, the major seismic reflectors at 0.46 s TWT (P1/K3 boundary) and 0.69 s TWT (K2/basement boundary) must be correlated with the top of lithologic Subunit IIIB (450.0 mbsf) and the top of lithologic Unit V (675.5 mbsf). Taking into account the velocity derived from the logging data, the seismic reflector at 0.31 s TWT (P2/P1 boundary) lies within Subunit IIA at 290 mbsf. Furthermore, the mean velocity for most of Subunit IIA is 1.87 km/s (0–290 mbsf) and is 2.13 km/s for the lower part of Subunit IIA and all of Subunits IIB and IIIA (290–450 mbsf).

The seismic reflector at 0.31 s TWT does not match any lithologic boundary. Since the seismic reflector at 0.69 s TWT obviously corresponds to the basaltic basement, it is possible to correlate the reflector at 0.59 s TWT (K2/K3 boundary) with the top of Subunit IIIC. With this assumption, the mean velocity calculated for Subunit IIIC and Unit IV is 1.62 km/s and is compatible with the measured compressional wave velocity completed on the very rare samples recovered in the hole. Consequently, the mean calculated velocity for Subunit IIIB is 2.23 km/s. The measured values for this subunit are extremely scattered and vary between 2.0 and 3.5 km/s; moreover, the limited number of samples did not allow us to estimate a significant mean velocity. The interpreted seismic section (*Rig Seismic* RS02-24) at Site 750 is given in Figure 43.

Based upon these correlations, a vertical velocity distribution model relating the different seismic sequences to the litho-

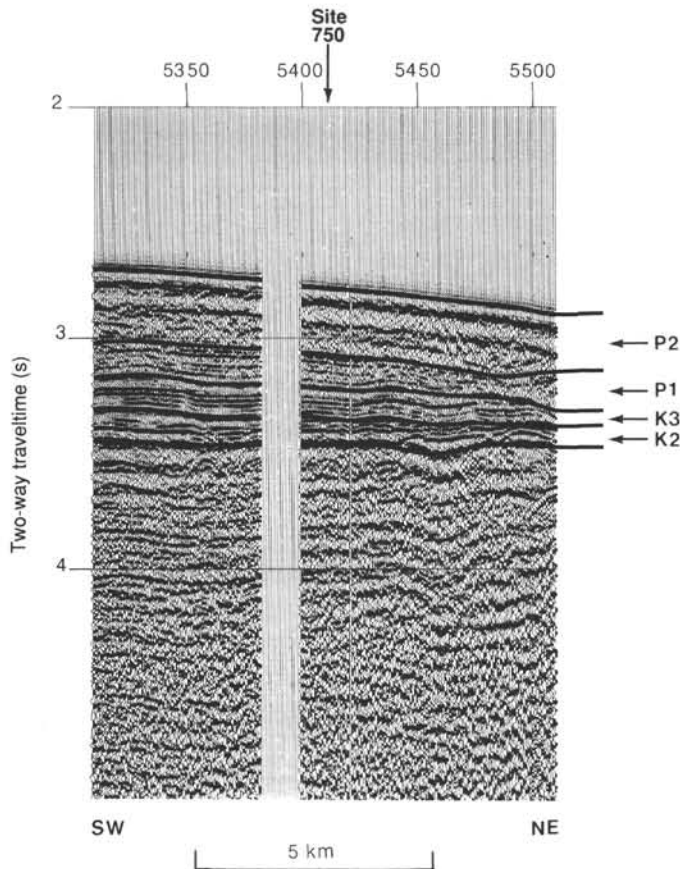


Figure 43. Interpretation of the *Rig Seismic* (RS02-24) seismic reflection profile at Site 750 with identification of the seismic sequences. The uninterpreted seismic section is shown on Figure 8. The correlation of the seismic sequences with the lithologic units is given in Figure 44.

logic units can be established for the sedimentary column at Site 750 in the eastern Raggatt Basin on the Southern Kerguelen Plateau (Fig. 44).

Site 750 is located about 4 km to the southwest of a northwest-trending, northeast-facing normal fault with a vertical throw of about 200 m (Fig. 2 and 43). To the northeast toward the normal fault, Sequence P2 thins by toplap. The thickness of the other sequences (P1, K3, and K2) remains fairly uniform close to Site 750 (see “Site Geophysics” section, this chapter).

Close to Site 750 the basement corresponds to a clear reflector overlying a series of dipping reflectors that almost parallel the basement reflector (Fig. 8 and 44). On the eastern flank of the Raggatt Basin, Sequence K1 disappears by onlap and Sequence K2 resting upon the basement is characterized by high-amplitude reflectors with medium continuity that drapes the preexisting basement topography. Sequence K3 is characterized by medium-amplitude reflectors with high continuity. Sequences P1 and P2 are rather transparent with high-continuity and low-amplitude reflectors (Coffin et al., in press; Colwell et al., 1988; Schlich et al., 1988; see also “Background and Objectives” and “Site Geophysics” sections, this chapter).

The basalts cored between 675.5 and 709.7 mbsf form the entire lithologic Unit V and are composed of a minimum of four lava flows (see “Igneous Petrology” section, this chapter). The basalts are compositionally transitional between normal mid-oceanic ridge basalts and oceanic island basalts.

The evolution of the eastern part of the Southern Kerguelen Plateau as derived from all these observations (see “Lithostratigraphy and Sedimentology” and “Biostratigraphy” sections, this chapter) and from seismic stratigraphy can be summarized as follows:

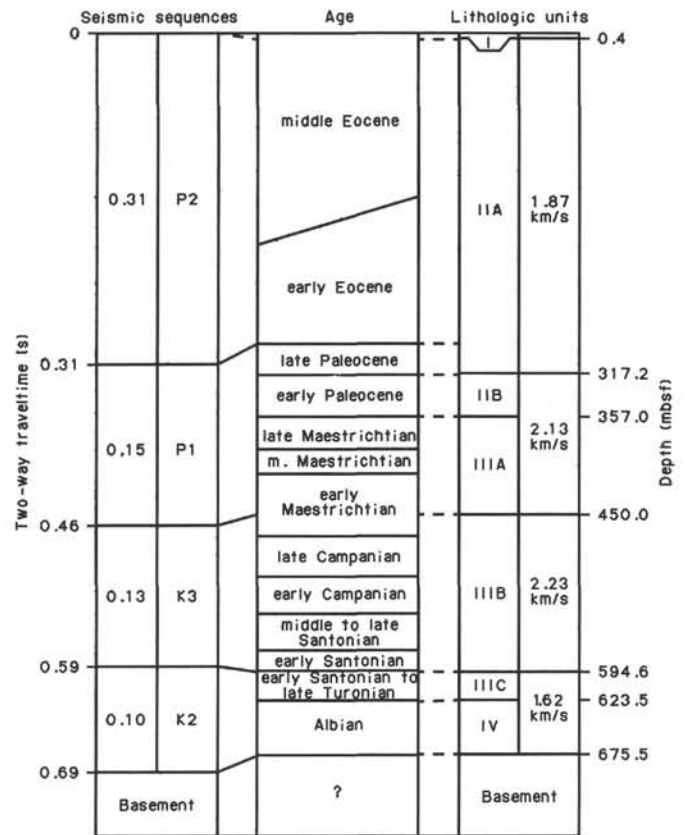


Figure 44. Vertical velocity distribution model for the sedimentary column at Site 750. Correlation of the seismic sequences with the different lithologic units.

igraphy and Sedimentology” and “Biostratigraphy” sections, this chapter) and from seismic stratigraphy can be summarized as follows:

1. Basalt flows (Unit V) covered the plateau over the region close to the site. These flows are relatively thick and massive; it is not clear from textural evidence whether the basalts were erupted at or near sea level.
2. During the Albian, sedimentation denotes fluvial conditions and consists of water-laid terrigenous claystones and siltstones with some sands and conglomeratic intervals (K2, Unit IV). The sedimentation evolved to open-marine deposits consisting of calcareous chalk with dark marl (K2, Subunit IIIC). During this time span, the plateau subsided from sea level to a depth of about 200 m (78–80 Ma).
3. During the late Campanian, open-marine sedimentation continued with intermittently silicified limestone and calcareous chalk, whereas the plateau remained at the same depth (K3, Subunit IIIB). The sedimentation rate is estimated at 5–10 m/m.y.
4. At about 75 Ma, a major tectonic episode affected the eastern edge of the Southern Kerguelen Plateau. Normal listric faults developed and are possibly related to the breakup between the Southern Kerguelen Plateau and the Broken Ridge–Diamantina Zone.
5. From 75 Ma to the middle Eocene (43 Ma), the sedimentation, mainly nannofossil chalk and ooze with some occurrence of chert, was essentially continuous with a sedimentation rate varying between 5 and 30 m/m.y. (P1, P2, Subunits IIIA, IIB, and IIA). During this period of time, the plateau remained at about the same depth.

6. A major erosional event scoured most of the sediments deposited at Site 750 after the middle Eocene.

SUMMARY AND CONCLUSIONS

Site 750 (proposed Site SKP-3D; 57°35.54'S, 81°14.42'E; water depth, 2030.5 m) is located on the Southern Kerguelen Plateau in the eastern part of the Raggatt Basin, west of the deep Labuan Basin, approximately 900 km south of the present-day Polar Front. Our primary objective was to recover an expanded Cretaceous section reflecting the early tectonic and depositional history of the Southern Kerguelen Plateau. The results were to be compared with those from Site 748, which was drilled through shallow-water, largely restricted Cretaceous marine sediments in the western Raggatt Basin, and with those from more open-marine sequences at Site 747 to the north and Site 738 (Leg 119) to the south. A second objective was to recover, if feasible, basement samples from the Raggatt Basin in a zone of dipping reflectors that we could compare with other Kerguelen Plateau basement sites (Sites 738, 747, and 749).

Beginning with this site on 14 April 1988, *JOIDES Resolution* resumed operations on the Southern Kerguelen Plateau following an unscheduled port call to Fremantle, Australia, requiring a transit of 17 days and 4400 nmi. The site was approved during the transit as a substitute for Site SKP-3B; it is located 18 km to the east on the same seismic line. The Paleogene sequence at the present site, however, is 140 m thinner than at Site SKP-3B, which would reduce drilling time by about 1 day; the Mesozoic sequence is of equal thickness at both sites. The basement reflector at Site 750 lies at about 0.69 s TWT below the seafloor, and three major seismic reflectors can be traced at 0.59, 0.46, and 0.31 s TWT.

Hole 750A was washed and interval cored using a rotary bit through middle and lower Eocene oozes, cherts, and cherts to 297.5 mbsf; below 143 mbsf the combination of cherts and heavy seas had their usual deleterious effect on core recovery, which was only 3% for the three rotary cores taken. After a 24-hr weather delay, continuous coring through Paleocene-Maestrichtian cherts to 423.3 mbsf yielded a nearly complete but drilling-disturbed Cretaceous/Tertiary boundary sequence at 348 mbsf; recovery was 47%.

The hole was ended at 460.5 mbsf by total bit failure (disintegration) after only 5½ hr of rotation, whereupon a successful logging run was made using a combination of seismic stratigraphy tools; a second run in rough seas using lithodensity tools was foiled by damage to the cable head. We suspended operations on 18 April 1988 with the hope of reoccupying the site after we drilled Site 751 (prospective Site SKP-2C) located 46 nmi to the west.

As it developed, we did reoccupy Site 750 on 20 April 1988 and washed Hole 750B with the RCB to 450 m, taking only one wash core on the way. After pulling a second wash barrel, the hole was continued with rotary or wash cores taken every 10–30 m through cherty Cretaceous cherts and limestones with the intention of maintaining a rate of progress of at least 10 m/hr. This rate was deemed necessary to reach basement before drilling time for the leg expired if the single bit were to survive to the projected total depth.

Drilling with a hard formation bit slowed considerably when the formation changed from marine limestone to terrestrial clay below 624 mbsf; however, a velocity inversion at that point considerably decreased the predicted depth to basement, which was encountered at 675.5 mbsf. Thereafter, a series of thick basalt flows were drilled with 67% recovery to a TD of 709.7 mbsf. This fulfilled the last remaining scientific objective, however abbreviated, for the Leg 120 shipboard participants, all of whom had made the long return trip to the plateau.

Throughout the final occupation of this site, the weather was remarkably good (the best for any hole during the leg), with winds generally steady between 20 and 35 kt and gusting between 45 and 55 kt only during brief snow squalls; this was perhaps the most important factor in the successful completion of this hole since operating in moderate seas considerably extended the life of the bit.

The following lithologic units were recognized at Site 750:

Unit I: depth, 0–0.37 mbsf; age, early Pleistocene to mid-Pliocene; diatom ooze and lag deposit. Repeated within the first core by a double punch of the drill string, this unit contains diatoms and foraminifers of early Pleistocene and mid-Pliocene age with a disconformity in between. The lag contains sands and ice-rafted pebbles with heavy manganese coatings; a disconformity occurs at the base.

Unit II: depth, 0.37–357.0 mbsf; age, middle Eocene to early Paleocene; nannofossil ooze, chalk, and chert divisible into two subunits.

Subunit IIA: depth, 0.37–317.2 mbsf; age, middle Eocene to late Paleocene; white nannofossil ooze, chalk, and chert.

Subunit IIB: depth, 317.2–357.0 mbsf; age, early Paleocene; white nannofossil chalk. Crosscutting gray dissolution seams are evident below 317 mbsf. Just above the Cretaceous/Tertiary contact, the white chalk darkens downward to an olive gray color. Dark specks are present, and there is a concomitant increase in magnetic susceptibility. The lowermost Danian nannofossil Zone NP1 is present, but it contains reworked Cretaceous material. The Cretaceous/Tertiary contact, which was disturbed by drilling, marks an abrupt change in lithology from well-consolidated Danian chalk to soft Maestrichtian ooze of the nannofossil *Nephrolithus frequens* Zone. The more clay-rich lower Danian section appears to show up as a positive excursion on the resistivity logs, which may allow a more precise placement of the base of this subunit.

Unit III: depth, 357.0–623.5 mbsf; age, late Maestrichtian to late Turonian; nannofossil chalk, chert, and intermittently silicified limestone divisible into three subunits.

Subunit IIIA: depth, 357.0–450.0 mbsf; age, late Maestrichtian to early Maestrichtian; nannofossil chalk and minor chert. Dissolution seams characterize this subunit along with burrows, laminae, and rare stylolites. Some pale purple laminae may represent redox changes; three gray laminae contained 50% zeolite. Microfossils are exceptionally well preserved in the upper Maestrichtian; echinoid spines are a persistent component and a brachiopod shell was found at 385 mbsf.

Subunit IIIB: depth, 450–594.6 mbsf; age, early Maestrichtian to early Santonian; intermittently silicified limestone and calcareous chalk, poorly recovered; bioclast fragments include small molluscs, crinoid columnals, and inoceramids.

Subunit IIIC: depth, 594.6–623.5 mbsf; age, early Santonian to late Turonian; chalk with dark clayey interlayers. Cenomanian microfossils are present but may be reworked; the darker clays may be redeposited. Pyritized wood fragments, a bivalve, and traces of glauconite are also present.

Unit IV: depth, 623.5–675.5 mbsf; age, Albian; red to dark grey brown silty claystone with charcoal and minor conglomerate. This unit consists of a broad range of water-laid terrigenous claystones and siltstones, with some sandy or conglomeratic intervals. Carbonized wood fragments from land plants are abundant as are coarse, authigenic siderite and pyrite grains and concretions. Where first sampled, this unit consists of a massive, plastic, reddish brown, silty claystone composed primarily of kaolinite, with up to 25% siderite (as coarse authigenic grains), 20% opaques, 6% pyrite, and 20% altered grains that may be derived from basalt.

The next core yielded a much darker, grayish brown clayey siltstone that is more fissile and richer in organic matter (up to 10%). A highly colorful, 25-cm-thick soft pebble conglomerate and brown sand displays grading, cross-stratification, and small-scale current bedding. Incorporated among the rounded to sub-rounded, 0.5–3 mm, silt- and claystone ferruginous grains are numerous large (centimeter scale) pieces of carbonized wood. Wood fragments are also enclosed within siderite-cemented claystones and a siderite concretion at the base of the unit. Shore-based palynological studies have yielded an Albian age for this richly fossiliferous unit.

Unit V: depth, 675.5–709.7 mbsf; basalt flows composed of moderately to highly altered plagioclase-clinopyroxene phryic basalt. At least four flows were recovered, of which the first flow represents the majority of the recovery, being a 11.5-m-thick massive basalt flow. The basalts were erupted in a sub-aerial or shallow subaqueous environment. The lower two flows are separated by a chilled margin and are overlain by highly altered volcanics. The flows are restricted in composition to olivine-hypersthene normative tholeiites. The secondary mineral assemblage consists of interlayered smectite, heulandite-clinoptilolite, calcite, and minor quartz veining.

From the seismic data, lithology, physical properties, and logging data, the major seismic reflectors at 0.46 s TWT (P1/K3 boundary) and 0.69 s TWT (K2/basement boundary) must be correlated with the top of lithologic Subunit IIIB (450.0 mbsf) and the top of lithologic Unit V (675.5 mbsf). Taking into account the velocity derived from the logging data, the seismic reflector at 0.31 s TWT (P2/P1 boundary) lies within Subunit IIA at 290 mbsf. Furthermore, the mean velocity for most of Subunit IIA is 1.87 km/s (0–290 mbsf). For the lower part of Subunit IIA plus Subunits IIB and IIIA (290–450 mbsf), it is 2.13 km/s.

The seismic reflector at 0.31 s TWT does not match any lithologic boundary. Since the seismic reflector at 0.69 s TWT obviously corresponds to the basaltic basement, it is possible to correlate the reflector at 0.59 s TWT (K2/K3 boundary) with the top of Subunit IIIC. With this assumption, the mean velocity calculated for Subunit IIIC and Unit IV is 1.62 km/s and is compatible with the measured compressional wave velocity completed on the very rare samples recovered in the hole. Consequently, the mean calculated velocity for Subunit IIIB is 2.23 km/s. The measured values for this subunit are extremely scattered and vary between 2.0 and 3.5 km/s; moreover, the limited number of samples does not permit an estimate of a significant mean velocity (Fig. 44).

Basement and sedimentary rocks drilled at this site provide interesting contrasts with those sampled elsewhere on the Kerguelen Plateau during this leg. In terms of incompatible trace element abundances, basalts from Site 750 are the most depleted, thereby extending the array defined by samples from Sites 747 and 749. They also show slight differences in incompatible element ratios, possibly indicating differences in source characteristics.

Nevertheless, Site 750 basement is transitional in composition between normal Indian Ocean MORB and Kerguelen and Heard island OIB lavas. The secondary mineral assemblage at this site indicates intermediate- to high-temperature alteration comparable with the temperature regimes defined at Sites 747 and 749. The alteration occurred under oxidizing conditions.

Following the emplacement of the uppermost basalts at this site, a considerable portion of the southern Kerguelen volcanic edifice was emergent during the Albian and subject to intense weathering in a warm temperate or subtropical climate (in marked contrast to the climate in this region today). Rainfall was sufficient to weather volcanics to kaolinitic clays. The actual source

rock may not have been entirely the tholeiitic basalts drilled at this site, but rather alkaline basalts located elsewhere in the rather extensive watershed (perhaps similar in composition to those drilled at Site 748).

The kaolinites accumulated in well-vegetated or forested, subaqueous or subaerial environments, perhaps on marshy flood plains. The soft-pebble conglomerates probably denote fluvial conditions, and the authigenic siderite crystals are characteristic of coal swamps. The numerous large pieces of charcoal (up to 5 cm) and high organic carbon contents of up to 10% further suggest a terrestrial setting. These sediments are visually similar but are in some ways mineralogically different from those penetrated but poorly sampled in lithologic Unit IV at Site 748; both, however, have high organic contents.

Foundering of this portion of the Kerguelen platform occurred by Cenomanian times. The oldest recovered chalks contain evidence of redeposition of inner shelf faunas and dark (organic-rich?) sediments into a deeper-water environment. As at Sites 747 and 748, the middle Campanian is missing, suggesting a plateau-wide disconformity (see Figure 4 in "Principal Results and Summary" chapter, this volume). By the late Campanian, however, subsidence had carried the site to upper slope depths. Sedimentation rates increased considerably and surface temperatures cooled, so that planktonic foraminifer assemblages changed from transitional to austral in character.

Only in the late Maestrichtian do the foraminifer and nannofossil assemblages lose their strong austral affinities, apparently indicating a progressive warming that leads up to the close of the Cretaceous period. By then, the site had deepened to perhaps bathyal depths. Conditions at this site during the deposition of these Upper Cretaceous chalks were consistently open marine, in strong contrast to the restricted late Albian–Turonian glauconitic siltstones and shallow-water Campanian–Maestrichtian glauconitic bioclastics that characterized the western Raggatt Basin (Site 748). Nor is there evidence of the Maestrichtian–lower Danian debris flows encountered at Site 747 to the north. The western Raggatt Basin stood structurally higher than the eastern portion of the basin throughout the Late Cretaceous, subsiding rapidly only at the end of the Maestrichtian, and Site 748 remains 740 m shallower than Site 750 today. These different histories are well reflected in our sedimentological and seismic stratigraphy records.

Surprisingly high sedimentation rates characterize the upper Campanian–Maestrichtian as well as the Danian. The latter, with a sedimentation rate of 11 m/m.y., spans 40 m of section at Site 750. Danian benthic foraminifer faunas are similar to those of the upper Maestrichtian; by then, the paleodepth of the site was approaching those of the present day. Sedimentation rates increased considerably to about 30 m/m.y. during the late early and late middle Eocene. These exceptionally high sedimentation rates denote high regional pelagic productivity. Except for the thin Pliocene–Pleistocene veneer and lag deposit, the remainder of the Cenozoic is missing at this site. The disconformity between the lower Pleistocene and mid-Pliocene noted at this site is also discernible at Sites 748 and 749 (see Figure 4 in "Principal Results and Summary" chapter, this volume).

In summary, the record at Site 750 broadens our understanding of the tectonic and geologic evolution of the Raggatt Basin and the Southern Kerguelen Plateau. It provides:

1. A fifth basement site (along with Leg 120 Sites 747, 748, and 749 and Leg 119 Site 738) to help characterize the basalts that underlie the plateau;
2. A record, albeit incomplete due to interval coring, of what appears to be the earliest sedimentation, both nonmarine and marine, recovered at any sites on the plateau;

3. An open-marine Cretaceous, predominantly slope depth, pelagic sequence in the eastern Raggatt Basin, which stands in stark contrast to the restricted and shallow-water section drilled in the western portion of the basin at Site 748;

4. Taken together with open-marine Site 747 to the north and Site 738 (Leg 119) to the south, Site 750 places constraints on the geographic extent and the nature of the sedimentological processes responsible for the development of the glauconitic facies in the west;

5. The most expanded high-latitude bathyal record of sedimentation to date through the critical Maestrichtian-Danian interval, a most important reference section for integrated biostratigraphic, biogeographic, and geochemical stratigraphy studies; and

6. An important deep-water control point for deciphering the tectonic and subsidence history of the Kerguelen Plateau, one which further suggests an eastward tilting of the Raggatt Basin and an eastward shift in the depocenter following the plateau-wide tectonic event near the end of the Cretaceous.

With penetration of basement in Hole 750B, basalt flows have been sampled at four Leg 120 sites. Since one of the primary objectives of this leg was to determine the nature and origin of the Kerguelen Plateau basement rocks, the following summary by our igneous petrologists is appropriate (see "Igneous Petrology" section, this chapter, and Fig. 40):

Basalts from Site 750 are more depleted in incompatible trace elements than any of the other basalts recovered on Leg 120. This may indicate that basalts from Hole 750B were produced by higher degrees of melting than those of Sites 747 and 749. Excluding the single (OIB) basalt flow drilled at Site 748, Leg 120 basalts show some intersite variation in incompatible element ratios, possibly indicating source heterogeneities.

Basalts from Sites 747, 749, and 750 are transitional in composition between normal Indian Ocean MORB (Price et al., 1986) and Kerguelen and Heard island OIB lavas (Storey et al., 1988). Compositionally, they show affinities with Nauru Basin basalts (Saunders, 1985), transitional basalts from the Southwest Indian Ridge (le Roex et al., 1983), and the oldest basalts from Kerguelen Island (Storey et al., 1988). The alkaline basalt lava from Hole 748 is quite distinctive in that it is extremely enriched in incompatible elements and has compositional characteristics typical of OIB-type magmatism.

REFERENCES

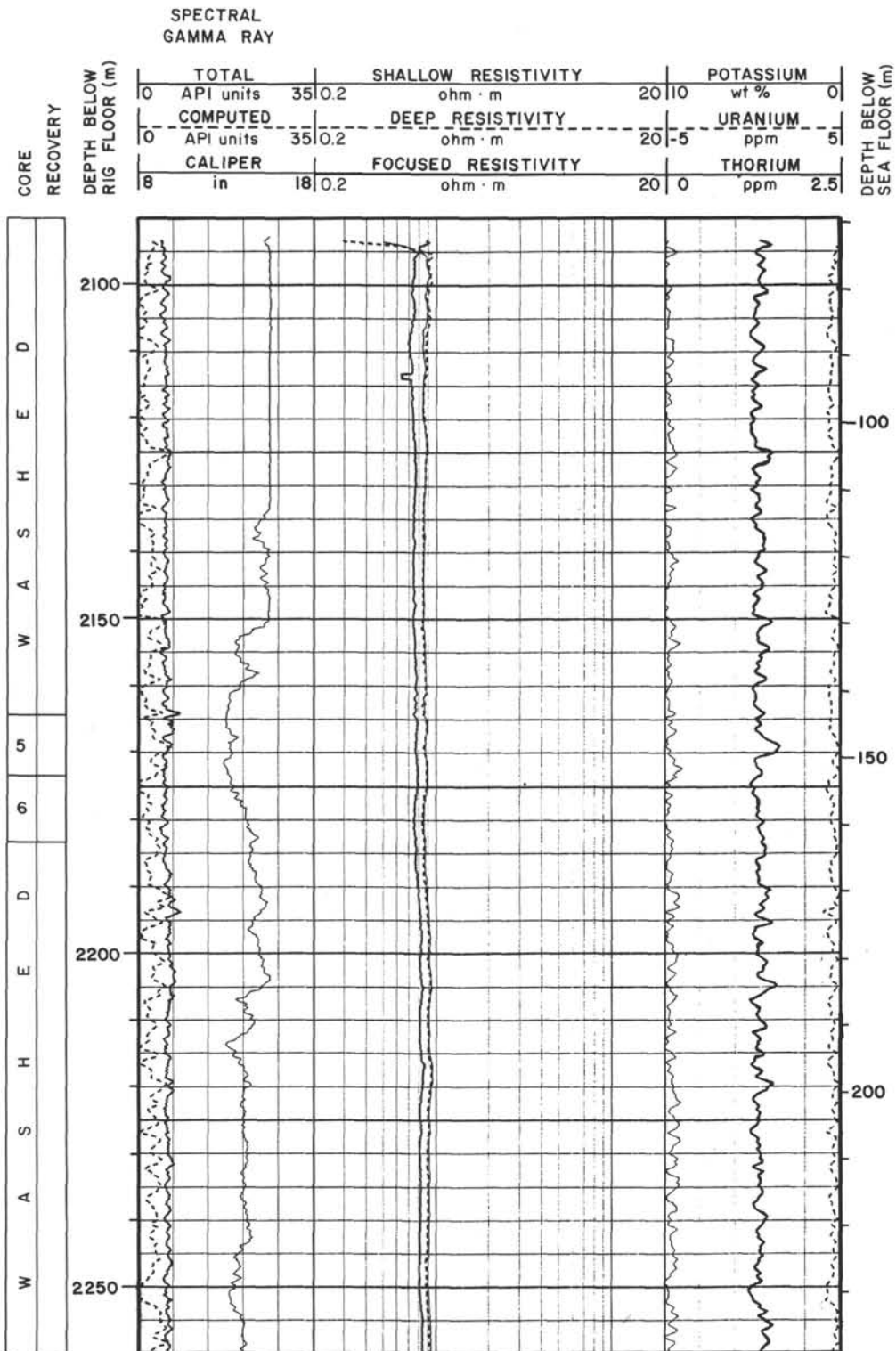
- Belford, D. J., 1960. Upper Cretaceous foraminifera from the Toolonga Calcilitite and Gingin Chalk, Western Australia. *Bull. Bur. Miner. Resour., Geol. Geophys. (Aust.)*, 57:1-198.
- Berggren, W. A., Kent, D. V., and Flynn, J. J., 1985a. Jurassic to Paleogene: Part 2, Paleogene geochronology and chronostratigraphy. In Snelling, N. J. (Ed.), *The Chronology of the Geological Record*. Geol. Soc. Mem. (London), 10:145-195.
- Berggren, W. A., Kent, D. V., Flynn, J. J., and Van Couvering, J. A., 1985b. Cenozoic geochronology. *Geol. Soc. Am. Bull.*, 96:1407-1418.
- Berggren, W. A., Kent, D. V., and van Couvering, J. A., 1985c. The Neogene: Part 2, Neogene geochronology and chronostratigraphy. In Snelling, N. J. (Ed.), *The Chronology of the Geological Record*. Geol. Soc. Mem. (London), 10:211-260.
- Bolli, H. M., 1974. Jurassic and Cretaceous calcisphaerulidae from DSDP Leg 27, eastern Indian Ocean. In Veevers, J. J., Heirtzler, J. R., et al., *Init. Rept. DSDP*, 27: Washington (U.S. Govt. Printing Office), 843-907.
- Boyce, R. E., 1976. Definitions and laboratory techniques of compressional sound velocity parameters and wet-water content, wet-bulk density, and porosity parameters by gravimetric and gamma ray attenuation techniques. In Schlanger, S. O., Jackson, E. D., et al., *Init. Repts. DSDP*, 33: Washington (U.S. Govt. Printing Office), 931-955.
- _____, 1977. Deep Sea Drilling Project procedures for shear strength measurement of clayey sediment using modified Wykeham-Farrance laboratory vane apparatus. In Barker, P. E., Dalziel, I. W. D., et al., *Init. Repts. DSDP*, 36: Washington (U.S. Govt. Printing Office), 1059-1068.
- Caron, M., 1985. Cretaceous planktic foraminifera. In Bolli, H. M., Saunders, J. B., and Perch-Nielsen, K. (Eds.), *Plankton Stratigraphy*: Cambridge (Cambridge Univ. Press), 17-86.
- Chen, P.-H., 1975. Antarctic radiolaria. In Hayes, D. E., Frakes, L. A., et al., *Init. Repts. DSDP*, 28: Washington (U.S. Govt. Printing Office), 437-513.
- Coffin, M. F., Munschy, M., Colwell, J. B., Schlich, R., Davies, H. L., and Li, Z. G., in press. Seismic stratigraphy of the Raggatt Basin, Southern Kerguelen Plateau: tectonic and paleoceanographic implications. *Geol. Soc. Am. Bull.*
- Colwell, J. B., Coffin, M. F., Pigram, C. J., Davies, H. L., Stagg, H.M.J., and Hill, P. J., 1988. Seismic stratigraphy and evolution of the Raggatt Basin, Southern Kerguelen Plateau. *Mar. Pet. Geol.*, 5: 75-81.
- Durand, B., and Monin, J. C., 1980. Elemental analysis of Kerogens (C, H, O, N, S, Fe). In Durand, B. (Ed.), *Kerogen: Insoluble Organic Matter from Sedimentary Rocks*: Paris (Editions Technip).
- Espitalie, J., Madec, M., Tissot, B., Mennig, J. J., and Leplat, P., 1977. Source rock characterization method for petroleum exploration. *Proc. 9th Annu. Offshore Technol. Conf.*, 3:439-448.
- Fox, P. J., and Stroup, J. B., 1981. The plutonic foundation of the oceanic crust. In Emiliani, C. (Ed.), *The Sea* (Vol. 7): New York (John Wiley), 119-218.
- Gieskes, J. M., and Peretsman, G., 1986. Water chemistry procedures on SEDCO 471—some comments. *ODP Tech. Note*, No. 5.
- Houtz, R. E., Hayes, D. E., and Markl, R. G., 1977. Kerguelen Plateau bathymetry, sediment distribution and crustal structure. *Mar. Geol.*, 25:95-130.
- Huber, B. T., Harwood, D. M., and Webb, P. N., 1983. Upper Cretaceous microfossil biostratigraphy of Seymour Island, Antarctic Peninsula. *Antarctic J. U.S.*, 1983 Review, 72-74.
- Katz, B. J., 1983. Limitations of "Rock Eval" pyrolysis for typing organic matter. *Org. Geochem.*, 4:195-199.
- Kono, M., 1980. Statistics of paleomagnetic inclination data. *J. Geophys. Res.*, 85:3878-3882.
- Lambe, T. W., and Whitman, A. E., 1969. *Soil Mechanics*: New York (John Wiley).
- Leclaire, L., Bassias, Y., Denis-Clocchiatti, M., Davies, H., Gautier, I., Gensous, B., Giannesini, P. J., Patriat, P., Segoufin, J., Tesson, M., and Wannesson, J., 1987a. Lower Cretaceous basalts and sediments from the Kerguelen Plateau. *Geo-Mar. Lett.*, 7:169-176.
- Leclaire, L., Denis-Clocchiatti, M., Davies, H., Gautier, I., Gensous, B., Giannesini, P.-J., Morand, F., Patriat, P., Segoufin, J., Tesson, M., and Wannesson, J., 1987b. Nature et âge du Plateau de Kerguelen-Heard, secteur sud. Résultats préliminaires de la campagne "N.A.S.K.A.-MD48". *C. R. Acad. Sci., Ser. 2*, 304:23-28.
- le Roex, A. P., Dick, H.J.B., Erlank, A. J., Reid, A. M., Frey, F. A., and Hart, S. R., 1983. Geochemistry, mineralogy and petrogenesis of lavas erupted along the Southwest Indian Ridge between the Bouvet triple junction and 11 degrees east. *J. Petrol.*, 24:267-318.
- Price, R. C., Kennedy, A. K., Riggs-Sneeringer, M., and Frey, F. A., 1986. Geochemistry of basalts from the Indian Ocean triple junction: implications for the generation and evolution of Indian Ocean Ridge basalts. *Earth Planet. Sci. Lett.*, 78:379-396.
- Quilty, P. G., 1973. Cenomanian-Turonian and Neogene sediments from northeast of Kerguelen Ridge, Indian Ocean. *J. Geol. Soc. Aust.*, 20:361-371.
- Saunders, A. D., 1985. Geochemistry of basalts from the Nauru Basin, Deep Sea Drilling Project Legs 61 and 89: implications for the origin of oceanic flood basalts. In Moberly, R., Schlanger, S. O., et al., *Init. Repts. DSDP*, 89: Washington (U.S. Govt. Printing Office), 499-517.
- Schlich, R., 1975. Structure et âge de l'océan Indien occidental. *Mem. Hors Ser. Soc. Geol. Fr.*, 6:1-103.
- _____, 1982. The Indian Ocean: aseismic ridges, spreading centers and oceanic basins. In Nairn, A.E.M., and Stehli, F. G. (Eds.), *The Ocean Basins and Margins: The Indian Ocean* (Vol. 6): New York (Plenum Press), 51-147.
- Schlich, R., Coffin, M. F., Munschy, M., Stagg, H.M.J., Li, Z. G., and Revill, K., 1987. *Bathymetric Chart of the Kerguelen Plateau*. [Jointly

- edited by Bureau of Mineral Resources, Geology and Geophysics, Canberra, Australia; Institut de Physique du Globe, Strasbourg, France; and Territoires des Terres Australes et Antarctiques Françaises, Paris, France.]
- Schlich, R., Munsch, M., Boulanger, D., Cantin, B., Coffin, M. F., Durand, J., Humler, E., Li, Z. G., Savary, J., Schaming, M., and Tissot, J. D., 1988. Résultats préliminaires de la campagne océanographique de sismique réflexion multitraces MD47 dans le domaine sud du plateau de Kerguelen. *C. R. Acad. Sci., Ser. 2*, 305:635-642.
- Shaw, C. A., and Ciesielski, P. F., 1983. Silicoflagellate biostratigraphy of middle Eocene to Holocene subantarctic sediments recovered by Deep Sea Drilling Project Leg 71. In Ludwig, W. J., Krasheninnikov, V. A., et al., *Init. Repts. DSDP*, 71, Pt. 2: Washington (U.S. Govt. Printing Office), 687-737.
- Sliter, W. V., 1976. Cretaceous foraminifers from the southwestern Atlantic Ocean, Leg 36, Deep Sea Drilling Project. In Barker, P. F., Dalziel, I.W.D., et al., *Init. Repts. DSDP*, 36: Washington (U.S. Govt. Printing Office), 519-573.
- Storey, M., Saunders, A. D., Tarney, J., Leat, P., Thirlwall, M. F., Thompson, R. N., Menzies, M. A., and Marriner, G. F., 1988. Geochemical evidence for plume-mantle interactions beneath Kerguelen and Heard Islands, Indian Ocean. *Nature*, 336:371-374.
- Tissot, B. F., and Welte, D. H., 1984. *Petroleum Formation and Occurrence*: Berlin-Heidelberg-New York (Springer-Verlag).
- Von Herzen, R. P., and Maxwell, A. E., 1959. The measurement of thermal conductivity of deep-sea sediments by a needle probe method. *J. Geophys. Res.*, 65:1557-1563.
- Worm, H.-U., and Banerjee, S. K., 1987. Rock magnetic signature of the Cretaceous-Tertiary boundary. *Geophys. Res. Lett.*, 14:1083-1086.
- Wright, A. A., Bleil, U., Monechi, S., Michel, H. V., Shackleton, N. J., Simoneit, B.R.T., and Zachos, J. C., 1985. Summary of Cretaceous/Tertiary boundary studies, Deep Sea Drilling Project Site 577, Shatsky Rise. In Heath, G. R., Burckle, L. H., et al., *Init. Repts. DSDP*, 86: Washington (U.S. Govt. Printing Office), 799-804.

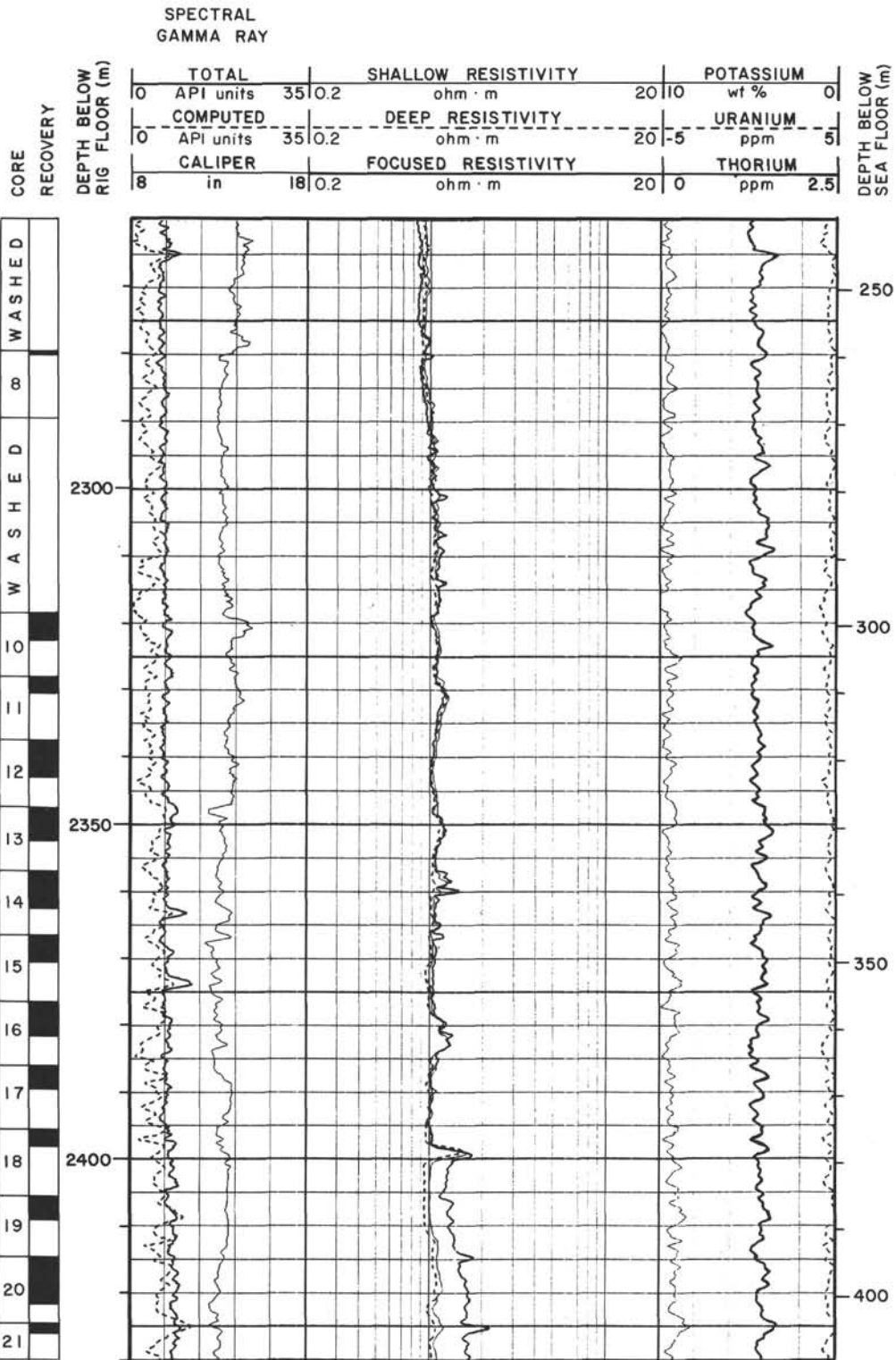
Ms 120A-112

NOTE: All core description forms ("barrel sheets") and core photographs have been printed on coated paper and bound as Section 3, near the back of the book, beginning on page 377.

Summary Log for Hole 750 A



Summary Log for Hole 750 A (continued)



Summary Log for Hole 750A (continued)

